NTNU – Trondheim
Norwegian University of
Science and Technology

Testing and Optimization of Nano Particles Reinforced PVAm/PVA Blend FSC Membranes for High Pressure Natural Gas Sweetening

Anders Sørheim

Chemical Engineering
Submission date: August 2012
Supervisor: May-Britt Hägg, IKP

Norwegian University of Science and Technology
Department of Chemical Engineering

Declaration of compliance

I declare that this is an independent work according to the exam regulations of the Norwegian University of Science and Technology (NTNU).

Trondheim, August 6th 2012

_____

Anders Sørheim

Preface

This Master's thesis was conducted at the Master's degree program for Chemical Engineering and Biotechnology at NTNU in the Department of Chemical Engineering. The main supervisor of this thesis was Prof. May-Britt Hägg and the co-supervisor was Dr. Ing. Xuezhong He, both with whom I feel very grateful and honored to have worked with. I would also like to recognize the continuous work with environmental friendly technology and outstanding gas separation membrane research at the Memfo group.

My deepest gratitude goes to my dear mom and dad, Anna Martha M. Sørheim and Jan Ove Sørheim, for being fantastic parents and for supporting me, being there for me and believing in me throughout my education.

A special gratitude goes to my supervisor Dr. Ing. Xuezhong He for always helping me out with practical and theoretical problems, and to Prof. May-Britt Hägg for her inspiration and kind and sweet-hearted nature. Helpful advice from Dr. Ing. Mohammad Washim Uddin and Inger Lise Alsvik have also been greatly appreciated. I am very grateful for all the valuable organizational help from Lisbeth H. Blekkan Roel in the department office. I would also like to mention in particular my fellow students Eivind Berstad and Markus Solberg Wahl for help, motivation, Friday porridge and wonderful coffee break talks.

Trondheim, August 6th 2012

Anders Sørheim

Abstract

Employing gas separation membranes for natural gas sweetening is a cheaper, simpler, more energy efficient and an environmentally friendly alternative to separate CO_2 from methane. Significant advances has been made in membrane science and technology over the last couple of decades, and especially novel polymer-based FSC membranes have the potential of commercialization in the natural gas treatment industry.

In this master's thesis, a selection of nanoparticle reinforced PVAm/PVA blend FSC membranes have been prepared and tested at high pressure for natural gas sweetening. An ultra-thin selective layer was prepared from commercial polyvinyl amine (PVAm) and polyvinyl alcohol (PVA) and incorporated with either carbon nanotubes or fumed silica, and was cast on the support materials polysulfone (PSf), polyvinylidene fluoride (PVDF) and cellulose acetate (CA). Permeation tests were carried out at a high pressure pilot scale membrane permeation rig, and the effect of pressure up to 80 bar was investigated. The permeate gas composition was analyzed with a gas chromatograph, and for a total of 11 different membranes, the CO_2 permeance and CO_2/CH_4 selectivity was calculated. Scanning electron microscopy was employed to analyze the morphology of the membranes.

Several preparational conditions such as nanofiller concentration, solution filtration and selective layer thickness were explored and yielded good results. One membrane in particular showed both high permeance and selectivity at high pressures, with a CO_2/CH_4 selectivity of 26.9 and a CO_2 permeance of 0.034 $m^3(STP)/m^2.h.bar$ at 60 bar and 30°C, with a feed gas flow rate of 0.120 m^3/h. The mechanical strength from the nanocomposite PVAm/PVA selective layer with an average thickness 0.670 μm on a PSf support showed good permeability and high selectivity for high pressures.

Sammendrag

Anvendelse av membraner for gasseparasjon i søtning av naturgass er et billigere, enklere, mer energieffektivt og mer miljøvennlig alternativ for å fjerne CO_2 fra metan. I løpet av de siste par tiårene er det blitt gjort betydelige fremskritt innen membranteknologi og membranforskning, og spesielt nye polymerbaserte FSC-membraner har potensial til å bli kommersialisert i markedet for naturgassrensing.

I denne masteroppgaven har et utvalg av PVAm/PVA-blandede FSC membraner forsterket med nanopartikler blitt preparert og testet ved høyt trykk for søtning av naturgass. Et ultra-tynt selektivt lag ble fremstilt av innkjøpt polyvinylamin (PVAm) og polyvinylalkohol (PVA) og innlemmet med enten karbonnanorør eller eimet silika, og ble støpt på støttematerialene polysulfon (PSf), polyvinylidenfluorid (PVDF) eller celluloseacetat (CA). Permasjonsforsøk ble utført i en pilotskala høytrykksrigg for membranpermeering, og effekten av opp mot 80 bars trykk ble undersøkt. Gasskomposisjonen av permeatgassen ble analysert med en gasskromatograf, og CO_2-permeansen og CO_2/CH_4-selektiviteten for til sammen 11 ulike membraner ble regnet ut. Skanningselektronmikroskopi ble tatt i bruk for å analysere morfologien til membranene.

Flere fremstillingsbetingelser som f.eks. konsentrasjonen av nanofyllere, filtrering av løsning og tykkelsen til det selektive laget ble utforsket og gav gode resultater. Spesielt én membran viste både høy permeans og selektivitet ved høyt trykk, med en CO_2/CH_4-selektivitet på 26.9 og en CO_2-permeans på 0.034 $m^3(STP)/m^2.t.bar$ ved 60 bar og 30°C, med en fødegasstrøm på 0.120 m^3/t. Den mekaniske styrken fra det selektive laget til nanokompositten PVAm/PVA med en gjennomsnittlig tykkelse på 0.670 μm på en støtte av PSf oppviste god permeabilitet og høy selektivitet ved høye trykk.

Contents

List of Figures

xiv

List of Tables

List of Symbols

Symbol	Explanation	Value/unit
Latin letters		
A	Area	m^2
C_A	Concentration of gas A	mol/cm^3
D	Diffusion coefficient	m^2/h
dC	Concentration difference	mol/cm^3
d_k	Kinetic diameter	$\mathring{A}$
dx	Distance difference	m
E	Tensile modulus	N/m^2
E_D	Activation energy	J/mol
E_P	Activation energy for permeation	J/mol
F	Force	N
F	Facilitated factor	-
J_A	Flux of gas A	m^3/m^2h
K	Equilibrium constant	-
k	Front factor	-
k	Boltzmann's constant	m^2kg/s^2K
l	Membrane thickness	m
M_m	Molecular weight	g/mol
M_n	Molecular number average	g/mol
M_w	Molecular weight average	g/mol
n	Slope	-
p_A	Partial pressure of gas A	bar
p	Polymer dispersity	-
p	Pressure	bar
p_feed	Feed Pressure	kPa
P	Permeability	$barrer$
P_0	Pre-exponential constant	-
q_p	Permeation flow rate	m^2/h
R_{CO_2}	Permeance of CO_2	$m^3(STP)/m^2hbar$
$\mathbb{R}$	Gas constant	$J/molK$
r	Stokes radius	m
S	Solubility	cm^3/cm^3cmHg
S_A	Solubility of gas A	cm^3/cm^3cmHg
S_0	Pre-exponential constant	-
T	Temperature	$°C$
T_c	Critical temperature	$°C$

T_g	Glass transition temperature	$°C$
v_f	Fractional free volume	
v_vdw	Van der Waals volume	cm^3/mol
w_i	Weight of component i	g
x	Distance	m

Greek letters

α	Selectivity	-
α	Mobility ratio	-
$\delta\alpha$	Thermal expansion coefficient difference	-
η	Viscosity	kg/sm
δH_S	Sorption energy	J/mol
ΔP_L	Upper pressure difference limit for facilitated transport effect	bar

List of Abbreviations

Abbreviation	Explanation
AA	Acrylic acid
AAM	Acrylamide
CA	Cellulose acetate
CCS	Carbon capture and storage
CH_4	Methane
CNT	Carbon nanotubes
CO_2	Carbon dioxide
DEA	Diethanolamine
DGA	Diglycolamine
$DMAEMA$	2-(Dimethylamino) ethyl methacrylate
$DNMDAm$	Diamino-N-methyldipropylamine
$ECBM$	Enhanced coal-bed methane recovery
ELM	Emulsified liquid membranes

EOR	Enhanced oil recovery
EGS	Enhanced geothermal systems
FSC	Fixed site carrier
FT_IR	Fourier Transform Infrared Spectroscopy
FTM	Facilitated transport tembranes
GPU	Gas permeance unit
LNG	Liquid natural gas
$MDEA$	Methyldiethanolamine
MEA	Monoethanolamine
$MWCO$	Molecular weight cut-off
$MMscfd$	Million standard cubic feet per day
$mscf$	Thousand standard cubic feet
MTR	Membrane Technology and Research Inc.
PAN	Polyacrylonitrile
PBO	Polybenzoxazoles
PEI	Polyetheleneimine
PES	Polyethersulfone
PFP	Perfluoropolymer
PIM	Polymer of Intrinsic Microporosity
PMP	Poly(4-methyl-2-pentyne)
ppm	Parts per million
$ppmv$	Volume parts per million
PSf	Polysulfone
PVA	Polyvinylaclohol
$PVAm$	Polyvinylamine
PVP	Polyvinylpyrrolidone
$PVSA$	Poly N-vinyl-γ-sodium aminobutyrate
$PVDF$	Polyvinylidene Fluoride
$RTIL$	Room temperature ionic liquid
SA	Sodium acrylate
SLM	Supported Liquid Membrane
Sm^3	Standard cubic meter = 1 m^3 at STP
STP	Standard temperature and pressure (273.15 K, 1 bar)
TMC	Trimesoyl chloride

1

1 Introduction

A push for cheaper and more efficient methods for natural gas sweetening has created leeway for gas separation membranes to emerge as a viable option for separating carbon dioxide (CO_2) from natural gas. Natural gas is the fastest growing fossil fuel in the world, and the global consumption increases with 1.6 % every year. It is also the cleanest of all fossil fuels with the smallest emission of CO_2 per mass unit. Whilst conventional technologies such as cryogenic distillation and absorption still dominate the global natural gas sweetening operations, technology based on gas separation membranes has contributed tremendously to the frontiers of research on CO_2 capture. Especially the commercial usage of polymer membranes accelerated in the 1980s as a result of novel synthetic polymers with unique separating characteristics. These include both high permeability in the membrane for the gas being separated, and a high selectivity over the other gases in the gas mixture, which in natural gas for most part is methane (CH_4). This results in both a high gas flow and a high purity of the product. Over the last 20 years, great progress has been made within the gas separation membrane technology, with main focus areas being the improvement of the membrane forming processes, the chemical and physical structures in the materials, and modular configurations of membranes implemented in the natural gas sweetening process [1, 2].

1.1 Background

Global warming has been literally a hot topic for more than three decades, and is one of the greatest challenges humanity is facing in the centuries to come, along with energy shortage and the ever growing world population, to mention but a few. The term "global warming" is used interchangeably with "climate change", with the latter perhaps being a more appropriate description, as the increase of global average temperature leads to an alteration of the regional climate patterns around the world, from both the increase and decrease of local annual temperatures to wind and precipitation anomalies.

The causes of climate change are mainly threefold. Natural factors such as the oscillations in solar radiation intensity and the minute changes in Earth's heliocentric orbit have been fluctuating over the course of billions of years, resulting in eons of varying global temperatures. Furthermore, natural processes like volcanic activity and changes in ocean circulation also constitute a major part of the temperature variations. But the problem with our re-

cent sudden temperature increase is that it is happening extremely fast in a geological sense, and this is mainly due to the anthropogenic change of the atmospheres composition, mainly caused by deforestation, burning of fossil fuels and the emission of hazardous green house gases like chlorofluorocarbons, methane and CO_2 [3].

Figure 1: The link between atmospheric CO_2 concentration and temperature from 1850 to 2009. [3]
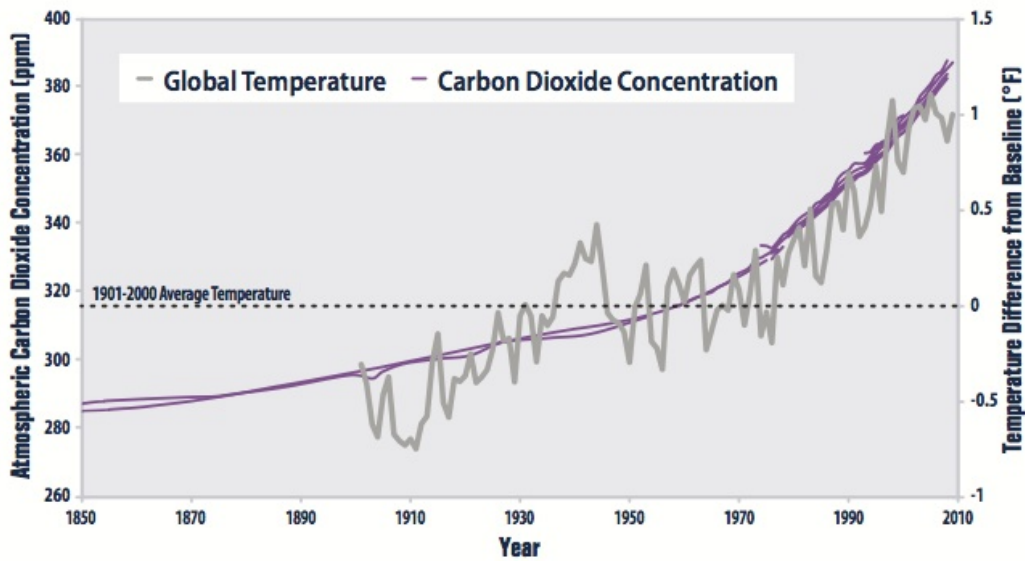
CO_2 has become the largest scapegoat for climate change because of the close correlation between temperature rise and CO_2 emission, as shown in Figure 1. From this it is clear that the concentration of CO_2 has risen almost exponentially from about 285 to over 380 parts per million (ppm) over the last 150 years, and over the same time the annual temperature has increased with over 1.5°C, with the current temperature already 1°C higher than the baseline temperature of the 20th century [3]. The concentration of CO_2 had remained at a more or less constant level until the beginning of the industrial revolution, where the burning of coal and subsequently oil started to pump billions of tons of CO_2 into the atmosphere. According to the Intergovernmental Panel on Climate Change (IPCC), the expected global temperature increase will be between 1.1°C and 6.4°C by 2100, depending on which of a number of possible climate change scenarios take place. From this, it is clear that the emissions of CO_2 need to be abated in order to minimize the menacing effects of global warming [4].

3

Table 1: Fossil fuel emission levels in lbs. per billion Btu of energy input [5]

Pollutant	Natural Gas	Oil	Coal
Carbon Dioxide	117,000	164,000	208,000
Carbon Monoxide	40	33	208
Nitrogen Oxides	92	448	457
Sulfur Dioxide	1	1,122	2,591
Particulates	7	84	2,744
Mercury	0.000	0.007	0.016

A gradual replacement of coal and oil with natural gas may help mitigating the global CO_2 emissions, as gas is the cleanest of all fossil fuels. When burned, natural gas on average emits only 71.3% and 56.3% the amount of CO_2 compared to oil and coal, as it primarily is composed of methane, whereas oil and coal consists of much more complex molecules with a higher ratio of carbon. The emissions of other harmful and environmentally unfriendly components such as SO_2, NO_x and mercury are also considerably lower as seen from Table 1, which makes natural gas a green energy source in the age of energy transitioning from fossil fuels to renewable energy sources. In addition to cleaner energy and lower CO_2 emissions, substituting natural gas with oil and coal may help better the air quality and smog problems in cities, as well as prevent acid rain. A more widespread use of natural gas as a fuel in motor vehicles could also lower the pollution in the transportation sector [5].

1.2 Natural Gas

Natural gas is a naturally occurring gas mixture consisting mostly of methane, but it can also be up to 20 % of other light hydrocarbons (mostly ethane) in content, along with containing other impurities such as carbon dioxide. Natural gas occurrence is usually due to biogenic and thermogenic processes on organic material working over time [5].

1.2.1 Applications and Consumption of Natural Gas

Natural gas is one of society's major energy sources, and has a vast number of applications ranging from the heating of buildings and generating electricity to manufacturing fertilizers and other important chemicals in the petrochemical industry. It is most frequently found in deep natural underground rock

formations both onshore and offshore, either by itself in coal beds, where it is adsorbed in the solid matrix of the coal, or in reservoirs with petroleum, also known as "associated gas" [6].

According to the International Energy Outlook 2011, natural gas is the fastest growing fossil fuel in the world, and the global consumption is estimated to become 168.7 trillion standard cubic feet in 2035, which make up an annual increase of 1.6 % from the 2010 amount of 113.1 trillion standard cubic feet, as shown in Figure 2. The energy produced by natural gas accounts for a total of 22.6% of the total energy consumption in the world. In Norway, the total production of natural gas in 2010 was about 233 billion standard cubic feet, which is approximately 6% of the total world production, and an increase of 3.1% from the previous year. 92% of this was exported to EU countries, primarily to Germany, Great Britain and France [1,7].

Figure 2: Projected global consumption of natural gas between 2008 and 2035 [5]
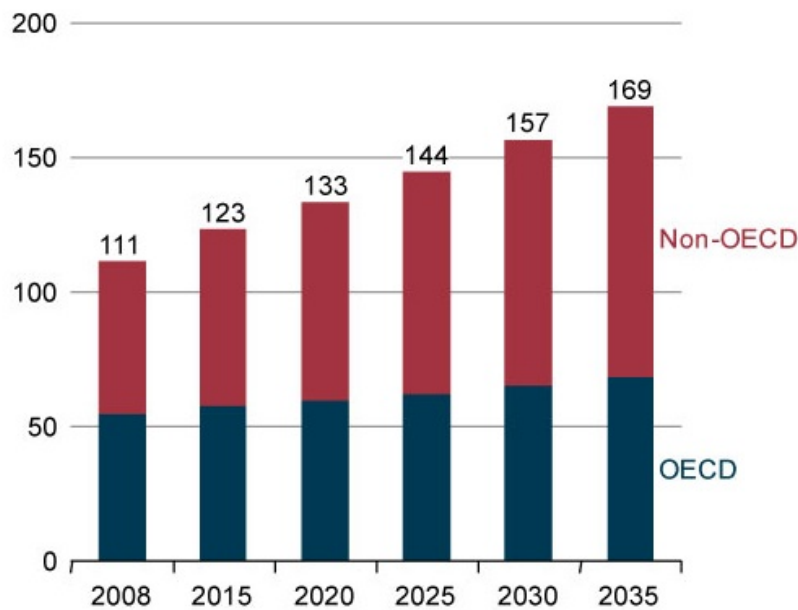
1.2.2 Natural Gas in Norway

The largest gas fields on the Norwegian shelf are Troll, Frigg, Gullfaks, Sleipner and Snøhvit. The latter two have implemented an innovative technology of sequestering carbon dioxide in either petroleum reservoirs or saline aquifers, also know as carbon capture and storage (CSS). The natural gas

produced from the Sleipner field contains nearly 9% CO_2, and since the completion of the world's first full-scale commercial CCS plant at the Sleipner site in 1996, over 10 million tons of CO_2 has been captured and injected into subsea saline aquifers. The CO_2 content of the Snøhvit field is slightly lower, between 5% and 8%, and here the separation of the natural gas and CO_2 from subsea wells is done at the onshore LNG (Liquid Natural Gas) plant in Hammerfest, with a full production of 700 000 tons of CO_2 per year since startup in 2007, see Figure 3. This gas is then re-injected into the well for enhanced oil recovery (EOR) [8].

Figure 3: Amount of CO_2 in tons injected (in red) versus emitted (in blue) for the years 2007 - 2010 for the natural gas field Snøhvit. [9]
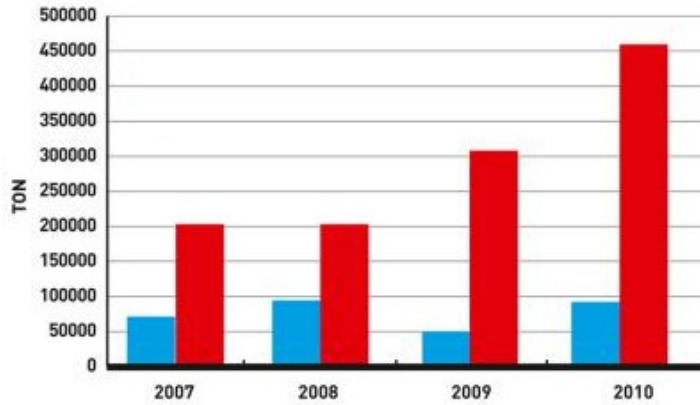
1.2.3 Composition and Impurities in Natural Gas

Traditional natural gas involve both associated and non-associated gas from wells, and varies quite a lot in composition. Inherently, natural gas contains a wide variety of gases and other contaminates, ranging from methane and other hydrocarbons, through oxygen, water and nitrogen, to unwanted acid gases like SO_2 , H_2S and CO_2. Technically, SO_2 is also an acid gas, but the removal of this gas is usually treated separately in a process called flue gas desulfurization [2]. Methane is usually the major constituent, but also nitrogen, water, ethane and carbon dioxide may comprise substantial proportions of the gas, depending on the location of the well, as seen in Table 2. Water is not shown in this list, as it is almost always, with some exceptions, present at wellhead conditions, and it usually assumed that the entering gas for sour gas treatment is saturated with water [6]. Other impurities that may appear in the natural gas stream are mercury (Hg), radon (Ra), oxygen O_2, and if the H_2S concentration is large enough, traces of carbonyl sulfide (COS),

carbon disulfide (CS2), elemental sulfur (S) and mercaptans [6].

Table 2: Some typical gas compositions [6]

	Canada (Alberta)	CO, US (Western)	Vietnam (Bach Ho)	Tunisia (Miskar)	NM, US (Rio Arriba)	TX, US (Cliffside)
Helium	0.0	0.0	0.00	0.00	0.0	1.8
Nitrogen	3.2	26.10	0.21	16.903	0.68	25.6
CO$_2$	1.7	42.66	0.06	13.588	0.82	0.0
H$_2$S	3.3	0.0	0.00	0.092	0.0	0.0
Methane	77.1	29.98	70.85	63.901	96.91	65.8
Ethane	6.6	0.55	13.41	3.349	1.33	3.8
Propane	3.1	0.28	7.5	0.960	0.19	1.78
Butanes	2.0	0.21	4.02	0.544	0.05	0.8
Pentanes +	3.0	0.25	2.64	0.630	0.02	0.5

1.2.4 Natural Gas Sweetening

Depending on the origin of the natural gas and whether it is associated or non-associated with oil, it usually contains from a few ppm to more than 50 vol% acid gases, and some gas wells even has a CO_2 portion of up to 70 vol% [10]. The pipeline specification for CO_2 in processed natural gas varies between the maxima of 2 and 2.5mole%, whereas the maximum allowed content of H$_2$S is at 5 mg/Sm^3 [11]. Approximately 20% of all the natural gas processed in the world contains excess amounts of CO_2, due to the vast volumes produced, even a small increment in efficiency for CO_2-removal will lead to considerable cost reductions [12]. Acid gases are undesirable in commercial sales due to their corrosiveness in presence of water, the high toxicity of H$_2$S, and the inability of CO_2 to combust and release heat when burned with oxygen, also known as calorific value, which is usually indicated by the Wobbe index [13]. In addition, their poisonous effect on catalysts, noxious influence on the environment and contribution to global warning are increasingly important reasons for their exclusion from the natural gas composition [2, 14]. In addition, CO_2 has a relatively high freezing temperature, which can lead to the forming of blocks of frozen CO_2, or "dry ice", that can clog equipment lines and damage pumps. The removal of the gases CO_2 and H$_2$S is commonly referred to as natural gas "sweetening" [15].

Conventional methods for natural gas sweetening are amine absorption and cryogenic fractionation, in addition to some minor processes like alkali salt

7

absorption, physical absorption and solid adsorption. However, these processes are quite costly, complicated, energy consuming and involve hazardous chemicals. The most commercialized technology, amine absorption, also suffers from corrosion of equipment and loss and degradation of solvent. Natural gas sweetening using membranes have the potential to overcome these disadvantages, and still provide an effective separation process, as membrane units are energy efficient, compact and reliable. This makes them particularly desirable for small productions or offsite separation such as offshore natural gas sweetening. Polymers are currently the only commercially available membranes for separation of CO_2 from methane, and are either packed in hollow-fiber or spiral-wound modules to achieve a high packing density for large gas volumes in the industry. One group of polymeric membranes that shows both high selectivity and high permeability is the facilitated transport membranes, where the flux in addition to the solution-diffusion mechanism is enhanced by a carrier that reacts reversibly with the CO_2 in the membrane [12, 16].

1.3   Objective of Thesis

The objective of this masters thesis was to optimize the permselectivity of a PVAm/PVA Blend FSC nanocomposite membrane for CO_2 separation from natural gas under high pressure, and to increase the mechanical strength of the membrane in order to sustain such high pressures. This was done by testing out different support membranes, different nanocomposite fillers and by varying the thickness of selective layer as well as the composition of the nanofillers, and observe the performance of the membrane at pressures from 10 up to 80 bar at a constant feed gas flow rate and sweep gas flow rate.

The motivation for this project was to contribute to advances in increased membrane CO_2 separation efficiency at high pressure and to optimize choice and preparation of membrane for producing a commercially competitive alternative for with a smaller carbon footprint compared to other separation processes. This separation process would not only cut down the emissions of CO_2, but also provide a viable alternative to the natural gas sweetening process and to enhanced oil recovery (EOR).

8

1.4 Outline of Thesis

This thesis is divided into six main chapters. Chapter 1 gives an introduction to the field of natural gas sweetening and an overview of the technologies competing with membrane separation of CO_2. It also provides a motivation for this work. Chapter 2 first covers a classification of different membranes used in membrane gas separation, with a primary emphasis on facilitated transport membranes (FTM) and the special case of fixed-site carrier (FSC) membranes. A theoretical background on polymer and gas properties and the transport mechanisms taking place in the FSC membrane follows, and the last part of the chapter is dedicated to the up-scaling and process design of natural gas sweetening processes employing membrane technology. Chapter 3 treats the existing literature on FSC membranes more thoroughly, comparing different materials used for selective layers, supports and nanofillers, in addition to focusing on various characterization techniques and the durability of FSC membranes. Chapter 4 describes the experimental procedures for preparation, SEM characterization and testing of the membranes as well as a description of the materials used to manufacture the membranes. Chapter 5 presents and discusses the results in accord with the theoretical background presented in chapter 2, and chapter 6 gives a brief conclusion of the masters thesis.

2 Membrane for Gas Separation

2.1 Advantages and Challenges of Membrane Gas Separation

Many membrane materials are permeable to the undesired gases in flue gas or natural gas, and therefore they provide a viable alternative for gas separation processes such as natural gas sweetening. For a membrane to be competitive with commercial separation processes like amine absorption, a CO_2/CH_4 selectivity of minimum 40 and a CO_2 permeance of 0.27 $[m^3(STP)/m^2hbar]$ is required [17]. It should also show resistance to plasticization and aging, have high thermal and chemical stability, utilize inexpensive commercial materials and be easy to upscale. If these requirements are met, membrane separation may present a score of beneficial advantages, such as [6, 15, 18]:

- Simple installation
- Installation for small size application and in remote locations
- Environmentally friendly in comparison to amine processes (No chemicals needed)
- Lower energy consumption
- Low capital investment compared to solvent systems
- Easy production scale up with addition of desired number of modules
- No moving parts for single-stage units
- Easy to operate and control
- High reliability and on-stream time
- Good weight and space efficiency
- Easy to combine with other separation processes

These advantages makes membranes especially attractive for offshore applications, as they can run unattended, there is no need to ass or regenerate chemicals and they have a good weight and space efficiency. However, there are also some disadvantages of membrane separation, a process which is currently still being investigated and improved. Some of the identified challenges are [6, 15, 18]:

- Short lifespan of many membranes

- Often have higher hydrocarbon losses compared to solvent system

- Difficult to meet the ppmv H_2S specifications, as H_2S and CO_2 usually have similar permeation rates

- Can not compete with large-scale amino plants due to little economy of scale of their modular nature

- Low stability to temperature, pressure and chemicals of many membranes

- Requires pretreatment of feed to remove liquids and particulates

- A trade-off between gas flux and selectivity, as defined by Robeson's upper bound

2.2 Classification of Membranes

Membranes can be classified in a number of different ways, depending on i.e. origin, material, morphology and manufacturing. A first distinction is between synthetic and biologically occurring membranes. Biological membranes are superior to technical membranes in terms of selectivity and flow properties and are therefore sometimes considered as a reference for the development of synthetic membranes. Synthetic membranes can be subdivided into solid and liquid membranes, where the former can be made of organic or inorganic materials. Morphologically the membranes can be divided into dense, non-porous membranes, which are always built asymmetrically, and porous membranes, which can be both symmetric and asymmetric. Whereas symmetric membranes are usually homogeneous, the asymmetric membrane has a separation-active layer on one of the sides, and thus can only be operated in one direction. The materials used in the commercially available membranes are divided into the major groups of inorganic materials and organic polymers, which can be of both natural or artificial origin. Most of the membranes produced today consist of macromolecular organic compounds, in which there are a broad range of polymers and polymer blends to choose from. Available polymer membranes of natural origin include the derivatives of cellulose, chitin and dextrins, whereas the polymers polyethylene, polypropylene and polyacrylonitrile predominate amongst the synthetic products [19].

A common approach to roughly categorize membranes separating CO_2 from methane and other gases is by the material they consist of, which can be either inorganic materials, polymers and composites (both inorganic and poly-

meric). Different membranes take use of different mechanisms for membrane gas separation, with the main types being Knudsen diffusion, molecular sieving, and the solution-diffusion mechanism illustrated in Figure 4 [20–22]. An overview is given in Figure 5.

Figure 4: Schematic representation of three of the possible mechanisms for membrane gas separation. [23]
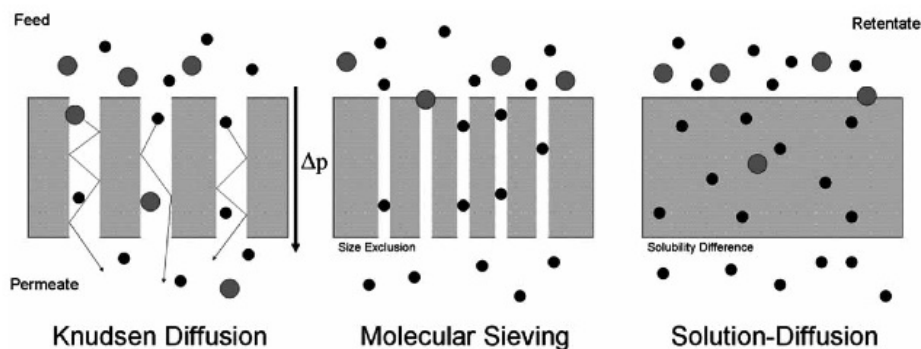
2.2.1 Common Polymeric Membranes

The polymeric membranes are generally more developed and commercially ready than other CO_2-selective membranes. For the separation of CO_2 from H_2, rubbery polymers such as polyacetylenes and organosilane modified porous glass are favored materials, mainly for their high selectivity and higher flux rates. When the gas mixture consists of CO_2/CH_4 or CO_2/N_2, glassy polymers dominate the industrial applications. Cellulose acetate is the most commonly applied membrane for natural gas sweetening. Recently the closely related material cellulose triacetate has also been put into use in a hollow fiber module at a natural gas sweetening process plant in the Gulf of Thailand. Polyimides have also attracted attention due to their relatively high stabilities in regard to heat, chemicals and stress, combined with high selectivity and permeability for CO_2. They can also overcome the plasticization problems that many cellulose acetate membranes encounter [15]. A detailed description of CA and PI membranes i given in the literature review section 9.

The performance of dense polymer membranes is mainly determined by their intrinsic properties rather than by pore size. Transport occurs mainly by solution-diffusion mechanism, where the gas molecules tend to move through channels of free volume between the polymeric structures. The membrane

Figure 5: An overview of CO_2-selective membranes [15, 24]
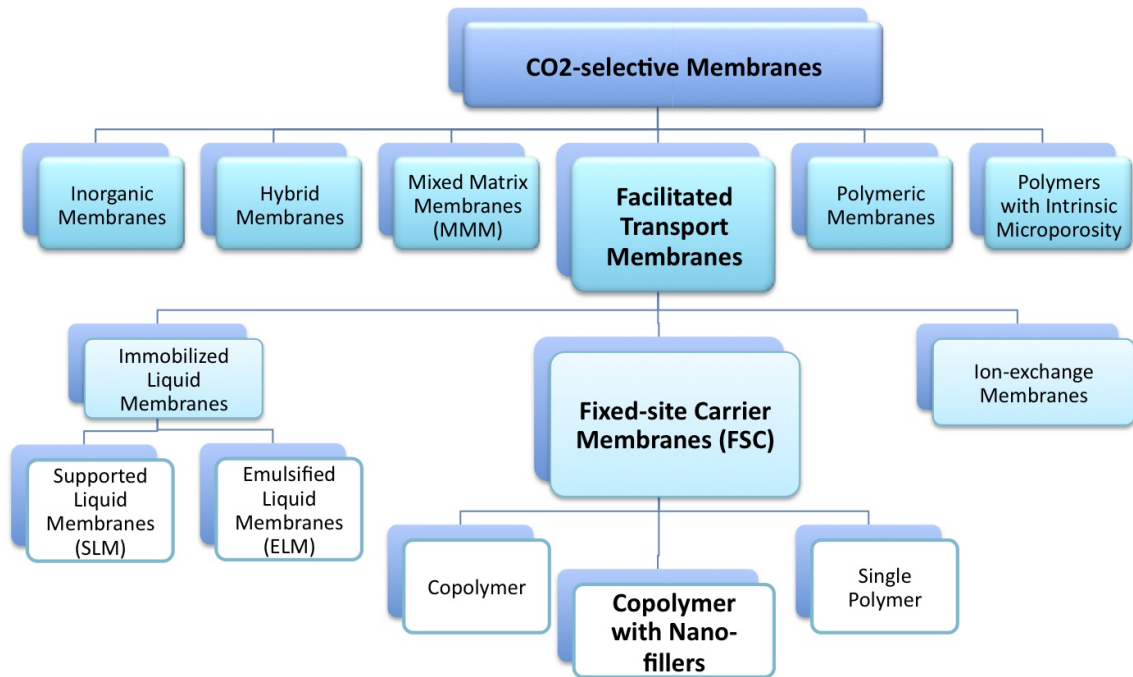
can both me a rubbery elastomer or a glassy polymer, and both PVA and PVAm are examples of dense polymeric membranes [15].

Porous polymer membranes are highly crystalline, and can be both hydrophilic or hydrophobic. They contain fixed pores in the range of 2-100 nm, dimensions by which selectivity is determined, and may be prepared by sintering, stretching, track-etching or phase inversion. Transport of gas through porous polymer membranes depends on pore size, and the flow will exhibit Knudsen diffusion for narrow pores and viscous flow for wider pores. Most polymeric membranes used in conventional gas membrane separation are porous, like polypropylene, polycarbonate, polyamide, cellulose acetate and polysulfone [15].

2.2.2 Inorganic Membranes

Besides the polymeric membrane materials, there has been great advancement of inorganic membranes over the past two decades. The advantages of

inorganic membranes over polymeric membranes are that they have higher resistance to high temperatures and pressures, they give better possibilities of cleaning and they are more resistant to corrosive and degrading chemicals. In addition, they offer easier and better options for more thoroughly regulating the separation performance. However, inorganic membranes are tied to higher investment costs and material costs, and they are generally more brittle and more susceptible to breakage from thermal expansion than organic membranes [19].

Inorganic membranes are typically made of ceramics, glass, metals, alloys and carbon, and there are many different types, and can roughly be divided into porous and dense membranes. Porous inorganic membranes are usually produced with a thin top layer cast on a porous metal or ceramic support. Membrane performance may be enhanced by modification of the surface. Depending on molecule size and pore size, transport may be driven by Knudsen or surface diffusion, capillary condensation, molecular sieving, or a combination of each of these. The transport in dense inorganic membranes such as metals and alloys occurs either by the solution-diffusion mechanism, or by charged particles in the membrane. High selectivities is achievable, but they yield low permeability [20–22].

Four of the most common inorganic membranes are carbon molecular sieves (CMS), alumina membranes, silica membranes and zeolite membranes. CMS membranes are produced by pyrolysis of thermosetting polymers. These membranes hold a narrow pore size distribution in the Ångstrøm dimensions, and can therefore separate molecules with very similar size. Transport is mainly through molecular sieving. They can also be applied as a top layer on a porous support material. CMS membranes possess high thermal and chemical stability, but can exhibit large changes in pore size in oxidizing environments. Alumina membranes exhibit high thermal and chemical stability as well, but may undergo undesired phase transition at relatively low temperature. Transport through alumina membranes is generally by Knudsen diffusion due to their mesoporous structure, and is usually used as support material. Silica membranes such as glass have surfaces which can be modified with organosilane compounds to tailor their pore size, and also the silica membranes show exceptional thermal, chemical, and structural stability in both oxidizing and reducing environments. Zeolite membranes are crystalline aluminosilicates with uniform pore structure and a small range of channel diameter at Ångstrøm dimensions. They are very efficient due to the ability to selectively adsorb molecules by size and polarity. Transport occurs by molecular sieving and surface diffusion mechanisms [20–22].

14

2.2.3 Mixed Matrix Membranes

Mixed matrix composite materials can be viewed as a combination of polymer membranes and molecular sieving materials. They consist of a continuous polymer matrix where either dense or porous inorganic materials are dispersed. Such particles may be zeolites, carbon molecular sieves (CMS), silica, carbon particles or carbon nanotubes. The resulting membrane displays advantages of both phases, such as the processability of polymers and the great gas transport properties and selectivity of molecular sieves. The only arising problem is the defects caused by poor contact at the interface between the polymer and molecular sieves, which leads to a lower performance. The separation through the membrane occurs according to the solution-diffusion mechanism, and is combined with either surface diffusion for dense fillers or molecular sieving in the inorganic phase of the microporous filler. Research on this issue by introduction of organic molecules has shown good progress, and MMMs definitely have a potential to provide both economic as well as high-performance gas separations. MMMs have attained a lot of focus as a group of membranes with very high expectations for the future in other fields as well [24, 25].

2.2.4 Hybrid Membranes

Hybrid membranes are porous inorganic membranes which are surface-modified with organic chemicals with high affinities for CO_2 to achieve both a high CO_2 flux and high selectivity, and have become an expanding field of research. They combine the high selectivity of dense polymeric membranes with the high permeability of porous inorganic membranes. Other properties can be designed as well, such as retaining the rigidity and thermal stability from an inorganic material as well as maintaining the flexibility of a polymer. The microstructure produced by this incorporation of organic molecules into the inorganic structure can be controlled either by cross-linking of the membrane, or by controlling the interstitial space occupied by the functional groups in the organic phase. A common method to prepare a hybrid membrane is by combining a sol-gel reaction with polymerization, and there are many different materials in use. For the inorganic support, it is common to select a ceramic such as α-alumina, γ-alumina, Vycor-glass and silica, and typical organic compounds are trichlorosilane, polyether and organisilane, to mention just a few [24, 26].

2.2.5 Polymers of Intrinsic Microporosity

Polymers of intrinsic microporosity (PIM) are polymers, inwhich the macro-molecular backbone can be designed to have a very high free volume inter-connected by micropores smaller than 2 nm , and which have gas adsorption properties similar to that of molecular sieves. In a rubbery polymer, the polymer chains are very flexible and give a high free volume. For a glassy polymer to also have a large degree of free volume, the chain mobility needs to be constrained and intense packing of the chains avoided. PIMs have backbones with kinks and rigid sequences, restricting the rotational movements around the backbone of the polymer. Many PIMs are incorporated with highly polar nitrile groups and five-membered aromatic rings to create a restrictive ladder structure in this backbone, such as the PIM-1 often prepared from the chemicals tetrahydroxy-tetramethyl-spirobisindane and dicyanote-trafluorobenzene. Various characterization techniques support the assertion that PIMs exhibit properties of molecular sieves. PIMs have been proven to have good processability and a high solubility coefficient for many gases, with CO_2 in particular. This gives high selectivity and permeability for a range of gas mixtures e.g. the separation of CO_2 from CH_4, which for PIMs can be found between the Robeson's upper bound of 1991 and 2008. Results also show that a membrane treated with methanol exhibit higher selectivity and permeance for this gas mixture than membranes treated with water or untreated membranes because of reversible swelling. The methanol-treated membrane have actually managed to surmount the Robeson's 2008 upper bound, with a CO_2 permeability of 2300 barrer and a CO_2/CH_4 selectivity of 18.4 [15, 27].

2.2.6 Facilitated Transport Membranes

Facilitated transport membranes (FTM) are among the most novel and attractive membranes for gas separation, and often polymer membranes with a support layer made up of a porous polymer and with a dense selective layer on top. Within the selective layer are carriers with a special affinity toward the permeating gas molecule, which enhances the permeability of the gas through the membrane by reacting reversibly with the permeating species. For a more detailed description of the mechanism, see section 2.4.2. This gives the FTMs higher selectivity and larger flux. The permeating gas dissolves in the upstream portion of the membrane and forms a complex with the carrier agent inside the membrane, which then diffuses through the membrane and releases the permeating gas on the downstream side of the membrane. The unloaded carrier then diffuses back to the feed side. The

membrane investigated in this project is of this variety. The main criteria for producing a FTM are the selection of suitable carrier with high affinity toward the desired molecules and an appropriate way of designing and fabricating the membrane, and there are four main types of FTMs: Immobilized liquid membranes, ion-exchange membranes, polymer/metal ion dispersions and modified polymer membranes, also know as fixed site carrier membranes (FSC) [15, 18].

Immobilized liquid membranes

Scholander [28] was the first to demonstrate a facilitated transport membrane, where he used hemoglobin as carriers for oxygen through a supported liquid membrane (SLM) with a very high O_2 selectivity. Ward and Robb [29] were among other to follow Scholander, and mixed a liquid solution of carriers for CO_2 in the pores of a microporous support as seen in Figure 6, with the liquid being held inside the support pores by capillary forces. The SLMs showed very good separation properties. However, the SLMs suffered from degradation issues, as the carrier solution would evaporate or get entrained with the gas stream and pushed out of the pores, leading to deactivation of the complexing carrier agent. To prevent this from happening, experiments were conducted to emulsify the liquid membrane, which could also potentially solve the problem of reproducibility and low interfacial area. These emulsified liquid membranes (ELM) have a stable emulsion of the organic and receiving phase, and a second emulsion of the first emulsified phase and the feed phase. This gives a high interfacial area between the phases, but have the drawback of being a batch process and requiring other compounds to stabilize and break the emulsions. Other methods of stabilizing the SLMs have been to add dense sealing layers or less volatile carrier solvents, but this type of membrane is still limited due to their inherent instability [15, 25, 30].

Figure 6: Supported liquid membrane [30]

17
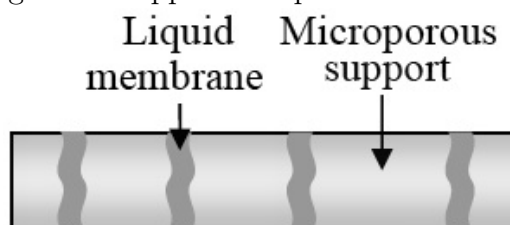
Ion-exchange Membranes

LeBlanc et al. took the concept of facilitated transport one step further, and proposed in 1980 an ion-exchange membrane for the separation of CO_2 from CH_4. This room temperature ionic liquid membrane (RTIL) has a negligible vapor pressure and has with that managed to overcome the problem of volatility and evaporation of selective layer, and by polymerizing these ionic liquids, ordered nanopores are created [25, 30]. RTILs may be described as organic salts that are liquid at room temperature, and they are nonflammable and have a high thermal resistance. The gas transport is similar to that in polymeric membranes, and firstly the gas molecules are absorbed into the liquid phase on the feed side, then diffuse through the membrane and are desorbed on the permeate side. Inside the membrane the permeating gas, usually CO_2, reacts reversibly with a mobile or fixed carrier, resulting in a higher CO_2 permeability and CO_2/CH_4 selectivity compared to nonreactive membranes [31, 32].

Fixed-site Carrier (FSC) Membranes

To overcome the limitations in liquid carrier membranes such as evaporation of carrier solution, entrainment with the permeating gas stream, and deactivation of the complexing carrier agent, another approach to prepare facilitated transport membranes is to introduce the carriers directly into the polymeric membranes. These carriers are covalently bonded to the polymer backbone, hence the name fixed-site-carrier. This means they have a restricted mobility and thus have a lower diffusivity than in mobile carrier membranes, but they give greater stability to the separation process as the carriers are not dissipated over time. This can be counteracted by water swelling of the membrane, which increases the diffusivity and thus the permeability [25].

The fixed carrier is quite often an amine group connected to the main chain of the polymer, and in the dry state, the acidic CO_2 is assumed to be subjected to the weak acid-base interaction between the CO_2 and the alkaline amine. In the wet state, on the other hand, it is theorized that the CO_2 reacts with water to yield HCO_3^-, which then reacts reversibly with the fixed amines. The bicarbonate is then transported through the membrane from the feed side to the permeate side by the fixed-site carrier like it is shown in Figure 12, and thus give a mobility comparable to that of the mobile carriers in liquid membranes [18, 25].

2.3 Important Properties Related to Polymeric Gas Separation Membranes

2.3.1 Polymer Properties

Molecular Weight

As polymers generally don't have a fixed homogenous chain length, but rather a wider distribution of size, an adequate way of expressing the chain length is the average molecular weight. This is an important property for the preparation and characterization of polymer membranes. There are two ways of denoting and calculating the average molecular weight, which are the number average M_n and the weight average M_w, as seen in Equation(2.1). The ratio between the weight and the number average is often referred to as polydispersity p, and is usually greater than 2 in commercially available polymers [18].

$$M_w = \frac{\Sigma_i w_i M_i}{\Sigma_i w_i} \tag{2.1}$$

Findings from literature show fairly weak effects of the molecular weight on permeability and diffusivity in gas permeation, and it has been concluded that the influence of polymer weight is insignificant and that end-groups of polymer chains does not significantly effect the transport properties. The slight difference can, however, be explained by the rise in glass transition temperature and that the increased chain length gives rise to a higher number of entanglements and to interaction sites, which then slightly changes the chemical, mechanical and physical properties of the polymer. An overview of the effects that high and low molecular weight polymers have on some properties are tabulated in Table 3 [2, 18, 33].

Table 3: The effect of low and high molecular weight on some polymer properties [2]

Polymer property	High MW	Low MW
Strength	Increases	Decreases
Viscosity	Increases	Decreases
Chemical resistance	Improves	Lowers
Required processsing temperature	Higher	Lower

Glass Transition Temperature

The polymer properties are greatly affected by the state of the polymer, which in most cases can be either rubbery or glassy, depending on the temperature. The delineation between these two states is called the glass transition temperature (T_g). When a non-crystalline polymer is heated, it will go from a glassy state, through a narrow temperature window where it undergoes a state transition, and finally end in a rubbery state. This glass transition temperature can be depicted in a log E – T diagram as seen in Figure 8, where E is the characteristic parameter for the tensile modulus. This is defined as the applied force F across the area A, also know as the stress, necessary to give a certain deformation or strain. In the glassy state the polymer has very limited mobility due to the fact that the segments are unable to rotate freely around the main bond. This restriction is overcome with sufficient thermal energy to surpass the glass transition temperature, and the polymer becomes rubbery. This state has a tensile modulus around three to four times smaller than in the glassy state, and the polymer now has a high degree of chain mobility [18].

The most important properties deciding the T_g are molecular weight, chain flexibility and chain interactions, which again depend on the type of atoms and bonds in the segment monomer constituting the polymer. The T_g is especially sensitive to the structure of the main and side-chains in the elastomer, wherein single bonds are more flexible than double or triple bonds because rotation around the bond is possible, and heteroatoms, aromatic and heterocyclic groups create a stiffer chain than carbon atoms. In addition, side groups of the monomer also play a slightly less important role of increasing the glass transition temperature for polymers with a flexible main group, whereas rigid main groups take very little effect of such side groups. Bulky side groups take up more space, and therefore the rotation around the main group is sterically hindered, and polar side groups give more interactions and hence help increasing the transition from rubbery to glassy state [18, 33].

As seen from Figure 7, T_g has a direct influence on gas permeability in rubbery polymers, with the permeability increasing as T_g decreases. This effects the diffusivity of the gas, as T_g is strongly related to free volume while the solubility is virtually independent of glass transition temperature. The slight scatter in the diagram is due to other factors influencing the permeability, such as side chain mobility. However, there has not been found such a general correlation between T_g and permeation properties in glassy polymers, even though they seem to have an opposite relation to T_g than for rubbery polymers. In other words, an increase in glass transition temperature often

leads to an increase in diffusivity and permeability. The factors influencing these parameters are complex, and it is generally viewed as more relevant to correlate transport properties in polymers by free volume than for T_g [33].

Free Volume

Other changes occurring in the transition from the glassy state to the rubbery state are changes in specific volume, specific heat, refractive index and permeability. Specific volume is the ratio of the volume to the mass, and is often known as the reciprocal of density. This implies that the density decreases with increasing specific volume, and hence increasing temperature. In rubbery polymers the specific volume also contains an increasing extent of free volume, which is defined as the fraction of the volume of the polymer unoccupied by the macromolecules themselves. Another definition is that the free volume is the volume at a certain temperature T subtracting the volume at 0 Kelvin, where molecules have no thermal energy and therefore are close-packed. The fractional free volume can thus be expressed as

$$v_f = v_{f,Tg} + \Delta\alpha(T - T_g) \tag{2.2}$$

where the first term denotes the fractional free volume at the glass transition temperature and the last term is the temperature difference times the difference of the thermal expansion coefficient at glassy and rubbery state. The fractional free volume for a number of glassy polymers has been found to be a constant, and is approximately 0.025 or 0.11, depending on whether it is based on the free volume concept of viscosity or that of the glass transition temperature [18].

Polymer free volume can also be defined as the fraction of the volume which is not occupied by the electronic clouds of the polymer. The importance of free volume for polymer membranes is that it gives a broader understanding of the transport of small molecules through the polymer. The increasing free volume gives more space for the molecules to diffuse through, and the larger fraction of free volume, the higher mobility of the penetrating species. If the free volume elements are interconnected, the distribution of the effective size of the micropores can also have an influence on the properties of the polymer [15, 18].

Figure 7: Permeability for nitrogen in various rubbers with different glass transition temperatures [33]
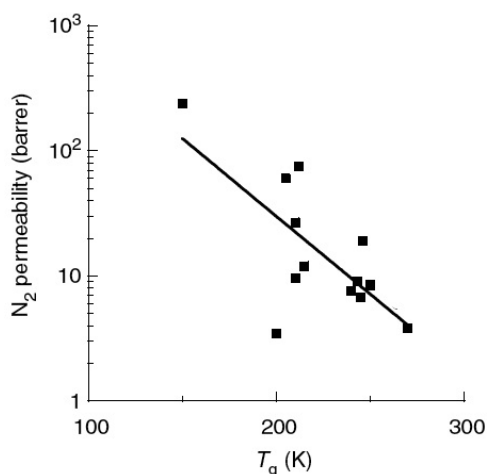
Figure 8: Tensile modulus E of a completely crystalline (a), a semi-crystalline (b) and non-crystalline polymer (c). [18]
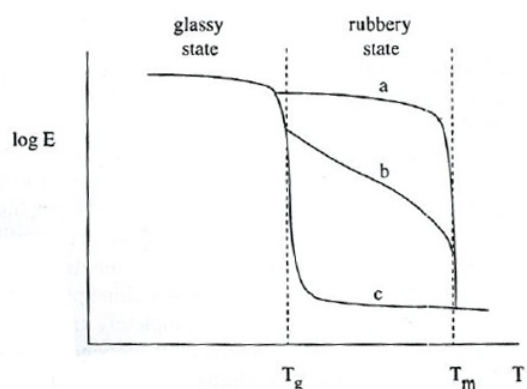
Crystallinity

Another important parameter determining the state of the polymer is the degree of crystallinity. The chains of the polymer can be packed in a regular pattern if the structural units are set in a very regular order, and can thus crystallize and increase the degree of crystallinity of the polymer. Polymers ordered in a syndiotactic or isotactic manner or with a very strong intramolecular interaction like hydrogen bonds are more inclined to be completely crystalline or semi-crystalline, the latter meaning the polymer has both an amorphous and a crystalline fraction. Copolymers derived from two or more monomeric species can usually not crystallize. Two types of crystallites are the so-called fringed micelles and spherulites.

Crystallinity influences both the mechanical properties as well as the transport properties of the polymer. This is because crystallites do not change their crystal lattice when passing through the glass transition temperature to the rubbery state. Semi-crystalline polymers will change slightly depending on the degree of crystallinity, but not as drastic as a completely non-crystalline polymer, as seen in Figure 8. Because of the low permeability of crystalline and semi-crystalline polymers they are usually not used for gas separation membranes. [18]

Polarity

Polarity arises from an unevenness in electron distribution and can be described by charge density, dipole moment, hydrogen-bonding capacity, dielectric constants and surface tension of bulk phase. The polarity of the membrane is caused by the dipole moment of its polar groups attached to the polymer backbone. These groups help to improve the properties of selectivity and permeability by an increasing interactions between the permeating gas species e.g. CO_2, and the polar groups like carbonyl or sulfone groups in polysulfone. In order for separation to take place, the polarity of the membrane must be close to the polarity of one of the permeating species. It is shown that the solubility selectivity increases with the concentration of polar groups in the polymer. This is partly because polar groups can decrease the fractional free volume and thereby improve the sieving ability of the polymer and the increase the diffusivity selectivity of CO_2/CH_4 [2,34].

Swelling

In a polymer system where there is an observed dependency on concentration, the diffusion coefficient may change due to the interaction between water or another low-molecular weight molecule like CO_2 and the polymer. This phenomena is called swelling and it increases both the penetrant concentration and the diffusivity of the penetrant species through the membrane. The diffusivity also depends on the concentration, and at lower degrees of swelling the effects of concentration will increase as the diffusion coefficient decreases, as seen in Figure 9. The degree of swelling can be defined as the weight fraction of penetrant inside the membrane relative to the weight fraction of the dry polymer. The increased swelling increases the mobility of the polymeric chains, and a diffusivity can be reached where it approximates that of liquid (ca. 10^{-9} m^2/s) [18]. A very high degree of swelling may lead to a collapse of the porous structure, and lower the permeability and selectivity of the membrane, including the porous support layers of composite membranes [35].

Plasticization

Plasticization is induced by condensable gases and vapors when a small molecule in the permeating gas is chemically similar to the polymer and sorb into it to such a degree that they create gaps between polymer chains. This then creates greater mobility and reduces the interactions between the chains, and the polymer becomes plasticized. In other words, the chain spacing and chain mobility in the polymer increases so that the diffusion and

Figure 9: Diffusion coefficients of components in a polymer as a function of the degree of swelling [18].
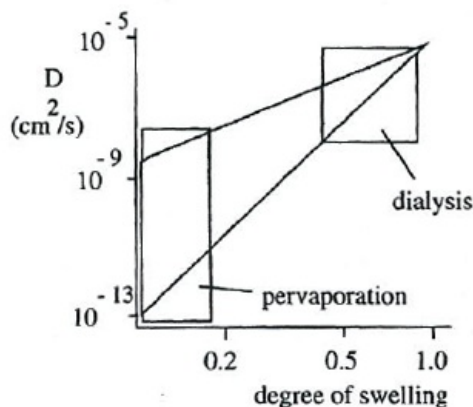
permeation coefficients of all penetrating gas species increase with increasing penetrant pressure. Plasticization phenomena significantly effect the membrane performance in the CO_2/CH_4 separation process. The polymer swells upon sorption of CO_2, which accelerates the permeation of CH_4. As a consequence, the polymer membrane loses its selectivity, and this is particularly present for CO_2 in highly selective membrane materials [27, 33].

Cross-linking

In an attempt to improve the gas separation performance and physical stability of a polymer membrane subjected to plasticization, the polymer or polymer blend may be cross-linked, which means that the polymer chains are randomly bonded to each other by covalent bonds as seen in Figure-10 [27]. A well-known example of cross-linking is the vulcanization of rubber, which converts rubber into a more durable material for use in e.g. tires via the addition of sulfur, which modifies the polymer by forming cross-links between the individual polymer chains.

Many investigations have shown that cross-linking may be a useful method for improving the separation characteristics of a polymeric gas separation membrane by decreasing the aforedescribed plasticization at high CO2 pressures. Two possible ways of preparing a cross-linked polymer is either through thermal annealing at relatively high temperature, or through formation of interpenetrating polymer networks, obtained by heating a the polymer blend with monomers or oligomers containing reactive acetylene end groups [36].

24

Figure 10: Architecture of a linear and a cross-linked amorphous polymer [27].

Amorphous linear polymer   Amorphous crosslinked polymer
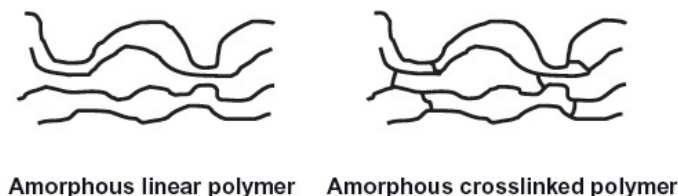
2.3.2 Robeson's Upper Bound

The performance of the membrane is evaluated based on two important parameters within the vernacular of membrane science, namely the permeance and the selectivity. The gas permeance is the molar amount of gas permeating a membrane of known area divided by the unit time and pressure difference across the membrane, and the selectivity is the ratio of the permeances of the two permeating gases in a binary gas mixture, which gives a value for the separation efficiency of the membrane [37].

Gas separation using polymeric membranes has for the past three decades emerged as a commercial unit operation, and it has been found that the separation factor for gas pairs varies inversely with the permeability of the more permeable gas of the specific pair, as is the case for the gas pair of CO_2/CH_4. An analysis of the literature data for this gas mixture published by Lloyd M. Robeson in 1991 reveals an upper bound relationship between selectivity and permeability, which can be represented by a log-log plot of the CO_2/CH_4 separation factor α versus the permeability P of CO_2. This results in a linear upper bound as shown in Figure 11, above which almost no values exist. The slope n of this line is given by Equation 2.3, where the constant k is known as the "front factor" [38, 39].

$$P_{CO_2} = k\alpha_{CO_2/CH_4}^n \qquad (2.3)$$

The slope of the linear Robeson's upper bound can be related to the difference between the gas molecular Lennard-Jones kinetic diameter of the two gases. That indicates that it is the diffusion coefficient which governs the separating capabilities of polymers for this gas pair. When the free space between the polymer molecules becomes smaller, the permeability decreases due to the decreasing diffusion coefficients, while the separation characteristics such as selectivity are enhanced. The upper bound correlation can

Figure 11: Upper bound correlation for CO_2/CH_4 separation. [39]
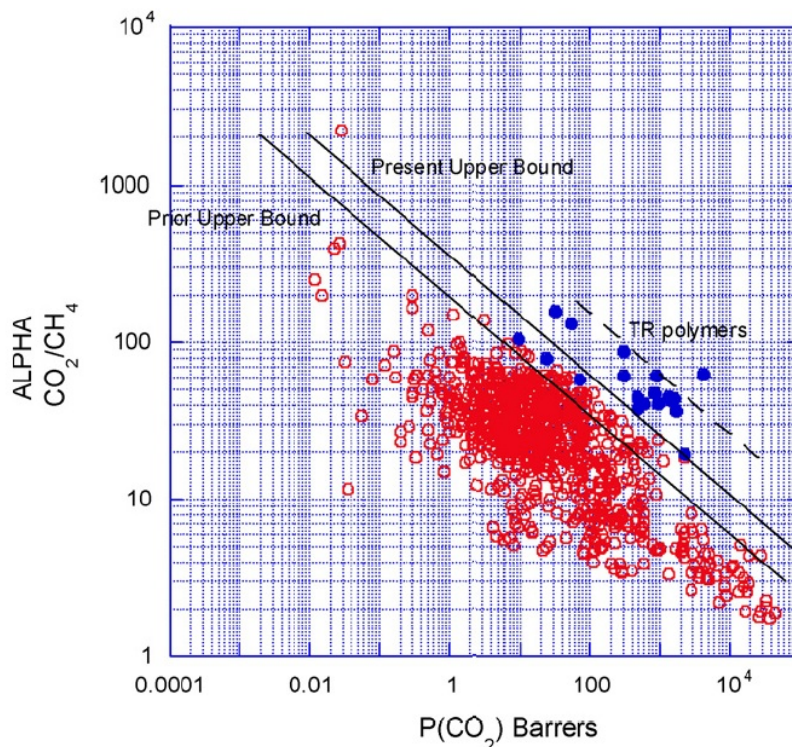
also be qualitatively determined as the point where the permeability changes from being mainly caused by the solution-diffusion mechanism to Knudsen diffusion [38, 39].

Since the first publication on the Robeson's upper bound in 1991, the upper bound position has had only minor shifts towards higher selectivity and permeability for most of the gas pairs, as seen from Figure 11, where the present upper bound is the 2008 update. These minor shifts are primarily due to novel membrane polymers with rigid, glassy structures, including ladder-type polymers [39].

Recent research on facilitated transport membranes has shown that their high permeability and selective make them eligible to surmount the Robeson's upper bound, and the fixed-site carrier membranes have in addition shown great stability for gas separation, which gives good reason to believe that the FSC membrane may play an important role in the future of natural gas sweetening with membranes [34].

26

2.3.3 Gas Properties

The diffusivity and solubility of gases in polymers are mainly determined by three factors; their size and shape, their condensability and their affinity for the polymer. Of all the gases present in natural gas, CO_2 exhibits unique chemical and physical properties which enables it to be separated from the other gases by polymeric membranes.

Size and Shape

Intuitively, the diffusivity of gases in the polymer membrane is sensitive to the size and shape of the penetrant gases, and the diffusion coefficient will increase with increasing molecule size, and also has a preference towards oblong versus spherical molecular shapes. When it comes to diffusion, it is the kinetic diameter, and not the van der Waals volume, which is determining for the separation selectivities, which is why the diffusion coefficient for CO_2 is higher than for CH_4, see Table 4 [40].

Table 4: Sizes of penetrating gas molecules [34].

Gas molecule	Van der Waals volume $(cm^3/mole)$	Kinetic diameter $(\mathring{A})$
CO_2	17.5	3.30
CH_4	17.2	3.80
N_2	-	3.64

The relation between the size of the molecule and the diffusion coefficient can be deducted from the Stokes-Einstein equation in Equation 2.4. The D is the diffusion coefficient, k is the Boltzmann's constant, T is the absolute temperature, η is the viscosity and r is the hydrodynamic radius of the gas molecule. The latter is also known as the Stokes radius, and is the radius of the hard sphere that would diffuse at the same rate as the mentioned molecule, and thereby including the molecules geometrical deviations [34].

$$D = \frac{kT}{6\pi\eta r} \tag{2.4}$$

Condensability

Another parameter affecting the solubility of gases in polymers is the condensability of the penetrating gas, that is to say at what temperature the

gas will condense. Usually the critical temperature T_c of the gas is referred to as a measure of condensability, and the solubility will go up as the critical temperature increases. This is why CO_2 is more soluble in most polymers than methane, as seen from Table 5 [34].

Table 5: Solubility and critical temperature of penetrating gas molecules [34].

Gas molecule	Solubility S $(cm^3/cm^3 \; cmHg)$	Critical temperature T_c $(^{\circ}C)$
CO_2	0.0120	31.0
CH_4	0.0035	-82.6
N_2	0.0015	-118.6

Affinity

The term affinity may be ambiguous, and the term gas polarity is more describing. Polarity of a molecule refers to a separation of electric charge leading to an electric dipole or multipole moment. A polar gas molecule will interact with polar molecules in the membrane through dipole-dipole intramolecular bonds and hydrogen bonds, and thus the CO_2 molecule with a linear dipolar will have greater affinity for a polar polymer molecules than the tetrahedral CH_4 with no overall dipole [18].

2.4 Gas Transport through Polymeric Membranes

Most of the gas separation processes undergone today is by dense (nonporous) membranes. This is because the achieved selectivity of separating two gases with a molecular radius difference of only 0.2-1.0 $\mathring{A}$ is very low using a porous membranes, as the pores would either let both gases through or retain them both at a specified pore size. Instead, other parameters such as solubility and diffusivity rather then molecule size directly determine the permeability of the different gases [18].

2.4.1 Solution-diffusion Mechanism

The solution-diffusion mechanism is the most widely used transport model for gas transport in dense polymeric membranes. In this model the permeants dissolve in the membrane material and then diffuse through the membrane down a concentration gradient. The gas transport can be divided into three

main parts, with the second one being by far the slowest, and therefore also the rate-limiting step [41]:

1. Dissolution: The gas dissolves into the feed side of the membrane with high pressure/chemical potential.

2. Diffusion: The gas diffuses through the polymeric membrane.

3. Desorption: The gas desorbs from the permeate side of the membrane with low pressure/chemical potential.

Diffusivity

The diffusivity, and consequently the gas transport through the membrane, can be described by Fick's first law, where the flux of the gas J_A is a function of the diffusivity coefficient D_A and the concentration difference C_A over a distance x as seen from Equation 2.5. The driving force is the concentration difference, which in the case of gases would be the difference in partial pressure, a correlation found from Henry's law where the concentration C_A equals the partial pressure p_A times the solubility S_A, as seen from Equation 2.6

$$J_A = -D_A \frac{dC_A}{dx} \tag{2.5}$$

$$C_A = S_A p_A \tag{2.6}$$

The diffusivity coefficient is dependent on temperature, which can be shown by the empirical Arrhenius relationship in Equation 2.7, where D_0 is the pre-exponential factor and E_D is the activation energy, which again is dependent on the gas size. The larger the molecule, the higher activation energy is needed [34].

$$D = D_0 exp(\frac{-E_D}{\mathbb{R}T}) \tag{2.7}$$

Solubility

As seen from the previous paragraph, the solubility of a gas is described by Henry's law, and like the diffusivity coefficient, the solubility coefficient is also related to temperature by the Arrhenius relationship, as shown in Equation 2.8, where S_0 is a pre-exponential constant and ΔH_s is the sorption

energy, which consists of both the enthalpy of condensation and the enthalpy of mixing [34].

$$S = S_0 exp(\frac{-\Delta H_s}{\mathbb{R}T})$$

(2.8)

Permeability

According to the solution-diffusion mechanism, the permeability of the penetrating gas is simply the product of the above-mentioned diffusivity and solubility (Equation 2.9), and when Equation 2.7 and Equation 2.8 are combined with this relationship, the new and more describing Equation 2.10 arises, with the resulting pre-exponential constant P_0 intelligibly being the product of the two previous pre-exponential constants, and the exponential factor E_p being the activation energy for permeation [34].

$$P_A = D_A \times S_A$$

(2.9)

$$P = P_0 exp(\frac{-\Delta H_s - E_D}{\mathbb{R}T}) = P_0 exp(\frac{-E_p}{\mathbb{R}T})$$

(2.10)

Permeance

Whereas the permeability describes the flow rate of the gas through an area of the polymeric membrane with a specific thickness and at a certain pressure, the permeance is useful when the thickness is unknown, and is defined as the flow rate through an area of the membrane at a certain pressure. The Permeance of a gas Pe_A is thus the permeability P_A divided on the thickness of the membrane l, represented in Equation 2.11 [18].

$$R_A = \frac{P_A}{l}$$

(2.11)

Selectivity

In addition to the permeability, the selectivity α is the most important parameter for measuring and comparing membranes for gas separation. It is a separation factor, and is defined as the ratio between the gas permeabilities of the permeating gas and the retentate gas. It can also be viewed on as the product of the diffusivity selectivity and the solubility selectivity, as

shown in Equation 2.12.Gas separation is usually achieved from the diffusion selectivity as they change more drastically than that of solubility [34].

$$\alpha = \frac{P_A}{P_B} = \frac{D_A}{D_B} \times \frac{S_A}{S_B} \tag{2.12}$$

2.4.2 Facilitated Transport Mechanism

In addition to the solution-diffusion mechanism there is another mechanism contributing to the gas transport especially in CO_2-selective membranes, namely the facilitated transport mechanism, which increases both the gas permeation and the selectivity. It is also called uncoupled transport, as opposed to the coupled transport to be mentioned later. In short, the facilitated transport mechanism describes a number of carriers within the polymer which help the penetrating gas molecules diffuse through the polymeric membrane. In the facilitated transport of gas molecules, the penetrant gas A reacts reversibly with a complexing agent C to from a solute-carrier complex like in Equation 2.13, and since this mechanism contributed in addition to the solution-diffusion mechanism, the total gas flux will be the sum of the both of them, as seen in Equation 2.14. The first term describes the already discussed Fickean diffusion whereas the second term describes the facilitated diffusion [18, 30, 42].

$$A + C \underset{k_r}{\overset{k_f}{\rightleftharpoons}} C \tag{2.13}$$

$$J_A = \frac{D_A}{l}(C_A, 0 - C_A, l) + \frac{D_A C}{l}(C_{AC}, 0 - C_{AC}, l) \tag{2.14}$$

The gas flux from the facilitated transport mechanism is usually faster the Fickean diffusion, and in the case where the reversible reaction is quite fast and the concentration of gas A in the carrier-solute complex AC is much higher than that of the free solute, the facilitated transport mechanism has a high facilitated factor F and becomes rate-determining. On the other hand, if the reaction is slow and the concentration of free gas A is much higher than that of the complex AC, the Fickean diffusion is rate-determining and the contribution from the facilitated transport mechanism can be neglected [18].

The facilitated factor F can be expressed in a complex equation consisting of the mobility ratio of the carrier to the solute α, the equilibrium constant

K and the Sheerwood number Sh, but can be simplified as shown in Equation 2.15 by assuming an excess of uncomplexed carrier C.

$$F = 1 + \frac{\alpha K}{1 + K} \qquad (2.15)$$

These facilitated carriers can be both mobile, like in liquid membranes, or they can be fixed, as in fixed-site-carrier (FSC) membranes, where the carriers are bounded chemically or physically to a solid polymer matrix, and so the carriers have quite a restricted mobility. It still enhances the gas transport by the facilitated transport mechanism by a an assumption called "hop and jump". An illustration of the mechanism for CO_2 permeation is shown in Figure 12 [43].

Figure 12: A proposed mechanism of facilitated transport in a FSC membrane [43]
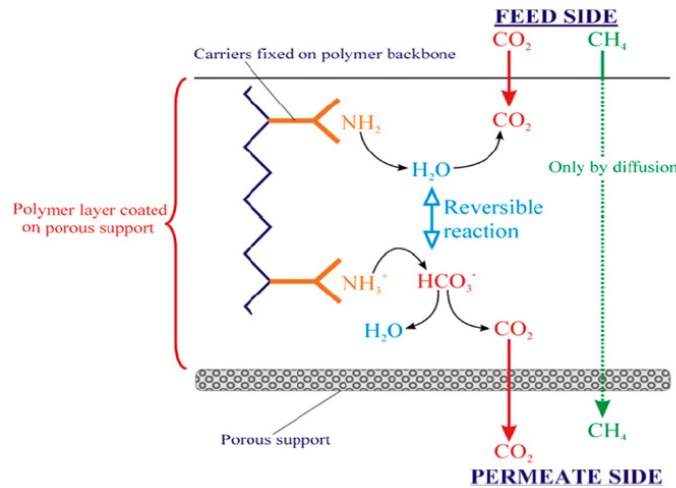
Carrier Saturation

Carrier saturation occurs at high pressure differences (or other large differences in driving force) when all the carriers species in the membrane are bound to solute molecules such as CO_2 in the case of FTM membranes, and increase in pressure will not result in an increased flux from the reactive pathway, as seen from Figure 13, and the facilitated transport membrane can not provide any additional facilitated transport. The upper limit for an observable facilitated transport effect is set at ΔP_L. Under this point, the majority of the transport is due to diffusion of the carrier-solute complex,

as the solution-diffusion transport is quite low, and decreases non-linearly proportional to the driving force [33].
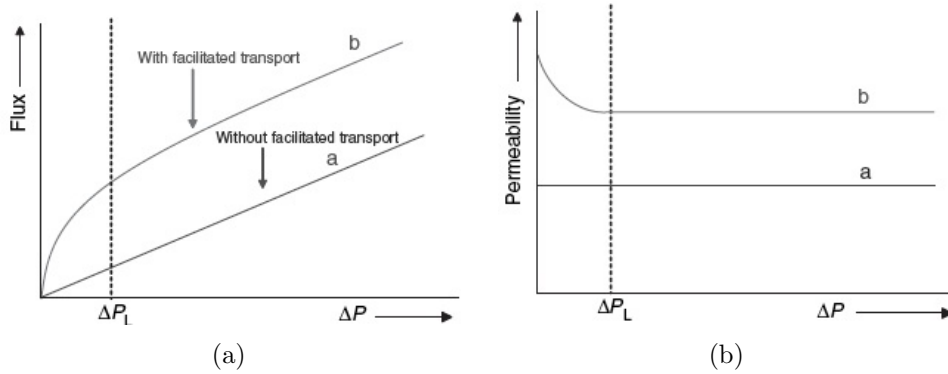
Figure 13: (a): A plot of resulting flux versus driving force in a FTM. (b): A plot of resulting permeability versus driving force in a FSC membrane [33]

2.4.3   Factors Influencing Flux and Selectivity

Coupling Effects

Coupling effects are the result of interactions between the components in a mixture giving different results when combined in comparison to when alone. One type of coupling effect is the coupled transport mechanism, which is similar to the aforementioned facilitated transport mechanism in that a carrier agent is incorporated in the membrane. But as the name suggests, the transport is undergone in couples, so the carrier transports two species across the membrane. If the concentration gradient of the other coupled species is large enough, it can be moved against its own concentration gradient [12]. The coupled transport can be either co-coupled or counter-coupled, depending on if the two components are moving in the same or opposite direction, respectively [18]. The coupling transport mechanism can arise e.g. when two gases are to be separated by a membrane, and the penetrating gas must compete with the other undesired gas to react with the carrier agent [12]. This may be an explanation for the lower values of selectivity and permeance in a gas mixture compared to those of pure gases [42]. This type of carrier facilitated process was actually the first to be developed, and originates from the early experiments in biology where researchers studies the natural carriers contained in cell walls. The process is sometimes erroneously named liquid membrane transport, as it often, but not always, contains liquid membranes [12].

33

Other types of coupling effects are the strong interactions between the gas mixture components and the membrane, causing swelling and plasticization of the membrane, and giving rise to competition in the diffusion route between the two gases [44].

Competitive Sorption

Competitive sorption is a phenomenon where the molecules of the gases in a gas mixture compete for the Langmuir void spaces in the membrane. This affects both the solubility within the polymer matrix and the adsorption in the Langmuir free volume [27]. For example will the presence of water vapor in the membrane affect the permeation of gas components with high affinity more than that of low affinity ones. A study on the effect of water vapor on a polymeric hollow fiber membrane for CO_2 separation from CH_4 showed that the CO_2 permeability decreased by up to 11% compared to a decrease of 1.5-7.5% with the presence of water vapor, and thereby decreasing CO_2/CH_4 selectivity [45]. As pressure increases, the CO_2 is also outcompeted by the higher concentrated CH_4 for the Langmuir sorption sites, which lowers the CO_2/CH_4 selectivity [46, 47].

Compaction

When the selective layer of a membrane is exposed to high pressure it becomes densified, or compacted, over time, which lowers the gas flux through the membrane. A study by Reinsch et al. [48] observed a collapse of 13.2% of the membrane thickness within just the first seconds, which was thought to come from compression of the substructure fabric support of the CA membrane. Within the next hour, the flux decreased by 10%, which could indicate a true compaction process happening at a slower rate. It is thought that an accumulation of contaminants from the gas stream could contribute to enhanced compaction rates in the membrane [27]. Membranes with a sponge-like structure are less affected by compaction than membranes with macrovoid structure, and the compaction is more likely to occur in the bulk layer with highest pore volume of the membranes [35].

Physical Aging

Over time, the permeation properties of thin dense membrane films have been shown to break down, and this effect increases with how thin the film is. The reason for it is that the polymer chains in the membrane film is slowly

reoriented in order to achieve a state of equilibrium, and the free volume is thus reduced. This also reduces the thickness of the membrane, which may slim down to half its thickness over a longer period of time. This type of compaction is, however, not driven by physical compressive forces such as pressure, but by thermodynamics and potential energy considerations. The physical aging effects has been reported for many polymers such as PSf, PPO and PI [27].

Fouling

Oil mist, particulates and other potential fouling materials must always be removed from the gas stream, or they will accumulate on the surface of the membrane and lead to fouling. This could lead to poor permeability and selectivity, and could also lead to plasticization of the polymer membrane. However, this is not usually a problem, as gas streams are thoroughly pretreated before entering the membrane module [12, 49].

Concentration Polarization

Concentration polarization can be found in most types of membranes, but is particularly an important issue in liquid separation such as ultrafiltration and reverse osmosis. For gas separation this is more easily controlled d with module configuration and flow directions, but can cause problems with high gas fluxes or highly selective membranes. The concentration polarization arises when there is an increase of the less permeable component in the boundary level close to the surface of the membrane, which inhibits the permeability of the permeating species, and thus lowers the selectivity [2,12].

2.5 Membrane Separation Process Design

2.5.1 Pretreatment of Natural Gas

The importance of good pretreatment of the feed gas was not applied in the early membrane plants, which caused damage by contaminants and liquids, but today this is controlled by better plant design and implementation of adequate pretreatment processes. In addition, modern membranes are more robust than just a couple of decades ago. In order to separate CO_2 from natural gas, the feed stream requires a pretreatment. This is mainly done to prevent excessive fouling in the membrane, to avoid plasticization of the

polymers and to avoid condensation of hydrocarbons on the membrane system. H_2S present in the natural gas can be absorbed on the amines in the selective layer of a FSC membrane, and may therefore affect the CO_2 separation performance of the membrane. Oil droplets and small particulates always need to be removed for any separating system, but it is also important to control the condensation on the membrane at a specific dew point [49,50].

The dew point of a component is the temperature where condensation starts, and the gas goes from a pure gas phase to a two-phase with both gas and liquid present. This temperature is dependent on the pressure of the gas and also the concentration of the heavy hydrocarbon component in the gas mixture. In the feed gas stream, these heavier hydrocarbons are well above their dew point, but as they don't permeate the membrane, they will accumulate in the retentate gas stream, and reach higher concentration levels, which increases their dew point temperature. In addition, the residue gas stream will expand as a consequence of most of the CO_2 permeating the membrane, and the Joule-Thompson effect will cool the residue gas by 10-15°C compared to the feed gas. This combination of effects can be sufficient to bring the gas into the two-phase region, and damaging condensation occurs. One way of avoiding this problem is to raise the feed gas stream temperature, but this will both be more energy-demanding and lower the selectivity of the membrane. The other solution is to remove water by method of glycol absorption, and cooling and condensation of C_6+ hydrocarbons before the feed stream enters the membrane system. Small amounts of heavier hydrocarbons ($C_{12}+$) can also be removed by temperature swing adsorption with carbon or silica. However, in many real pretreatment processes, both heating and removal processes are applied [49].

Figure 14: An adapted flow-chart of stages in a pretreatment process, with minimum pretreatment requirements are shown in dark boxes [49].

The amount of pretreatment necessary depends on both the membrane of choice and the composition of the feed gas. As an example, membranes made from cellulose acetate or polyimide are very sensitive to water, and therefore require a more thorough pretreatment process than a perfluoropolymer membrane. If it in addition were to separate a natural gas containing high levels of CO_2 and a high content of higher hydrocarbons, it would require a maximum pretreatment process. If the gas stream, on the other hand,

contained very little higher hydrocarbons and a relatively small amount of CO_2, only a few steps would be required in the minimum pretreatment process. A flow-chart of potential steps in a pretreatment process between the raw feed gas stream and the entrance to the membrane system is illustrated in Figure 14, where the three dark boxes depict the minimum pretreatment requirements, whereas all the steps would need to be include for a maximum pretreatment [47, 49].

2.5.2 Handling of Separated CO_2

Traditionally, the CO_2 separated from the acid natural gas in sweetening processes have been vented into the atmosphere. However, as the awareness of global warming due to CO_2 emissions have grown as mentioned in section 1.1, other usages have been found for the excess CO_2. Injection of CO_2 into deep geological deposits or in deep saline aquifers have been used for CO_2 storage, as well as enhanced CO_2 uptake in arboreal areas. However, for direct usage of CO_2 as feedstock, there are a number of processes, both already in use and with great future potential. A selection of major possible processes where CO_2 are currently in use or in development for being used are listed in Table 6, as well as their predicted cumulative demand within 2020. In addition to this list, CO_2 is also currently being used in water treatment, food processing, preservation and packaging and horticulture, to mention a few [51].

Table 6: CO_2 reuse technologies [51]

Technology	Demand 2011-2020
Enhanced oil recovery (EOR)	>500 Mt
Enhanced coal bed CH_4 recovery (ECBM)	20 - 100 Mt
Urea yield boosting	20 - 100 Mt
Carbonate mineralisation	20 - 100 Mt
Polymer processing	5 - 20 Mt
Algae cultivation	5 - 20 Mt
Concrete curing	5 - 20 Mt
Bauxite residue carbonation	5 - 20 Mt
Liquid fuel production (Methanol)	5 - 20 Mt
Enhanced geothermal systems (EGS)	<5 Mt
Liquid fuel production (Formic Acid)	<5 Mt

As seen from Table 6, recovery of CO_2 in the oil and gas production to promote enhanced oil recovery (EOR) is the largest application of CO_2. In

EOR, high pressure CO_2 is pumped back into the depleted oil reservoir, where it diffuses through the formation and is partially dissolved in trapped oil reserves. This oil then swells and becomes less viscous, and is therefore driven towards the production wells, and the excess CO_2 is sequestered. The dissolved CO_2 (between 50 and 67%) will return to the surface with the extracted oil, where it is recaptured and re-injected in order to prevent release into the atmosphere. By this method, the inaccessible oil that could not be reached by conventional technologies can be reached and exploited. Generally, the injected CO_2 needs to have a purity of minimum 95vol%. EOR from CO_2 is considered a commercially mature technology, and was first taken in use in the 1970's. It can increase the original oil recovery by 7-23%, and its use depend on many physical properties of the oil reservoir. It is usually only a viable solution if the depth of injection is more than 600m and the pressure is over 100 bar. Temperature, angle and permeability is also factors that need to be taken into consideration, and the potential use of EOR is therefore very specific to location. Today, the use of EOR is for most part dominated by onshore wells in the US, where about 50 Mt of CO_2 is injected per year, producing 250,000 barrels of oil per day [25, 51].

Yang et al. [52] compared models of two different membrane process designs with cross-flow; one with a single stage system and another with a two-stage recycling system. For a single-stage system, a membrane with a selectivity of over 50 was needed to achieve a product purity of 98% and a maximum methane loss of 2%. A membrane with selectivity of only 20 yielded a CH_4 recovery of only 90% with the same product purity. However, introducing a second membrane unit fulfills the former requirement for a membrane with selectivity of 20. The advantages with one-stage systems are that they are don't require recompressing and that they don't have any moving parts, which makes it very competitive to other technologies, especially if the permeate gas with low pressure can be put to use [49]. Due to its simplicity, a one-stage systems will always have a lower investment cost than a multistage process, but will have higher gas processing costs [53]. More complex processes introducing other membrane units are possible, especially when heavy hydrocarbons and H_2S need to be removed from the natural gas. The latter can either be separated together with CO_2 or in separate stages and then isolated [54].

2.5.3 Membrane Modules

The technical arrangement of membranes is called a module. The optimization of the membrane process requires both an optimal single module and a

corresponding optimal connection of the modules in the process. The choice of module greatly depends on the application of the optimized conditions for the membrane separation process, and is usually a compromise between the different requirements, as many of the module properties contradict each other [19].

Some of the desirable module characteristics are as follows [19]:

- Good, uniform flow across the membrane without any dead zones

- High packing density

- Mechanical, chemical and thermal stability

- Low manufacturing and operating costs

- Cleanability

- Fouling tendency

There are a number of different ways to construct a membrane module depending on the area of application, some of which are the plate-and-frame module, tubular module, capillary module, hollow fiber module and spiral-wound module. However, for gas separation the most common modules in use are the latter two, which will be covered more thoroughly [18].

Spiral-wound Module

The spiral-wound module was the first to be commercialized and is similar to the modules applied in many water treatment processes. It is basically a plate-and-frame module coiled into a tube with a collection pipe in the center. Spacer material is glued along three of the edges of the membrane and permeate-side to form an envelope, and the feed-side spacer is placed on top to act as promoter for turbulence, as a turbulent gas stream has a lower tendency to lead to concentration polarization than a laminar flowing stream. For an illustration of the spiral-wound module with specific denoting of the different layers see Figure 15. The packing density of this type of module is quite high, and ranges from 300 - 1,000 m^2/m^3 depending on the module geometry and on the spacer material employed between the sheets of membrane. An average fabrication cost lies between \$10-100 per m^2. The module has a high mass transfer rate, but is harder to clean than other types of modules [18, 19, 47].

Figure 15: Schematic presentation of a spiral-wound module for gas separation [18].
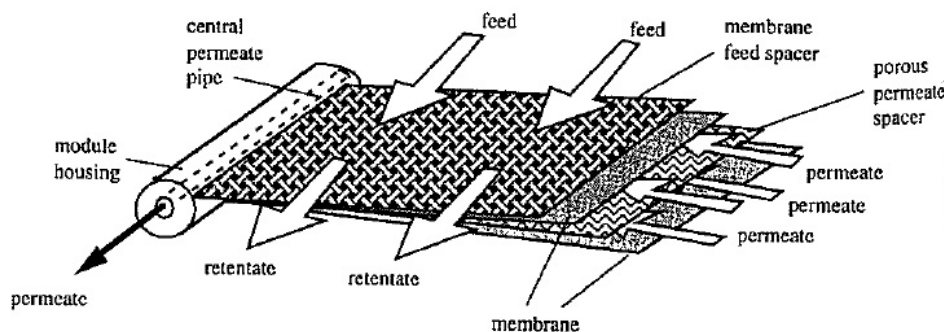
Hollow Fiber Module

Hollow fiber modules are a more recent development, with each module containing thousands of fibers in a shell, each typically with a diameter between 40-500 μm. They can be arranged in a u-shaped way, and may be attached in only the end plate, or the fibers could be stretched and affixed on both sides. There are two types of configurations, depending on if the feed stream enters inside the fiber and permeates through the fibers ("inside-out"), or it enters from outside the fibers ("outside-in"). For modules used in gas separation, a preference for the "outside-in" configuration dominates due to a lower pressure loss inside the fiber and to gain a higher membrane area, as shown in Figure 16. This, and the option of placing the feed counter-current, co-current and cross-flow gives the hollow fiber module a high flexibility in operation. A typical module for hollow fiber membranes is shown in Figure 17. The hollow fiber module have a very high pressure stability, and can attain a packing density of up to 30,000 m^2/m^3, which is by far the highest of all the modules and gives a high membrane are per unit of volume. The fabrication costs are considerably lower than for spiral-wound modules, and lies between \$2-5 per m^2 [18, 19, 47].

2.5.4 Plant Design

To make membranes competitive with amine absorption, a low gas flow rate and high content of CO_2 in the natural gas stream is required, as seen from the diagram in Figure 18 [47]. This minimizes the loss of methane and the advantage of amine absorption plants with high economy of scale plays a less important role. It was found that an amine/glycol plant was equal in cost

Figure 16: Special hollow fiber construction for gas separation [18].
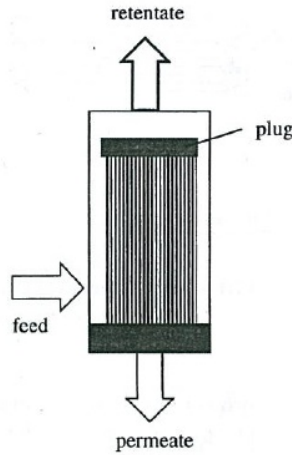
Figure 17: Hollow fiber module for gas separation [21].
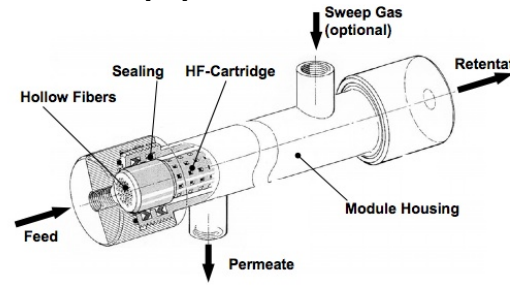
with a membrane plant for the separation of CO_2 from natural gas when the CO_2 content was 11% and the feed gas flow rate was 30 MMscfd [55]. Beyond this values, a combination of membrane gas separation and amine solvent absorption may be used if the CO_2 content in the feed gas is sufficiently high enough, inwhich a single stage membrane unit removes the majority of CO_2, and the retentate is processed in a second amine absorption unit. This reduces both the size and the cost compared to process system with only amine absorption. An example of use of such a design may be employed in a offshore natural gas field, where the membrane unit is installed on the offshore site and sent through pipelines to be further processed onshore to meet the pipeline specifications [47].

Simple Design

As the driving force for gas transport across the membrane for membrane gas separation is a concentration difference, and hence partial pressure difference between the feed side and the permeate side, there is a need for either a compressor on the feed side or a vacuum pump or a sweep gas flow on the permeate side, or in many cases both. The compressor increases the pressure of the entering gas stream, and the vacuum pump decreases the pressure of the permeating gas stream to maximize the pressure ratio across the membrane. Such a configuration is illustrated in Figure 19. Exchanging the vacuum pump with a sweep gas flow will decrease the partial pressure of the desired permeate gas to maximize the partial pressure ratio [18].

41

Figure 18: A comparison of membrane separation and amine absorption technologies for natural gas sweetening with regard to feed gas flow rate and CO_2 concentration in the feed gas [49].
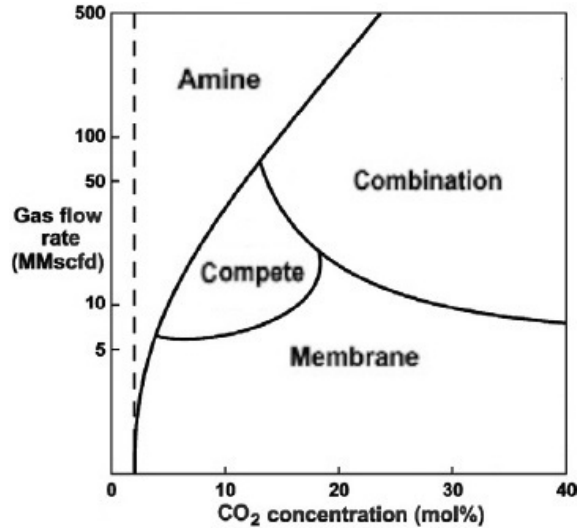
Figure 19: Schematic drawing of a membrane gas separation process [18].
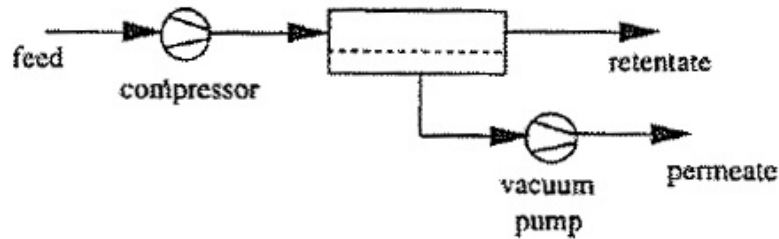
Two-stage Design

A typical two-stage membrane process design example is given in Figure 20, where the natural gas containing acid gas is introduced to the first and largest membrane unit. This unit separates CO_2 from the natural gas to a level that meets the pipeline specification standards (usually 2%). In order to recover CH_4 from the permeating gas stream, which can contain up to 12% of the feed methane, permeate stream is compressed and introduced to a second smaller membrane unit, which again separates the CO_2, and a second permeate stream of typically 86% CO_2 is sent to the vent, while the retentate stream is recycled with the feed stream to the first membrane unit. This cre-

ates an acceptable level of methane loss of around 1.5%. A third membrane unit could also be installed to decrease the methane loss or to increase the purity of the retentate product, but this would demand another compressor and membrane unit, and is usually not economically justifiable [47]. In order for the permeate gas from the first membrane unit to be sent to the second unit in the two-stage system it needs to be compressed. The energy needed was estimated to be about 107.5 $KJ/m^3(STP)$ including a conversion factor of 3-4 between heat and electricity. This is about 6-8 times less than the required energy for an equivalent amine absorption process [52]. A technical and economical analysis by L. Peters et al. [56] from NTNU presents a similar two-stage design, but includes the need for gas cooling between the first and second membrane module and at recycling, as well as an additional compressor after the second membrane module, which will give additional energy costs.

Figure 20: A typical two-stage plant membrane process design for natural gas sweetening, with a CO_2 permeance of 100 GPU and a CH_4 permeance of 5 GPU [49].
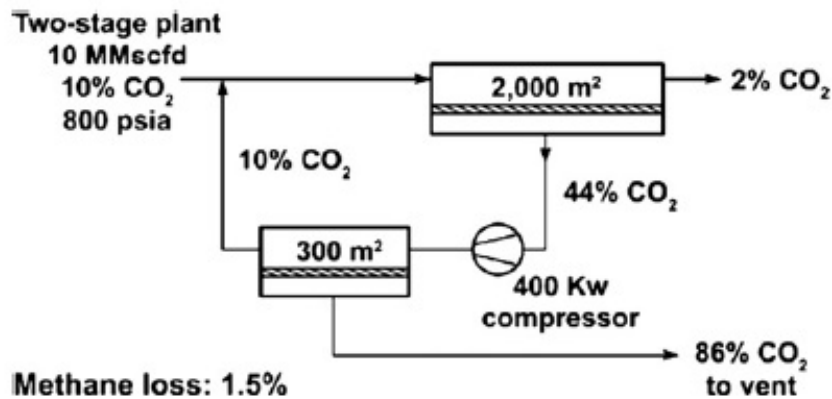
Offshore Design

For offshore natural gas sweetening of high concentration CO_2 gas another type of system design may be applied to lower the CO_2 content sufficiently to be piped to shore without the potential danger of pipe corrosion, and for further removal of CO_2 at natural gas sweetening plants onshore. This design combines a one-stage and a two-stage system, as seen in Figure 21. After being pretreated, the feed gas is sent through two similar membrane modules, inwhich the first module reduces the CO_2 content from 30% to 14.6%, and the second one lowers the content further down to 7.9%. The

first permeate stream is can be either vented or reinjected into the well, while the other with a lower CO_2 content is compressed and introduced into a third and smaller membrane module. The retentate from this module containing 70% methane is then recycled with the feed gas stream, whereas the permeate with a relatively high CO_2 purity is vented or reinjected. In total, there is a methane loss of 7%, which could be decreased to 3-4% by improving the total separating design either by an increase of compressor size or enlarging the first membrane module unit. This however depends on the situation, as there is a trade-off between the acceptable cost of methane loss and the cost of larger equipment and higher energy consumption. Such an offshore membrane process design is already the preferred natural gas sweetening method over amine absorption for natural gas containing high concentrations of CO_2, and may gain more terrain with an ever-increasing efficiency and current developing of novel membrane technology [49].

Figure 21: An offshore flow design combining a two-stage and one-stage membrane system to for natural gas sweetening of feed gas with high CO_2 [49].
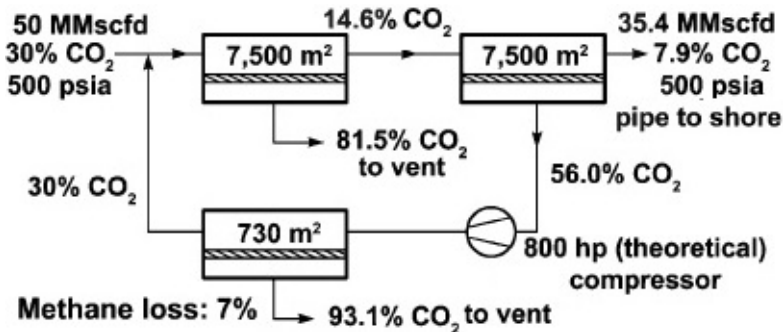
2.5.5 Simulation and Optimization

A comparison of the amine absorption process and membrane separation for three different cases of natural gas sweetening was performed by L. Peters et al. [56] by simulation and optimizing parameters such as membrane stage areas and compressor duty. The technical analysis was performed with Aspen Hysys with a special membrane model package named "ChemBrane". The membrane in use was the PVAm/PVA FSC membrane with PSf as support layer. Both single-stage designs and two-stage designs were simulated, but the simulation process for a two-stage membrane design for case 1 will be investigate closer, as seen in Figure 22. The feed conditions of case 1 were given to be 10mole% CO_2 and 90mole% CH_4, with a feed gas flow of 18560

kmol/h. The feed temperature was 8°C and had a pressure of 115 bar. The permeate pressure of the first membrane stage was set to 2.5 bar, and the permeate pressure of the second membrane stage to 1 bar. The desired CO_2 content in the first retentate stream was maximum 2mole% and in the second permeate stream 90mole%.

Figure 22: A process flow chart of the two-stage membrane design used for simulation and optimization [56]
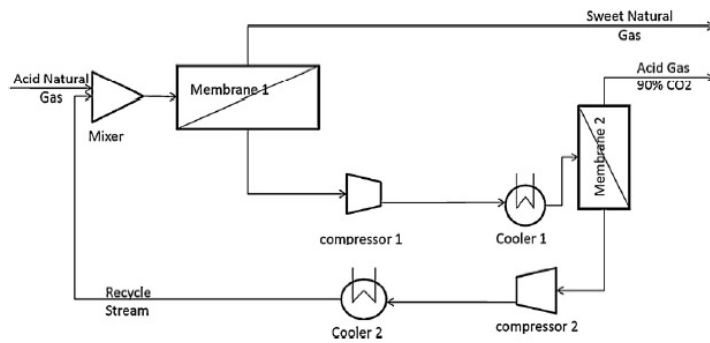
The results from the simulation gave a required area of the first membrane stage to be almost constant at 8141 m^2, whereas the required membrane are of the second stage decreased with increasing feed pressure as seen from Figure 23(a), which indicated that the correlation between the first compressor and second stage membrane area is very strong, as pressure is the driving force for the membrane separation ability. The specific CO_2 capture duty from the first compressor plotted with feed gas pressure for second membrane stage is shown in Figure 23(b), and shows a minimum at 986 $kJ_{elec.}/kg$ CO_2 captured, which gives a second stage feed pressure of 24 bar and an optimized area at 2863 m^2, resulting in a total minimum required area of 11004 m^2. This minimum in specific CO_2 capture duty is due to both the fact that more energy is needed to compress a feed stream than a retentate or permeate stream as formulated by Favre et al. [57], and that an increasing feed pressure on the second membrane stage reduces the total size of the second retentate stream recycled back to the first membrane stage. In total, the required compression energy was found to be 15440 kW, the product first retentate flow 18389 kmol/h, and the second permeate flow 200.5 kmol/h. An overall CO_2 recovery was at 33.5% with a 90mole% purity in the retentate stream, giving a CH_4 loss at 0.11% [56].

(a) Impact on membrane area   (b) Impact on spec. CO2 capture duty
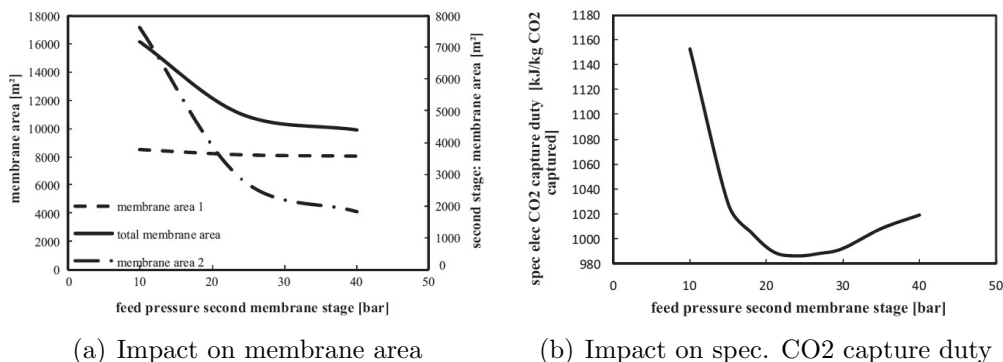
Figure 23: Impacts of increasing pressure [56]

2.5.6 Up-scaling and Economic Analysis

Depending on the drying of solvent and thermal annealing, the cost of membranes may vary significantly, but a typical cost for a spiral-wound module of the turnkey type used in natural gas processing lies around US$500 per square meter. This includes both the actual cost of the membrane, the connecting valves, support structure, module housing and the instrumentation. This only makes up between 10–25% of the total cost of the natural gas treatment plant. Most of the cost is associated with the compressors required in the process design to recompress the gas between the modules and for recirculation, and with operations needed for pretreatment of the gas, which varies depending on the type of membrane [58].

However, for the simulation performed in the previous section, a price of US $50 per m^2 for the PVAm/PVA FSC membrane on PSf support including the spiral-wound module was estimated, and the other identified major investment costs for the membrane plant were the heat exchangers and the compressors. For the sizing and costs of the heat exchangers, a method by Biegler and Guthrie [59, 60] was used, and for the compressors an expression by Bhide et al. [61] was used. Other assumptions made by L. Peters et al. was a membrane life of 4 years and a replacement cost of 25 US$/$m^2$, and all costs were updated to a 2008 Chemical Engineering Cost Index. An overview of the economic parameters, including total capital investment and gas processing cost is given in Table 7. The results were that the total capital investment costs were 14 US $ and the gas processing costs 0.12 US $ per thousand standard cubic feet of product. In the comparison it was found that the investment costs for single stage membrane design were very much lower, and only slightly lower gas processing costs, but yielded a much higher CH_4 loss (1.6%). Compared to other studies on membrane plant design for nat-

46

ural gas sweetening, L. Peters et al. achieved a lower gas processing source, mainly due to a higher feed gas pressure and the high CO_2/CH_4 selectivity and CO_2 flux of the novel membrane in use [56].

Table 7: Economic parameters for a membrane-based natural gas sweetening plant [56]

	Value	Unit	Source
Wellhead price for natural gas	4.2	$/MMBTU	[62]
Cost for electricity	0.07	$/kWh	[56]
Cost for cooling water	0.01	$/t	[63]]
Cost for process water	0.6	$/t	[63]
Membrane cost	50	$/$m^2$	[56]
Membranes replacement cost	25	$/$m^2$	[56]
Membrane life	4	Year	[56]
Direct labor	15	$/h [25 MMSCFD feed]	[64]
Working time	8	h/d	[64]
Overall labor cost	2.15	Direct Labor	[64]
Maintenance cost	0.05	TCI	[61]
Capital recovery cost	0.277	TCI	[61]
Plant on stream factor	0.97		[56]
Total capital investment	14	$/mscf product	[56]
Gas processing cost	0.12	$/mscf product	[56]

3 Literature Review

This chapter is dedicated to previous research and literature on both conventional methods for natural gas sweetening, and on FSC membranes and polymeric membranes with nanofillers. The first section will describe a couple of other processes competing with membrane technology for natural gas sweetening. The next section is threefold, and will first treat a selection of the different polymers investigated for the selective layer, in which the facilitated transport mechanism occurs, and report the most important results of CO_2 permeability and CO_2/CH_4 selectivity. A special attention will be paid to the polymer blend of polyvinyl amine and polyvinyl alcohol, as this copolymer is the material used for selective layer in the experimental part of this thesis. Then follows a review on some of the support membranes used in FSC membranes, with additional weight on polysulfone, as well as cellulose acetate and polyvinylidene fluoride, and the third subsection will deal with the nanofillers experimented on in the experimental part of the thesis. A third section is dedicated to different methods of membrane characterization observed in literature, whereas a last section will investigate some of the most influential parameters for stability and durability in FSC membranes.

3.1 Conventional Methods for Natural Gas Sweetening

In order to remove H_2S and CO_2 from the combustible hydrocarbons, several different sweetening processes are employed. The most conventional methods are cryogenic fractionation process and reversible absorption by aqueous solvents such as monoethanolamine (MEA) and diethanolamine (DEA), which are energy consuming and in the case of absorption environmentally hazardous ways of ridding the natural gas of CO_2. A comparison among some of the important design parameters for the most common natural gas sweetening processes are shown in Table 8 [14,65]. Other methods in commercial use are amine chemical solvent absorption, alkali salt chemical solvent absorption, physical solvent absorption and molecular sieve adsorption, as shown in Figure 24 [6].

3.1.1 Amine Absorption

The most commonly used technology for natural gas processing is amine absorption. Amines are a group of organic compounds formed from ammonia,

Figure 24: An overview over most common processes for natural gas sweetening [6]
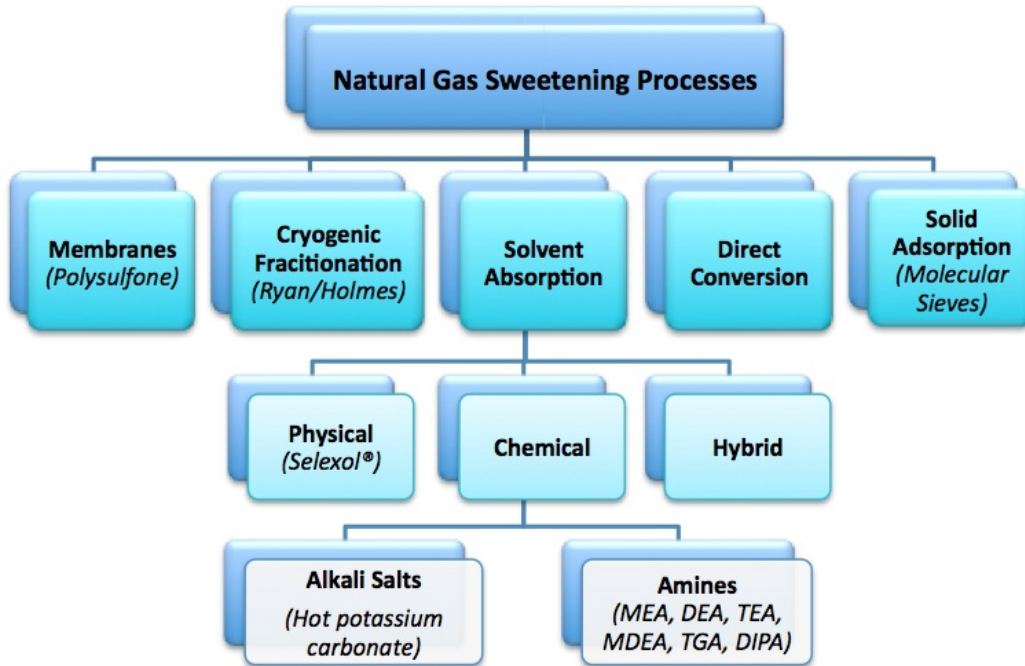
where one or more of the hydrogen atoms in the ammonia is replaced with another hydrocarbon group. When only one H-atom is replaced, a primary amine is produced, and when two or three H-atoms are replaced, the product is a secondary or tertiary amine, respectively. Their reactivity decreases with the number of hydrocarbon replacements, so primary amines are the most reactive. In absorption processes, alkanoamines are most widely used, as they have a OH-group attached to the replaced hydrocarbon group, which lowers their volatility. They are usually dissolved in water in concentrations ranging from about 10 to 65wt%. The acid gases will first dissolve in the the amine solvent through physical absorption, and will then chemically absorb to the weakly basic amines through a acid-base reaction. The physical absorption with the liquid is controlled by the partial pressure of the gases and the chemical absorption is governed by the reactivity of the dissolved species. The most used alkanoamines are monoethanolamine (MEA), diethanolamine (DEA), diglycolamine (DGA) and methyldiethanolamine (MDEA). The amine absorption technology has high capital costs, high energy consumption for the regeneration of absorbents and potential environmental pollution, but are generally insensitive to partial pressures of CO_2 and H_2S and can reduce

these gases to ppm concentrations, and thereby give a high purity product [6, 66].

Figure 25: A typical amine absorber-stripper process for natural gas sweetening [49]
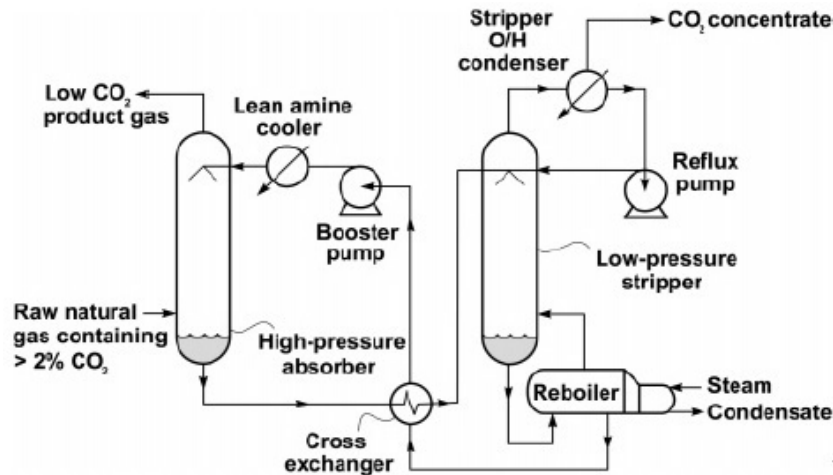
For an amine absorption process, typically two towers are used as seen in Figure 25, where the gas is absorbed in a countercurrent flow of lean amine solution in the first tower, and the rich amine solution is stripped using lower pressure and higher temperatures in the second tower. The regenerated amine solution then passes a heat-exchanger and is recycled to the first absorber tower. These towers are large and expensive vessels, and the higher CO_2 content in the natural gas, the bigger the equipment and more amine solution is needed. The equipment also requires a high degree of maintenance, in particular to avoid corrosion from the highly corrosive products from amine degradation, but also due to the need for careful monitoring of heating and cooling of the solution in recirculation. This requirement for regular maintenance and operation monitoring makes amine absorption unsuited for natural gas sweetening at remote location [49].

Some of the disadvantages of the amine absorption process may be improved by membrane contactors, where the membrane acts as a barrier between the gas phase and the amine absorbent liquid phase, letting only the component to be removed from the gas mixture to diffuse through the membrane contactor and into the liquid amine absorbent. This will reduce the size and weight of the equipment, making the absorption process viable in offshore natural gas sweetening processes. The gas and liquid flow rates can be adjusted individually, and there is no loss of solvent due to elimination of liquid entrainment, flooding and channeling [25].

3.1.2 Cryogenic Fractionation Process

For liquid mixtures, distillation is the most ubiquitous process of separation, and as vapor pressures of CO_2, H_2S and methane are quite different, distilling the natural gas stream could be a good method for natural gas sweetening. However, when CO_2 becomes concentrated in its liquid phase it freezes, despite a relative CH_4/CH_4 volatility of 5:1. Thus, a the maximum attainable vapor concentration of methane lies only at 85-90 mol%. This problem can be solved by a number of techniques, but the novel Ryan/Holmes process proposed in 1982 is the most widely applied process. Here, a solvent is added to the mixture to alter the behavior of the separating system by changing the relative volatility of the two gas components in a process called extractive distillation. The solvent phase, which often is a mixture of propane and heavier hydrocarbons, is then fractionated in another column to produce a higher purity of the product. Even though this process can reach higher puritiy and have good economics for large-scale natural gas sweetening, the cryogenic process has a very low flexibility due to the concentration sensitivity in the feed can affect the purity of the product directly. It is also less reliable than the membrane and absorption processes, as it has a high requirement for pre-treatment of the feed due to possible freezing of contaminants leading to shut-down [6, 65].

3.1.3 Alkali Salt Absorption

The chemical solvent absorption process using alkali salts is quite similar to the amine absorption process, in that CO_2, but also H_2S, react chemically with the solution after being physically absorbed in the alkali salt solution. The most common alkali salt process in use is the hot potassium carbonate process developed in the 1950s in the US. When the CO_2 reacts with the lean solution of potassium carbonate in the absorber, it undergoes a complex reaction pathway, but in the end water and a rich solution of potassium bicarbonate is produced. The CO_2 is then released from the rich solution in the stripper, partially by simple pressure reduction from about 21 to 1.3 bar and partially by steam. The stripped solutions is recirculated to the absorber without the need for reheating by heat exchanger, as the heat of solution for potassium carbonate absorption of CO_2 is quite small and the temperature difference between the absorber and stripper is about 5°C (110-115°C) [6].

3.1.4 Physical Solvent Absorption

Physical absorption processes involve only one reaction, namely the physical absorption of CO_2 in the solvent, with no chemical reactions occurring. Solvents such as Rectisol® and Selexol® are most commonly used, and the latter is a polyethelene glycol with a varied chain length depending on its use. Advantages of physical absorption are that the required energy to regenerate the solvent is lower than for chemical absorption, and that partial dehydration occurs in the separation process, creating a much lower requirement for drying in comparison with chemical absorption. The physical solvents can also be chosen for selective removal of sulfur compounds, and the separation can also be processed at temperatures close to ambient temperatures. However, the physical absorption process works best with feed compositions with low concentrations of heavier hydrocarbons, as these will be strongly absorbed by the physical solvents. The process involving Selexol® can reduce H_2S and CO_2 concentrations down to 4 ppmv and 50 ppmv, respectively, and can remove all mercaptans, CS_2, and COS from the feed stream [6].

3.1.5 Solid Adsorption

Acid gases may be separated from natural gas by adsorption on a solid surface. Iron sponges and zinc oxides may be used, but the most prevalent material is molecular sieves. The acid gases physically adsorb on the surface of the synthetic zeolites in the molecular sieves, letting the methane pass through. Unfortunately, water is also adsorbed onto the adsorbent bed, which causes limited applications of molecular sieve adsorption. Adsorption isotherms for CO_2 and H_2S on molecular sieves with a nominal diameter of 5 Å at room temperature exhibit a logarithmic curve when plotted with pressure, indicating that both gases are easily adsorbed at low pressures down to 0.01 bar. The molecular sieves are regenerated by heating, where the adsorbed component is desorbed when the energy exceeds the binding energy of the Van der Waals forces between the adsorbent and the adsorber. However, to reduce the H_2S concentration to 6 mg/m^3, the bed requires a regeneration temperature of 315°C for an extended time period [6].

A study by Chi and Lee in 1973 focused on the coadsorption of CO_2, H_2S and water from a natural gas mixture onto an adsorption bed of 5Å molecular sieves. It showed that CO_2, having a concentration of almost 16 times that of H_2S was adsorbed instantaneously and saturated the molecular sieve bed, resulting in a zero CO_2 content of the exit gas stream. However, the CO_2 molecules in the adsorption bed was quickly displaced by the amount of

H$_2$S accumulated in the system, and after half an hour the CO$_2$ content of the exiting gas stream was higher than that of the inlet gas stream, due to an addition of CO$_2$ desorbed from the molecular sieves to the existing CO$_2$ content in the feed stream. A similar behavior with H$_2$O replacing H$_2$S happened on a slower time scale, leading to a maximum H$_2$S content in the outlet gas stream of 120% to that of the inlet gas stream after approximately 6 hours [67].

Table 8: Comparison of important design parameters for three natural gas sweetening processes [65]

	Membranes	Absorption	Cryogenic
Operating flexibility	High (CO$_2$>20%) Low (CO$_2$ <20%)	Moderate	Low
Response [a]	Instantaneous	Rapid (5–15 min)	Slow
Start-up [a]	10 min	1 h	8–24 h
Turndown	Down to 10%	Down to 30%	Down to 30-50%
Reliability	100%	Moderate	Limited
Control requirement	Low	High	High
Ease of expansion	Very high	Moderate	Very low
Energy requirement	0.5–6 MJ/kg_{CO_2}	4–6 MJ/kg_{CO_2}	6–10 MJ/kg_{CO_2}

[a] Response to variations and start-up after variations.

3.2 Membranes for Natural Gas Sweetening

3.2.1 Commercially Available Membranes

Nearly all the membranes commercially available today are polymeric in nature, and exhibit both good thermal and chemical resistance and are easy to process into membrane modules. Almost all of them are glassy polymers, as these give a high gas selectivity and good mechanical properties. They have a simple flow configuration and low-maintenance operation, but despite all these advantages, polymer membranes are still not an economically viable replacement for amine absorption in most natural gas sweetening processes. For this the current CO$_2$ flux and CO$_2$/CH$_4$ selectivity is too low, and would need to reach a value of at least 40 to be able to change the competitive position of membranes in the natural gas sweetening industry. The three main types of commercial membranes are cellulose acetates, polyimides and perfluoropolymers [15, 47, 68].

Cellulose Acetate Membranes

Almost 80% of the marked share for natural gas sweetening membranes is dominated by membranes made of cellulose acetate (CA), diacetate or triacetate, which originated from the reverse osmosis industry. Their chemistry is a cellulose backbone with hydroxyl groups substituted with acetyl groups, and thereby reducing the chain packing and enhancing the flexibility and mobility of the polymer chains as the hydrogen bonding from the hydroxyl groups are reduced, increasing gas permeability as a result [69]. Because of their commercial use for nearly 30 years, they are often used as industrial standards for comparison purposes. Cellulose acetates are usually employed for gas streams with high CO_2 content between 10-20% or more, or in offshore platforms where space is a limiting factor [70]. Drawbacks with cellulose acetate membranes is that they are susceptible to plasticization by CO_2 and heavy hydrocarbons, which can change the separation performance, reduce the mechanical strength and accelerate the aging effect, leading to membrane failure [71]. They also have a quite low CO_2/CH_4 selectivity of around 12-15 under normal operating condition, which is much lower than that calculated from pure gas measurements [68]. With gas mixtures, the gases permeating the membrane will compete for the sorption sites in the Langmuir void spaces, as is the case for all polymer membranes, and the permeability will decrease with higher pressures compared to that of pure gas transport [72]. The major two manufacturers of cellulose acetate membranes for natural gas sweetening are Cameron with their Cynara®asymmetric hollow fiber modules, and UOP Separex™spiral wound modules from Honeywell [73, 74].

Polyimide Membranes

A commercial alternative to cellulose acetates that emerged about a decade later are the polyimide (PI) membranes, which in addition to their higher CO_2 permeability and CO_2/CH_4 selectivity have better thermal and chemical stability, and they are easy to prepare. Polyimides as rigid, have a high glass transition temperature and a high-melting point, and they consist of segments of diamine-diahydride which have been polymerized by condensation. Both the diamine and dianhydride may be varied to create a wide selection of tailored membranes with different properties. Some examples are Matrimid 5218, 6FDA-TAPOB and ODPA-IPDA [15,33,47]. In the modeling of natural gas process, the replacement of cellulose acetate membranes with polyimide membranes results in a reduction of required membrane area of 40% and a reduction in compressor duty with 35%. The membrane loss is also cut down with 75% in comparison with the cellulose acetate membranes [17]. These ad-

vantages, in addition to a higher CO_2/CH_4 selectivity of around 20-25 under normal operating conditions, has slowly started to replace cellulose acetate in commercial natural gas sweetening processes [68]. The disadvantages of polyimide membranes are that they require a more expensive pretreatment process, they are more expensive and there is a larger discrepancy between the separation performance calculated from pure gases than for mixed gases due to competitive sorption compared to cellulose acetate membranes. In addition, the membrane undergoes the aforementioned polymerization at high pressures and they are impacted by minor impurities in the natural gas [27]. Polyimide membranes have been commercialized by both UBE industries and by Air Liquide, in a product called Medal, which consists of both polyimide and polyaramides in a hollow fiber module configuration [75].

Perfluoropolymer Membranes

As opposed to cellulose acetates and polyimide membranes, membranes made from perfluoropolymers (PFP) display a very high chemical and thermal resistance, and show a better resistance to polymerization form CO_2 and higher hydrocarbons. They consist of a polymer backbone with fluor-containing substituent groups. The most common perfluoropolymer is poly-(tetrafluoroethylene) (PTFE), where all four hydrogen atoms are substituted with fluor-atoms [76].This highly crystalline polymer is not very suitable for membrane gas separation due to its poor separation properties, but exchanging the fluor-atoms with more bulky groups containing fluor has lead to a lower chain packing, a very high free volume, and hence to better gas separation properties. Some examples of these polymers are Cytop$^©$, Teflon AF$^©$and Hyflon AD$^©$ [33]. Some other advantages of perfluoropolymer membranes is that they are easy to process for membrane manufacturing and a very high gas permeability. They are quite hydrophobic and organophobic, which makes them eligible for gas streams with high water and higher hydrocarbon content that otherwise would lead to plasticization. Drawbacks are that their very high permeabilities cause a lower CO_2/CH_4 selectivity, and that the materials needed to prepare the polymer is quite expensive, so cheaper material alternatives are continually being investigated [47]. An example of a commercialized perfluoropolymer membrane for natural gas sweetening is the Z-top$^®$membrane developed by the Membrane Technology and Research Inc. (MTR) [77].

Table 9: Some commercially available membranes [73–75, 77]

Membrane	Company	Material	Configuration
Cynara®	Cameron	Cellulose Acetate	Hollow fiber
UOP Separex™	Honeywell	Cellulose Acetate	Spiral wound
Z-top®	MTR Inc.	Polyimide	Hollow fiber
Medal	Air Liquide	Teflon AF©	Spiral wound

Membranes in Development

A wide variety of both polymeric and inorganic material membranes for natural gas sweetening are currently being investigated and constantly improved in order to gain access to the commercial market. Many are already past the lab scale testing and are ready for pilot scale testing, but considering that polymer membranes have been subject to scrutinizing research over the last three decades with only a couple of polymers being commercialized, there is reason to believe that not many of the novel CO_2-separating membranes will survive the pilot scale testing stage. However, some membranes still show a promising potential for future commercialization, such as FSC membranes [47]. For a more detailed description of different types of membranes for gas separation, and particularly natural gas sweetening, see section 2.2.

3.3 Materials for FSC Membranes

3.3.1 Polymers in Selective Layer of FSC Membranes

Polyvinyl Amine and Polyvinyl Alcohol Copolymer

When it comes to research on the copolymer FSC membrane treated in this thesis, Polyvinyl Amine (PVAm) and Polyvinyl Alcohol (PVA), a majority of the literature stems from the MEMFO group at NTNU and the diligent and innovative work of Professor May-Britt Hägg and her group of researchers, Ph.D. students and more. The first focus was FSC membranes made of PVAm cast on PSf support, which were investigated for both natural gas sweetening and CO_2 capture from flue gas, which separates CO_2 from N_2. M. Sandru et al. obtained a CO_2 permeance of 0.28 $m^3(STP)/(m^2 hbar)$ and a CO_2/N_2 selectivity of 197 at a feed pressure of 2 bar, and the membrane exhibited stable performance over time [78]. Later, PVA was added to increase mechanical strength to the polymer blend by creating a supporting network through entangling of the polymeric chains [79]. In particular the

investigations conducted by Dr. Ing. Liyuan Deng have led to great progress in the field of CO_2 separation and natural gas sweetening by PVAm/PVA FSC membranes.

In her 2009 article, a polymer blend of PVAm and PVA was cast on a PSf support membrane with a MWCO of 50,000. The percentage of PVA in the copolymer ranged from 20% to 60%. Before casting, the polymer solution was stirred overnight and subjected to ultrasonic mixing for 2 min, and after applying a calculated amount on the support, the membrane was dried at 45°C for 5 hours and then cross-linked by heating at 90-120°C for 1 hour. For the separation of CO_2 form N_2, a CO_2 permeance of 0.58 and 0.13 $m^3(STP)/(m^2hbar)$ was obtained at 2 bar and 15 bar of feed pressure, with CO_2/ N_2 selectivities of 174 and 94, respectively [79]. Using the PVAm/PVA FSC membrane to separate CO_2 from natural gas was later tested out, and a CO_2/ CH_4 selectivity of up to 45 and 40 was found at feed pressures of 2 and 15 bar, and the CO_2 permeance at 2 bar was documented to be up to 0.3 $m^3(STP)/(m^2hbar)$. The conclusion of the experiments was that the membrane showed high CO_2 permeability and selectivity, as well as having both good reproducibility and stable performance [13]. Another study focusing on the water swelling behavior and permeation performance of CO_2 exhibited a CO_2 permeance of 0.55 $m^3(STP)/(m^2hbar)$ [80].

Poly(2-(N,N-dimethyl) Aminoethyl Methacrylate)

An early research on FSC membranes with amines as carrier agent was performed by H. Matsuyama et al. at the Kyoto Institute of Technology in 1995. By a technique called plasma-graft polymerization, they created a composite polymer membrane on a microporous polyethylene substrate from 2-(N,N-dimethyl) aminoethyl methacrylate (DMAEMA).They tested the membrane for a mixture of CO_2 and N_2, and found good permselectivity in both dry and water swollen conditions. However, they did not investigate the selectivity and permeance of CO_2 in regards to CH_4 [81].

This was on the other hand done when in 2004, a group of researchers from Zhejiang University and the Development Center of Water Treatment in the Chinese city of Hangzhou led by J.-n. Shen, finished experiments on copolymer composite membranes containing PolyDMAEMA. This copolymer was synthesized from acrylic acid (AA) and DMAEMA and coated on a PSf support membrane with a molecular weight cut-off (MWCO)of 48,000. The membrane measured the permeation rate and selectivity of pure gases at 26°C presented in Table 10. The thickness of the selective layer was measured to

be between 18.6–31.0 μm, and the membrane dried for 24 hours in room temperature before being thermally cross-linked in an oven for 3 hours at 120°C [82]. The following year the same group repeated the aforementioned experiments with not only pure CH_4 and CO_2, but with a gas mixture of 1:1 volume ratio as well, which led to a decrease in both selectivity and permeance due to coupling effects, which is tabulated in Table 10 [83].

Poly N-Vinyl-γ-sodium aminobutyrate

Y. Zhang et al. from the Chemical Engineering Research Center at Tianjin University produced in 2002 a new FTM material for CO_2 separation. This was synthesized through the hydrolysis of polyvinylpyrrolidone (PVP), which after hydrolysis yielded Poly N-Vinyl-γ-sodium aminobutyrate (PVSA) and was cast on a selection of different porous support membranes, with the best one being 50,000 MWCO PSf. The membrane was subject to permeation tests of both pure CH_4 and CO_2 with results shown in Table 10, and a binary mixture of the two, operating at pressure between 250 and 67,000 Pa. It was concluded that the composite membrane possessed better CO_2 permeance and selectivity compared to other FTMs in literature [20].

The PVSA was two years later combined with sodium acrylate (SA) to produce the copolymer PVSA–SA by a team led by Z. Wang at the Tianjin University. Only 50,000 MWCO PSf was used as support membrane, and the CO_2 selectivity and permeance for both pure and 1:1 volume ratio gas mixture are tabulated in Table 10 [84].

Polyallyl Amine and Polyvinyl Alcohol

J. Zou and W.S. Winston Ho from Ohio State University published in 2006 an article about their study on CO_2-selective polymeric membranes containing amines in cross-linked polyvinyl alcohol. The experiments showed great results in separating CO_2 from gas mixtures such as CO_2/ H_2, CO_2/ CO andCO_2/ N_2 [85]. The year after a similar membrane was developed in the Chemical Engineering Research Center of Tianjin University led by Y. Cai, where a blend polymer of polyallyl amine (PAAm) and PVA was cast on a PSf support membrane. The permeance and selectivity of both pure CO_2 and CH_4 and a 9:1 volume ratio of the binary gas mixture CH_4/ CO_2 was investigated, and the latter results are listed in and Table 10. For the gas mixture, a selective layer of 20wt% PAAm showed the highest CO_2 permeance, whereas different PAAm contents yielded the highest selectivity depending on the pressure [86].

Polyetheleneimine and Polyvinyl Alcohol

M. Wang et al. at Tianjin University studied in 2009 the effects of pressure and temperature on a FSC membrane for the CO_2 separation from natural gas, a composite membrane consisting of a blend of polyetheleneimine (PEI) and PVA on a PSf support membrane. The gas mixture consisted of a 9:1 volume ratio of CH_4/ CO_2, and the best achieved CO_2 selectivities and permeances as listed in Table 10. In this experiment four different membranes were manufactured in an identical manner, but still results showed a variance between lowest and highest values of 22% and 25% in selectivity and permeance, respectively [87].

3,3-Diamino-N-Methyldipropyl Amine and Trimesoyl Chloride

Yet another research team (X. Yu et al.) from Tianjin University prepared in 2010 a new FSC membrane with amino carriers for the capture of CO_2. The composite membrane had a 6,000 MWCO PSf support with a thin film selective layer on top consisting of a polymerization of 3,3-Diamino-N-methyldipropylamine (DNMDAm) and trimesoyl chloride (TMC), in short named poly(DNMDAm-TMC). The permselectivity of the membrane was investigated for the two gas mixtures N_2/ CO_2 and a 9:1 volume ratio of CH_4/ CO_2. The good results were thought to be mainly due to the thin film thickness and the tertiary amino groups, and can be seen in Table 10, with a TMC concentration of 0.0226 mol/l and a DNMDAm concentration of 0.006 mol/l [88].

Polylvinyl Pyrrolidone

In 2001, a novel membrane material was obtained by Y. Zhang et al. at Tianjin University with two kinds of CO_2 carriers. The selective layer on top of the MWCO 50,000 PSf support was a polymer synthesized from polyvinyl pyrrolidone (PVP) by a radical polymerization and hydrolysis, which opened up the five-membered pyrrolodine ring, and thus freeing the carboxylate anion and downgrading the tertiary amine to a secondary amine, both important CO_2 fixed carriers. Permeation tests of both pure and a 1:1 volume ratio of the gas mixture CH_4/ CO_2 resulted in better CO_2 selectivity and permeance than other FSC membranes previously reported in literature, see Table 10 and Table 10 [89].

Polyvinyl Pyrrolidone and Acrylamide

The following year Y. Zhang et al. combined the N-vinyl pyrrolidone and acrylamide (AAM) in a 7:3 mass ratio to prepare a polymer composite membrane very much alike the hydrolyzed PVP membrane, but with two segments in the polymer chain. The additional segment contained an extra carboxylate anion, which yielded better permselectivity for the binary mixture in accordance with an enhanced facilitated transport, as shown in Table 10 [42].

Table 10: Comparison of permeation rates of CO_2 and CO_2/CH_4 selectivity for mixed gas permeation tests for a selection of FSC-membranes

Year	Selective Layer	p_feed [kPa]	Permeance [$cm^3(STP)/cm^2sPa$]	α [−]	Ref.	Ratio
2001	PVP	1.32	5.93×10^{-7}	212	[89]	Pure
		65.3	0.19×10^{-7}	80		
2001	PVP	1.07	2.81×10^{-7}	51	[89]	1:1
		33.33	0.075×10^{-7}	16		
2002	PVP-AAm	1.6	3.41×10^{-7}	47	[42]	1:1
		73.3	0.11×10^{-7}	15		
2002	PVSA	2.6	6.00×10^{-7}	210	[20]	Pure
		66	0.15×10^{-7}	77		
2004	PVSA-SA	105.4	0.069×10^{-7}	46.8	[84]	1:1
		173.0	0.056×10^{-7}	16.0		
2005	DMAEMA-AA	3.5	2.30×10^{-7}	47	[83]	1:1
		32.5	0.22×10^{-7}	21		
2007	PAAm-PVA	100	0.195×10^{-7}	58	[86]	9:1
		1300	0.055×10^{-7}	9		
2009	PEI-PVA	120	0.255×10^{-7}	52.5	[87]	9:1
		1300	0.083×10^{-7}	17.5		
2010	DNMDAm-TMC	110	0.885×10^{-7}	37	[88]	9:1
		1500	0.398×10^{-7}	12		

3.3.2 Polymers in Support Layer of FSC Membranes

Several different support membranes have been tested and investigated over the last 20 years. Some show excellent CO_2 permeance whereas others give a very high CO_2/CH_4 selectivity, but it is hard to find a material that exhibits both qualities due to the "trade-off" relationship between selectivity and permeability for the dense polymer membranes, as coined by Robeson
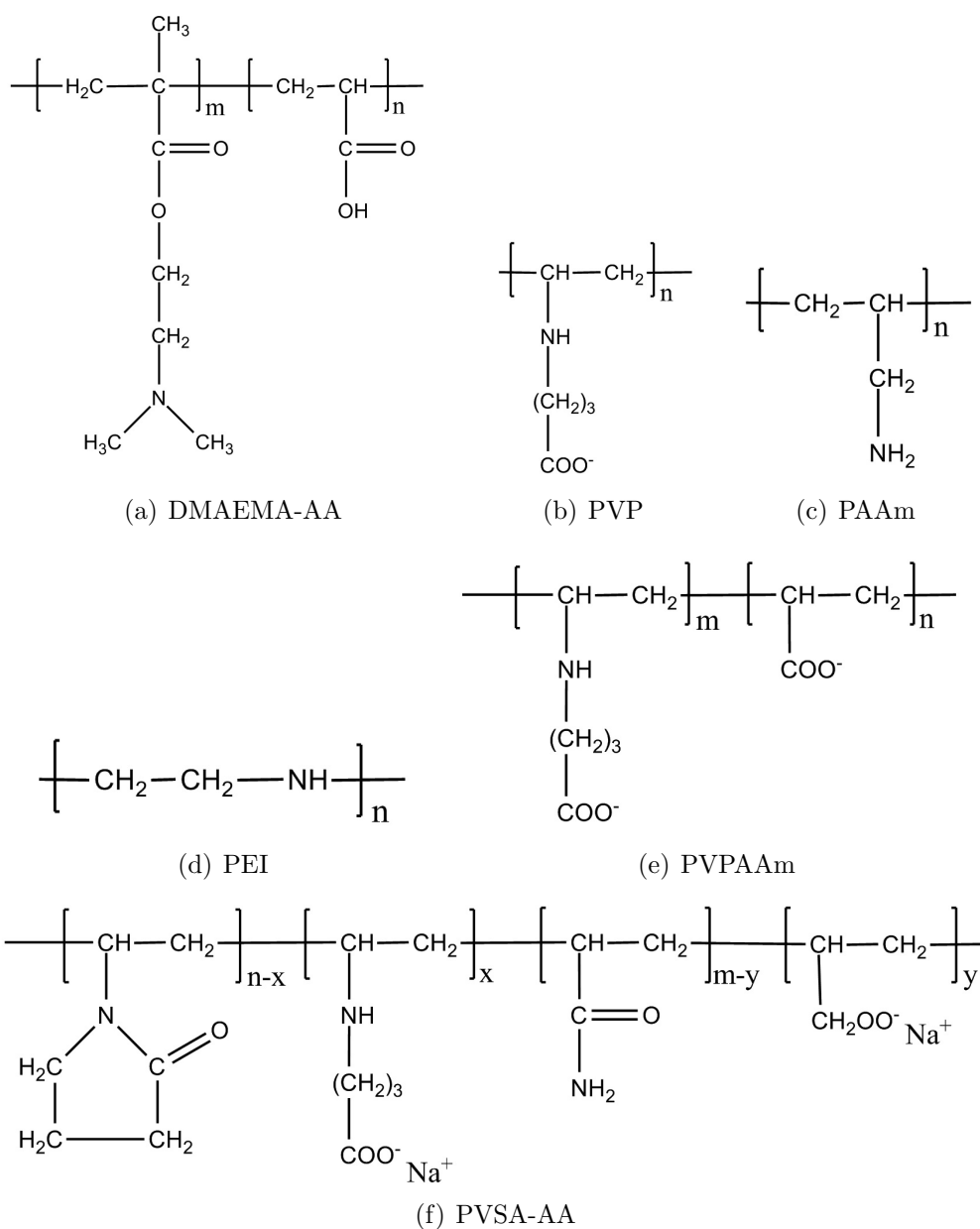
Figure 26: Molecular structures of polymers from literature

handbook. Typical support polymers for FSC membranes are cellulose ac-
etate (CA), polysulfone (PSf), polyethersulfone (PES) and polyacrylonitrile
(PAN). A study of the three latter support polymers by Y. Zhang et al.
showed that PSf had both better CO_2 selectivity and permeance compared
to the other two. It was argued that the sulfone groups favor the solubility

of CO_2, as they are quite similar in structure to CO_2 [20].

Another study was performed by T.-J. Kim et al. at NTNU, where they compared the five support membranes PSf (MWCO 20,000 from DSS), PSf (MWCO 30,000 from Osmonics), CA, PAN and PES with a selective layer of PVAm on top. For a pressure of 2 bar and room temperature, it showed that the CO_2 permeance of PSf manufactured by DSS was moderately good, but that its CO_2 selectivity was greater than any of the other membranes with a factor of 40 compared to the next best membrane, as seen in Table 11. The big difference between the two PSf membranes was explained by their difference in MWCO, as there should be a reasonable difference between the MWCO of the support membrane and the selective membrane. In that case, the PVAm of the selective layer had a MWCO of 39,000, which caused it to leak into the support instead of forming a layer on top [43]. The MWCO of the support (which also is a measure of the porosity of the support) can therefore directly have an influence on both the selectivity and permeance of CO_2, so the membrane may be tailored for the desired characteristics. A low MWCO (e.g. 20,000) yields a high purity product whereas a high MWCO (e.g. 50,000) gives a high flux [78].

Table 11: Comparison of permselectivity for PVAm on different support membranes [43]

Support	PSf (DSS)	PSf (Osmonics)	CA	PAN	PES
CO_2 permeance[a]	0.00837	0.0063	0.099	0.0327	0.00388
α **(CO_2/CH_4)**	1143	26.9	17.3	5.1	6.5

[a] Permeance in units of $[m^3(STP)/m^2barh]$.

3.3.3 Nanofillers in Selective Layer of FSC Membranes

There exists very little reported literature about implementation of nanofillers in FSC membranes, except from previous studies at NTNU by L. Cheng and M.-B. Hägg [90]. However, mixed matrix membranes (MMMs) have been developed where nanofillers are mixed within a polymer matrix, so a lot of experience may be drawn from the existing re search on MMMs. In addition, composite films of multiwalled carbon nanotubes (CNTs) in PVA has been reported by W. Chen et al. [91], hybrid membranes of PVA/CNTs by F. Peng [92] and Z. Wang explored the reinforcing efficiency of carbon nanotubes in PVA composites in his Ph.D. thesis [93].

Table 12: Selectivity and CO_2 permeability of a selection of polymeric membranes [25, 79]

Polymer	P_{CO2} [$Barrers$]	Selectivity [$-$]
PTMSP	37,000	2.01
Poly(4-methyl-1-pentyne)	10,700	1.98
Silicone Rubber	4,550	3.18
Poly(4-methyl-1-pentene)	84.6	5.68
PPO	65.5	16.0
Tetrabromobisphenol A Polycarbonate	4.23	33.6
Polysulfone	4.9	23.3
PC	6.8	19
TMPC	18.6	21
HFPC	24	23
TMHFPC	111	24
TBPC	4.2	34
TBHFPC	32	36
TB=TBHF-co-PC	16	34
PMDA-ODA	2.71	45.9
PMDA-MDA	4.03	42.9
PMDA-IPDA	26.8	29.7
PMDA-DAF	0.15	71.6
6FDA-ODA	23	60.5
6FDA-MDA	19.3	44.9
6FDA-IPDA	30	42.9
6FDA-DAF	32.2	51.1

Fumed Silica

Merkel et al. added up to 30 vol% of non-porous fumed silica (FS) with average size of 10 nm to an ultra-permeable, reverse-selective nanocomposite membrane made of poly(4-methyl-2-pentyne) (PMP), and achieved both a considerable higher permeability of CH_4 than that of pure PMP. This was thought to be because of the disruption of polymer chain packing induced by the fumed silica and as a result of a subtle increase in free volume [94]. Z. He et al. also incorporated several types of non-porous, nanosized, fumed silica fillers into a PMP membrane in order to manipulate the chain packing of the molecular polymer. This increased n-butane permeability up to four times and doubled the n-butane/methane selectivity compared to the pure PMP

membrane. From this, it seems as though the silica-filled hybrid PMP membrane shows completely opposite gas permeation behavior compared to other hybrid membranes of polymers filled with non-porous inorganic nanoparticles [95].

The use of nanosized fumed silica (Aerosil R106) was also investigated by M. Wahab et al. as fillers in polysulfone for a hollow fiber mixed matrix membrane (HFMMM). Here, the fumed silica particles increased the CO_2 permeability by 12%-16%. This stimulation of permeability at all loadings of FS was speculated to be proof of a interaction between the fumed silica and CO_2. At a low loading of 0.1wt%, the CO_2/CH_4 selectivity reached almost 33 as seen in Figure 27, whereas the selectivity at a high loading of 10 wt% was much lower, at about 7.4. By using SEM images, this could be explained by a severe agglomeration of fumed silica fillers at higher loadings, leading to a higher permeation of CH_4 and hence a lower selectivity. The incorporation of fumed silica was also proven to increase the glass transition temperature and the thermal stability of the membrane [96].

Figure 27: CO_2/CH_4 selectivity for PSf-FS HFMMMs at various loadings. [96]
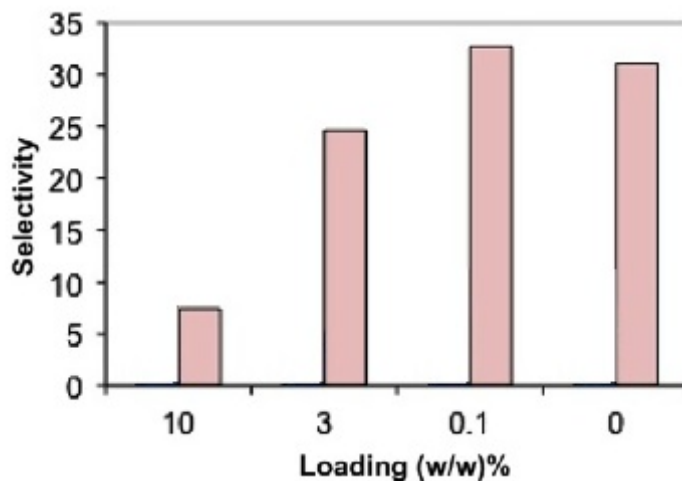
Titanium Oxide

V. Bhardawaj et al. incorporated several types of nanofillers, including titanium oxide TiO_2 with an average size of 150 nm, into a polysulfone spinning solution in an attempt to enhance the mechanical strength and to increase CO_2 selectivity of the membrane. At a concentration of 5wt% TiO_2 in PSf,

Table 13: CO_2 and CH_4 permeabilities and CO_2/CH_4 selectivity of pure PMP, PMP/FS and PMP/TiO$_2$ nanocomposite membranes at 35°C and 2 bar [97]

| Nanofiller | Permeability [a] | | Selectivity |
	CO_2	CH_4	CO_2/CH_4
0 (Pure PMP)	1790	6700	3.7
15 wt% FS	2010	7130	3.5
25 wt% FS	2510	8720	3.5
35 wt% FS	3620	11250	3.1
15 wt% TiO$_2$	1980	6980	3.5
25 wt% TiO$_2$	2460	8430	3.5
35 wt% TiO$_2$	3420	10970	3.2

[a] Permeability in unit of Barrer (1 Barrer $= 10^{-10} cm^3 (STP) cm / cm^2 s cmHg$).

the CO_2 permeability only increased with 4%, whereas the CH_4 permeability increased with 75%, leading to a decrease in CO_2/CH_4 selectivity from 41 to 29.5 compared to the neat PSf membrane. Still, the mechanical strength was bettered with addition of titanium oxide nanofiller 89 . Another paper by Y. Kong et al. discusses the experiments of a nanocomposite membrane blended from TiO$_2$ sol and polyimide (PI) solution. For all the tested gases (H$_2$, O$_2$, N$_2$ and CH$_4$), permeability increased with increasing TiO$_2$ content up to 40wt%. Both H$_2$/N$_2$ and O$_2$/N$_2$ selectivities first dropped with lower TiO$_2$ content, but increased at higher content, whereas the H$_2$/CH$_4$ decreased with increasing TiO$_2$ content [98]. Investigations on TiO$_2$ nanoparticle filled PMP nanocomposite membranes have also been performed at NTNU by L. Shao et al., using a cross-linked PMP membrane. Several types of nanoparticles were added in an attempt to raise the gas permeability lost due to cross-linking. From Table 13 one can see that permeability for both CO$_2$ and CH$_4$ increased with increasing content of TiO$_2$ in the PMP, but that the selectivity dropped slightly from 3.7 to 3.2 [97].

Carbon Nanotubes

Novel nanocomposite membranes with single walled carbon nanotubes dispersed in a polysulfone matrix as seen in Figure 28 was prepared and characterized by S. Kim et al., and experiments at feed pressure of 4 atm showed that the gas permeability of the membranes increased with increasing weight fraction of carbon nanotubes. CO$_2$ permeability increased from 3.90 to 5.19 Barrers with a CNT load of 10wt%, whereas the CH$_4$ permability increased from 0.17 to 0.28 Barrer. The articled concluded that the addition of carbon

nanotubes in a polymer matrix improved permeability of small molecules and some selectivites by increasing the diffusivity, and predicted an even better permselectivity with the incorporation of future CNTs with diameters less than 10 Å [99].

Figure 28: Cross-sectional FESEM image of 10 wt.% unmodified single-walled nanotube in a polymer matrix, with arrows indicating the nanotubes [99]
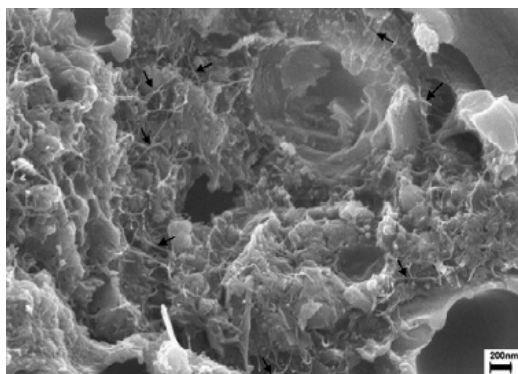
3.4 Characterization of FSC Membranes

3.4.1 Thermal Analysis

Differential scanning calorimetry (DSC)

Differential scanning calorimetry (DSC) is a technique investigating thermal properties, and can be used to detect phase transitions in the polymer, such as the glass transition temperature and melting temperature. It measures the difference in the amount of heat required to increase the temperature of a dry polymer sample compared to a reference sample over a wide range of temperatures, and plots the heat flow versus temperature. A graph of DSC measurements of the PVAm/PVA blend and its pure components is seen in Figure 29. A melting point for PVA is clear at around 220°C, whereas the PVAm and the PVAm/PVA blend have no obvious melting temperatures, as PVAm is a highly crystalline polymer and is mixed in a homogenous blend with PVA [79, 86].

Thermal Gravimetric Analysis (TGA)

Thermal Gravimetric Analysis (TGA) is an easy technique to analyze degradation of a material through thermal reactions like evaporation, decomposition and gas absorption. The TGA measures the difference in mass (usually weight loss) over a period of time while heated to very high temperatures ($> 500°C$) as a function of temperature, and can be used to examine the decomposition behavior of a polymer. An example of a TGA graph can be seen in Figure 30, where the thermal degradation of unfilled and a variety of silica-filled PSf matrix membranes is shown [34, 100].

Figure 29: DSC graph for the polymers PVA, PVAm and PVAm/PVA blend [79]
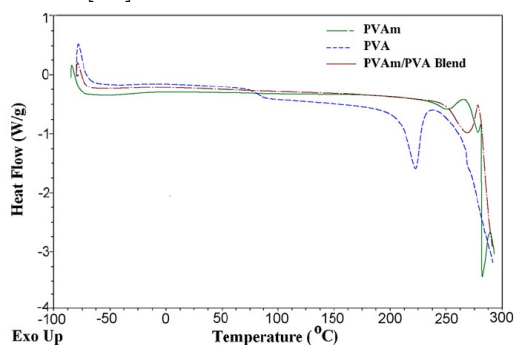
Figure 30: TGA graph for silica-filled PSf matrix membranes [100]
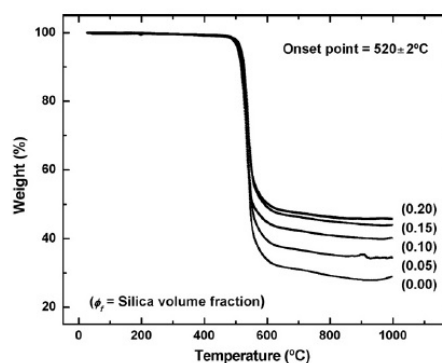
3.4.2 Chemical Structure

Fourier transform infrared (FT-IR) Spectrometry

A Fourier transform infrared (FT-IR) spectrometer can record the FT-IR spectrum of polymer solution by dripping it on a salt plate and let the solvent evaporate off under an infrared lamp, which gives a thin polymer film sample. This provides knowledge about the intra-molecular bonds and atoms in the structure of the molecule, as each single and double bond will have different absorption peaks for different wave numbers. Both stretching vibrations and symmetrical and asymmetrical bending vibrations will establish the existence of single and double bonds as they are measured by the spectrometer. This is a commonly used characterization technique to determine the structure of the molecule in the polymer [86]. An example of FT-IR spectrum of the FSC membrane PVAm/PVA blend on PSf is given in Figure 32, where the band

near 1090 cm^{-1} can be assigned to the combination of –C–O–C– bond and
≡C–OH bond [79].

¹H NMR Spectrometry

Proton nuclear magnetic resonance (NMR) spetrometry can be used to detect
protons in the polymer structure, and thereby confirm the structure of a
polymer. It records chemical shifts in parts per million (ppm) relative to
an internal standard, which often is tetramethylsilane (TMS), and lines at
different ppm are assigned to different functional groups in the polymer as
seen in Figure 31. For instance will lines near 1.2 and 1.7 ppm be assigned
to the protons of methylene and methine groups, and lines at 2.7 ppm to
methylene groups adjacent to amine groups. In order for the polymer to
be analyzed, it is often dissolved in deuterium oxide and chemical shifts are
recorded at a specific frequency (typically 600 MHz) [86].

Figure 31: An example of how a ¹H
NMR Spectrum for a polymer may
look like [86]
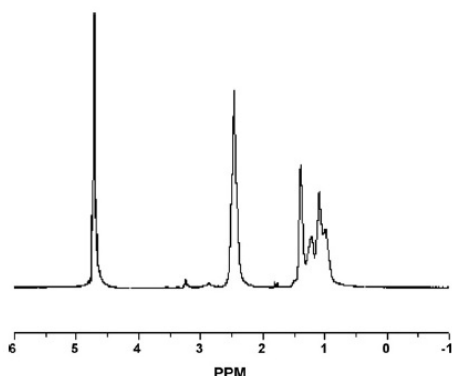
Figure 32: FT-IR specter of the FSC
membrane PVAm/PVA blend on PSf
[79]
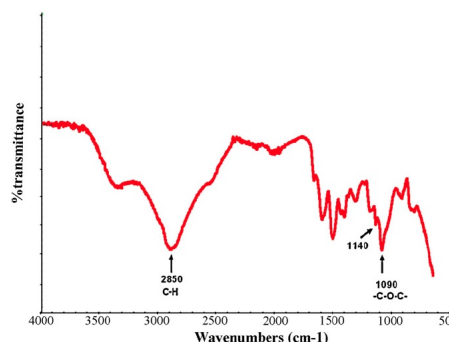
X-ray diffraction (XRD)

X-ray diffraction (XRD) spectrometry can be used to investigate the crystal
structure, chemical composition and the physical properties of polymers by
analyzing the intensity of scattering beams from x-ray radiation. It can also
be used to investigate the variance of crystallinity in a blend polymer at
different compositions, or to find the difference in a polymer before and after
cross-linking. An example of XRD spectrometry graph showing the difference
between a heated and a non-heated cross-linked PVAm/PVA copolymer can
be seen in Figure 33 [79, 86].

X-ray photoelectron spectrometry (XPS)

X-ray photoelectron spectrometry (XPS) can measure the elemental composition in a polymer, as well as empirical formula, chemical state and electronic state of elements in the polymer. An example of an XPS analysis is using Mg Kα as a radiation source to take spectra with an electron emission angle of 45∘. The spectrum plots intensity with the binding energy, and shows peaks for different atoms like O, N and C as seen from the XPS spectrum of a PVAm/PVA blend in Figure 34, which in this case shows that the content of oxygen in the membrane increases from 18% to 22% after heat cross-linking, and may indicate the formation of cross-linking chain (–C–O–C–) in the blend network [79, 88].

Figure 34: XPS spectrum of a PVAm/PVA copolymer [79]

Figure 33: XRD spectrum of a PVAm/PVA copolymer [79]
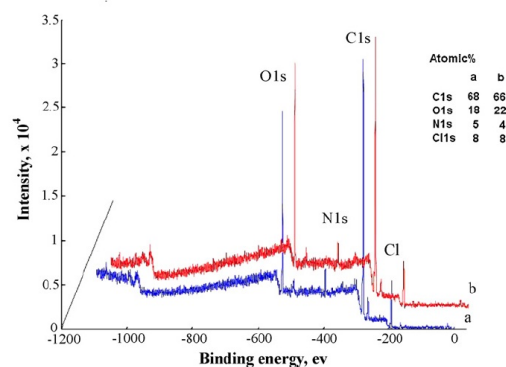
3.4.3 Gravimetric Analysis

Swelling Capacity Tests

A rather simple technique may be performed to measure the swelling capacity of a polymer membrane. This is demonstrated in [34], where PVAm/PVA blend membranes were cast and dried before saturated with water and weighed. The samples were subsequently weighed every day until the mass of the membrane was constant. The mass between the first saturated sample and the dry sample was the mass gain from water of the swollen membrane. From this the swelling degree could be calculated as well, by dividing the evaporation loss by the mass of the dry membrane, and multiplying with 100.

3.4.4 Morphological Analysis

Scanning Electron Microscopy (SEM)

Scanning Electron Microscopy (SEM) is probably the most used technique to analyze the surface or cross-section surface of a membrane. It allows for sensitive structures to be examined at a high magnification [27]. Thickness of membranes and membrane films can be measures, as well as shape, distribution and size of pores in porous membranes. The membrane sample is coated in a conductive material, e.g. gold, and is radiated by an electron beam. This allows for a much greater resolution than regular microscopes, which are restricted by the longer wavelengths of visible light. Several examples of SEM-pictures of the membranes tested in this thesis can be seen in section 5.1.

3.5 Durability and stability of PVAm/PVA Blend FSC Membrane

The durability of the membrane studied in this master thesis was investigated for durability and stability at high pressure (up to 80 bar) by M. W. Uddin at NTNU in his 2012 Ph.D. thesis. The effect on the membrane of components naturally present in natural gas such as H_2S, water, heavy hydrocarbons and aromatics was studied, alongside impurities such as glycols and corrosion inhibitors. With this novel knowledge, the need for necessary pretreatment conditions for natural gas sweetening using this kind of FSC membranes could be elucidated and better understood. The FSC membrane in use was the PVAm/PVA blend on PSf support, and a number of parameters were tested thoroughly. It was found that the presence of higher hydrocarbons such as pentane and higher, aliphatic hydrocarbons, benzene and toluene reduced the permeability of both CO_2 and CH_4 due to partial chemical cross-linking, and this negative effect was intensified with higher temperature, whereas the selectivity remained unchanged. The effects of H_2S, n-hexane and propane were not that detrimental to the membrane performance, and showed only a decrease of 16% after two weeks of exposure under high relative humidity conditions, whereas the membranes were the least affected by glycols such as MEG and TEG, and actually caused a slight increase in gas permeance due to extra bounded water accommodating the diffusion transport in the membrane. The presence of ethane and propane also reduced the gas permeance through the membrane due to competitive sorption, but the membrane regained its permeation capacity after removing

these gases. In addition, it was found that the membrane did not undergo plasticization in the pressure of 7 to 80 bar. The thesis concluded that the main areas of improvement were to strengthen the membrane in order to resist compaction and to secure the water content in the membrane for the carrier effects to have full effect [101].

3.6   Summary from Specialization Project

In the fall of 2011 a specialization project was carried out in the course TKP 4530 Environmental Engineering and Reactor Technology. The main supervisor of this project was Prof. May-Britt Hägg and co-supervisor was Dr. Liyuan Deng, and the title of the project was "Testing and optimization of CNTs reinforced PVAm/PVA blend membrane for natural gas sweetening at high pressures". One membrane was prepared with a selective layer of 5:1 PVAm/PVA and 1wt% CNTs on a PSf MWCO 20,000 support membrane. This membrane was tested at different feed and sweep gas flow rates at pressures ranging from 10 to 80 bar, and the highest CO_2/CH_4 selectivity of 26.7 was found at 40 bar for all feed gas flow rates above 500 ml/min. At this point the highest CO_2 permeance of 0.0587 $m^3/m^2.h.m^2$ was found at a feed gas flow rate of 2000 ml/min.

4 Experimental Procedures

4.1 Materials

4.1.1 Selective Layer

The selective layer of the experimental membrane was a polymer blend consisting of the two polymers PVAm and PVA in a ratio of 5:1, see Figure 37. The blend was reinforced with either CNTs or SiO_2.

Polyvinylamine

PVAm is a linear polymer with a repeating unit with a molecular weight of 43 g/mol, which include a primary amine group directly attached to the carbon main chain. It has a glass transition temperature of 45°C and is amorphous. PVA is usually prepared indirectly from either a Hoffmann rearrangement from polyacrylamide or by polymerization and hydrolysis of protected vinylamines. The structural formula for PVAm can be seen in Figure 35.

The utilization of PVAm is primarily because of its cationic nature of the primary amine groups under neutral or acidic conditions, as with the acidic CO_2 gas. The polymer is therefore not stable in air because it will react with CO_2 in the atmosphere [102].

For the preparation of the membrane in this project, the commercially available salt polyvinylamine hydrochloride (PVAm· HCl) with a molecular weight of 340,000 g/mol from BASF was used. This salt is quite stable and is soluble in water, formamide, ethylene glycol and some alcohol/water mixtures, but not in common solvents like acetone, alcohols, dimethylformamide, and methylene chloride [102, 103].

Figure 35: The repetitive unit of polyvinylamine
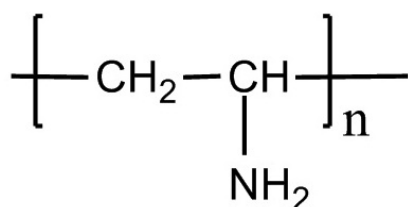
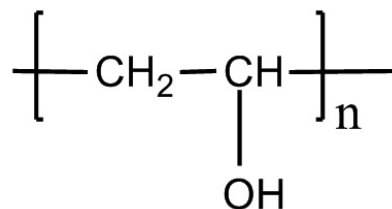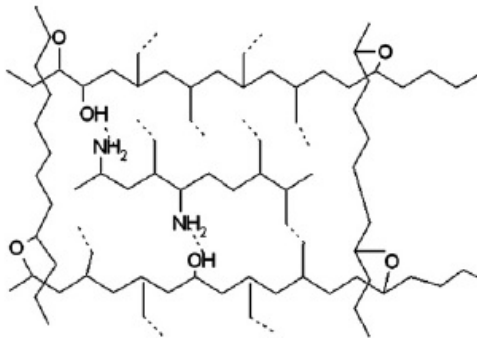Figure 36: The repetitive unit of the polyvinyl alcohol

Figure 37: PVAm/PVA blend polymer framework [79]

Polyvinyl Alcohol

Similar to PVAm, PVA is a linear polymer with a repeating unit as shown in Figure 36 with a molecular weight of 44 g/mol, which include a primary alcohol group directly attached to the carbon main chain. It has a glass transition temperature of 85°C and exhibits semi-crystalline properties, even though it is an atactic polymer. This is due to its strong hydrogen bondings [18]. As a result, PVA has an amorphous density in room temperature of 1.26 g/cm^3 and a crystalline density of 1.35 g/cm^3 [102].

The application of PVA in the membrane blend investigated in this project is partly due to the mechanically strong polymer matrix it provides. This strong chain framework contributes to a stable separation and to a higher permeance due to the efficient ultra thin selective layer [79].

PVA is completely soluble in water and is useful as an industrial, medical, and biomimetic material, and is commonly used as a thickener in some suspensions and emulsions. It can be prepared by polymerization and alcoholysis of vinyl acetate [102, 103].

For the preparation of the membrane in this project a 90% hydrolyzed PVA powder provided by Sigma Aldrich with a molecular weight of 72,000 g/mol was used.

4.1.2 Nanofillers

Carbon Nanotubes

Carbon nanotubes (CNT) were first discovered in 1976, but had no application at the time, and was later in 1991 rediscovered by Iijima. CNTs are

73

tube-shaped materials made of carbon, having a diameter typically ranging from less then 1 nm to up to 50 nm. The graphite layers are rolled up in a continuous unbroken hexagonal mesh with the carbon molecules at the apexes of the hexagons, like represented in Figure 38. Carbon nanotubes can appear in many different structures, lengths, thicknesses, and in various types of helicity and numbers of layers [104, 105].

Nanocomposites reinforced with carbon nanotubes have a potential of having extraordinary specific stiffness and strength, and they represent great opportunity for application. CNTs have unique properties which makes it a suitable filler in the polymeric membrane to enhance its mechanical strength and improve the membrane swelling capacity. The CNTs have an extremely high tensile strength, and the best specific strength of known materials, more than 30 times that of high-carbon steel. The thermal stability and permeation properties are also improved, the latter one being as result of the nano-spacer effect, which loosens the packing of the polymers at high pressure [34, 106].

(a)   (b)
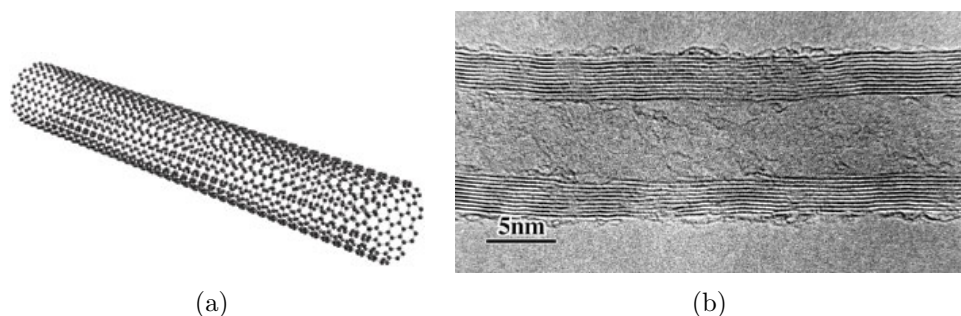
Figure 38: (a): A nanoscale representation of a carbon nanotube. (b): TEM picture showing the layered structure of a multiwalled carbon nanotube [106]

Fumed Silica

Fumed Silica (FS) (SiO_2) is a silica powder produced from the hydrolysis of silicon tetra chloride ($SiCl_4$) with an oxy hydrogen flame, which then reacts with water and yields hydrochloric acid and fumed silica. Due to the preparation method of fumed silica it is often called pyrogenic oxide, and it has unique and invaluable properties like low moisture absorption and high mechanical stability, and it can optimize the rheological properties of the desired filling substance, properties which combined display a high level of versatility of usage of fumed silica. Its morphology is chain-like particles, which forms three dimensional networks when mixed with liquids. This can

trap the liquid and make it more viscous, which serves a purpose when coating porous surfaces, as it becomes more resistant to absorption by the substrate. The major applications for fumed silica are in coatings, adhesives, cosmetics, cements, sealants and as a filler for rubbers and plastics, as in e.g. polymer membranes [107, 108].

When dispersed in amorphous and glassy polymer membranes with high free volume, it has been assumed that the fumed silica particles disrupt the chain packing at the interfaces, as the membranes in experiments exhibited an increase of gas solubility and a sustained gas diffusivity. This can be explained by the larger free volume being able to host more molecules [27]. Other investigations on mixed-matrix membranes embedded with fumed silica have been shown an increase in both selectivity and permeability for the penetrant with largest molecular structure. This too was accredited an increased free volume in the polymer from chain packing disruption [95, 109].

Two types of FS from the company Evonik Industries were used in the preparation of four different membranes in this thesis. Two membranes had the selective layer impregnated with AEROSIL®150 fumed silica in concentrations of 0.1wt% and 1.0wt%. AEROSIL®150 is a 99.8% pure hydrophilic fumed silica powder with a specific surface area of 150 ± 15 m^2/g and with an average size of 14 nm [110]. In the other two membranes, a type of fumed silica called ACEMATT®3300 were applied in concentrations of 0.1wt% and 1.0wt%. ACEMATT®3300 is a hydrophilic advanced polymer-treated thermal silica with a very good matting efficiency and high transparency. It has an average particle size of 9.5 μm and a specific surface area of 195 m^2/g and a purity of more than 99% SiO_2. This large particle size was not discovered before after the membranes were prepared and tested, due to erroneous labelling of the ACEMATT®3300 container [111].

4.1.3 Supports

Polysulfone

Polysulfone, usually abbreviated PSf, but PS and PSO can also be found in literature, is an amorphous polymer with a high performance, and have both very good chemical and thermal stability. It has a glass transition temperature of 190°C, and is often used as a hydrophilic porous membrane for ultrafiltration and as a support material for composite membranes utilized in many reverse osmosis, nanofiltration and some gas separation membranes [18, 112]. PSf has a CO_2 permeability of 5.6 barrer compared to a CH_4 permeability of 0.25 barrer at 35°C [12].

Experiments conducted by Y. Zhang et al. [20] indicate that polysulfone is the best alternative for use as a support membrane in a composite membrane for the separation of CO_2/CH_4 gas mixture, with polyethersulfone also being a viable alternative. The explanation to the superior support properties of polysulfone is that gases have an affinity to dissolve in polymers with a similar chemical structure, and the CO_2 is chemically quite comparable to the sulfone group and therefore reaches a higher solubility in the interfacial layers [20].

For the preparation of most of the membranes in this thesis, a PSf ultrafiltration flat sheet membrane (DSS-GR61PP) with a MWCO of 20,000 g/mol from the manufacturer Alfa Laval was used. In addition, A PSf membrane with a MWCO of 10,000 g/mol (DSS-GR81PP) was tested. Both PSf layers were supported by a polypropylene fiber support.
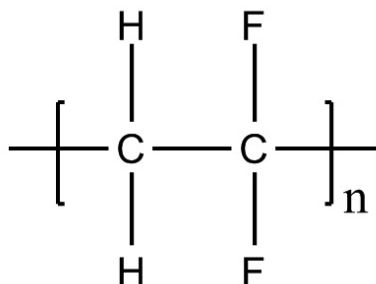
Figure 39: The repetitive unit of the support polymer PSf
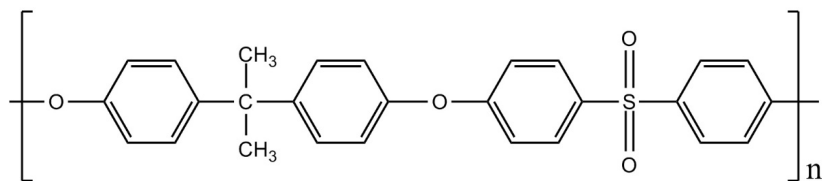
Polylvinylidene Fluoride

Polyvinylidene fluoride (PVDF) was one of the first fluoropolymers to be discovered and has a great number of applications in industry (e.g. separation of uranium isotopes by gaseous diffusion) due to its high chemical and thermal stability. It has also gained scientific and industrial attention over the years because of the polymers excellent electrical properties, its durability and its biocompitability. The chain of PVDF has a backbone consisting of only single bonds, which makes the polymer quite flexible. The glass transition temperature of amorphous PVDF lies quite low, at T_g = -40°C and the room temperature density is $\rho = 1.68 \ g/cm^3$. It has a complicated crystalline structure, with three different chain conformations. The average price of one kilogram PVDF on the market is about 20 \$. PVDF can be spun into fibers or drawn into films, and besides its uses in electronics and in transducer technology, it is widely used as packing material in food and pharmaceutical industry. Its heat and chemical resistant properties also makes it goo for metal coatings and coating of equipment used in petrochemical, electric and nuclear industries [102].

This polymer is also widely used in micro- and ultrafiltration [113], but has also been used in gas separation membranes, such as in the early experiments performed by El-Hibri and Paul in 1986. They they found that uniaxial drawing of PVDF reduced gas permeability and diffusivity, whereas these parameters were increased by annealing, caused by a mixture of amorphous and crystalline regions in the PVDF. The solubility of CO_2 in the polymer was found to be about six times higher than predicted by the correlation with the Henry's law sorption coefficients [114]. PVDF was also used as the support membrane by Sridhar et al. in 2007, on which a thin film of poly(ether-block-amide) was applied. For the separation of CO_2 from CH_4, a permeance and selectivity in the range from 3.0 to 4.8 GPU and 18 to 25 were achieved, respectively [115].

For the preparation of the PVDF membrane in this thesis, a PVDF ultra-filtration flat sheet membrane (FS61PP) with a MWCO of 20,000 g/mol from the manufacturer Danish Separation Systems (DSS) AS was used. The PVDF layer was supported by a polypropylene fiber support.

Figure 40: The repetitive unit of the support polymer PVDF

Figure 41: The repetitive unit of the support polymer CA
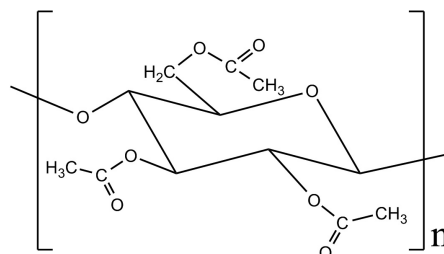
Cellulose Acetate

Cellulose acetate (CA) is one of the most tested and used materials in polymer membranes for gas separation, and has a long history of practical applications. It was initially produced for reverse osmosis and desalination of sea water, but is presently also the most popular membrane and the industrial standard for the separation of CO_2 from CH_4 and other light hydrocarbons and has been installed in membrane plants for natural gas sweetening for almost three decades [6, 27, 112].

CA is a polysaccharide thermoplastic with a repeated molecular structure shown in Figure 41 and a molecular weight of 139,14 g/mol, and it is pro-

duced as the derivative acetate ester of cellulose [12]. Due to its strong intermolecular hydrogen-bonds between the hydroxy groups it has a high level of crystallinity, which makes it is a relatively glassy polymer. Even though it is hydrophilic by nature, often carrying charged groups on the surface, its crystallinity prevents it from dissolving in water [112]. The polymer is easy to produce, is mechanically tough and chemically resistant towards chlorine, but has a limited usage in acids and bases, as it has a pH range of 4 - 6.5. The glass transition temperature of CA lies between 10 - 124°C, and has a CO_2 permebility of 10 barrer compared to a CH_4 permeability of 0.36 barrer at room temperature. It has a reported selectivity of the two gases between 10-20, and is commonly used in a spiral wound or hollow fiber module [12, 112].

For the preparation of the CA membrane in this thesis, a CA ultrafiltration flat sheet membrane (CA600PP) with a MWCO of 20,000 g/mol from the manufacturer Alfa Laval was used. The layer was supported by a polypropylene fiber support.

4.1.4 Gases

The feed gas used in the permeation experiments was a gas mixture containing 10 mol% CO_2 in CH_4 at 200 bar provided by AGA in a 50 L flask.

The sweep gas used in the permeation experiments was N_2 with a purity of $\geq 99.999\%$ provided by YaraPraxair in a 50 L flask.

4.2 Membrane Preparation

4.2.1 Preparation of PVAm/PVA Solutions

1. **Solution of PVAm**: A calculated amount of PVAm HCl powder was weighed in a glass bottle and mixed with distilled water to make a 5 wt% solution. It was placed on a rotating machine overnight to dissolve the polymer completely.

2. **Solution of PVA**: A calculated amount of PVA was dispersed in distilled water to make a 5 wt% solution. To dissolve PVA in water the solution was heated to 90°C for one hour and then placed on a rotating machine overnight.

3. **Solution of nanofillers**: A calculated amount of CNTs and FS were dispersed in distilled water to make a 0.1 wt% and 1wt% solution. Five

solutions were made:

- 0.1wt% CNTs was used to prepare membranes #1-7
- 0.1 wt% AEROSIL®was used in membrane #8
- 1.0 wt% AEROSIL®was used in membrane #9
- 0.1 wt% ACEMATT®was used in membrane #10
- 1.0 wt% AEROSIL®was used in membrane #11

4. **Adding nanofiller solutions to a PVAm solution**: A calculated amount of nanofillers aqueous solutions and a calculated amount of PVAm aqueous solution were added to a glass bottle and mixed by an ultrasonic mixer at 2 minutes with 5 seconds pulse and 60% amplitude. The solution was then sonicated in 30 minutes with 10 seconds pulse and 20% amplitude.

5. **Adding PVA solution to the nanofiller/PVAm solutions**: A calculated amount of PVA aqueous solution was added to the CNTs dispersed PVAm solution to and sonicated in 2 minutes with 5 seconds pulse and 20% amplitude.

6. **Filtering**: To remove contaminants, polymer particles and nanofiller agglomerates that were not dissolved, the solution was filtered using a syringe and a $5\mu m$ filter. For membrane #1 the filtrated solution was re-filtrated with a $2.5\mu m$.

7. **Dilution**: In order to achieve a thinner membrane, membranes #2 and #3 were diluted by adding with 50% and 100% water to the solution, respectively.

A summary of the different membranes prepared is given in Table 14.

4.2.2 Casting of Membranes

The solutions were cast on a PSf, PVDF and CA ultrafiltration support membranes. The procedure is developed to mimic dip coating and gives a selective layer in the range of $0.2 - 1\mu m$.

1. **Attaching**: A 100 x 120 mm support membrane was taped to a 100 x 150 mm glass plate. Different support membranes were used:

- PSf 20,000 MWCO support was used for membranes #1-3 and #7-11

Table 14: Summary of the different membranes prepared in this thesis

#	Support	Nanofiller	Dilution	Filtration
1	PSf 20,000	1wt% CNT		2.5 μm
2	PSf 20,000	1wt% CNT	50 %	5 μm
3	PSf 20,000	1wt% CNT	100%	5 μm
4	PVDF 20,000	1wt% CNT		5 μm
5	CA 20,000	1wt% CNT		5 μm
6	PSf 10,000	1wt% CNT		5 μm
7	PSf 20,000	1wt% CNT		5 μm
8	PSf 20,000	1wt% AEROSIL®FS		5 μm
9	PSf 20,000	10wt% AEROSIL®FS		5 μm
10	PSf 20,000	1wt% ACEMATT®FS		5 μm
11	PSf 20,000	10wt% ACEMATT ®FS		5 μm

- PVDF 20,000 MWCO support was used for membranes #4

- CA 20,000 MWCO support was used for membranes #5

- PSf 10,000 MWCO support was used for membranes #6

2. **Washing**: The support membranes were washed with 50°C tap water for 10 minutes to remove the hydrophilic protecting layer, and then washed with distilled water.

3. **Application of solution**: The solution was dripped on the support membrane using a pipette and rolled out with a glass syringe to obtain an even distribution. The membrane was placed in an upright position to make the extra solution flow off. The procedure was repeated with the membrane placed up side down to reduce thickness differences and secure a defect free membrane.

4. **Drying**: The membranes were dried by placement in an oven at 45°C overnight.

5. **Heating**: Physical cross-linking was obtained by placing the membranes in a heater at 105°C for 1 hour.

4.3 Characterization of Membranes with SEM

All the membranes prepared and investigated in this thesis have been characterized with a scanning electron microscope (SEM) of the type S-3400N

from Hitachi High Technologies America Inc. The membrane samples were cut in strips and submerged in liquid nitrogen for 20 minutes to obtain a high enough brittleness for the selective layer to be cracked open with a nice and smooth interface. However, the polypropylene woven layer under the PSf had to be cut over with a sharp knife. The samples were then cut into 10x5 mm bits ant attached to small bolts and fixed to a metal holder with 5 other samples. These were coated with gold particles in a coating machine, before they were inserted into the SEM. Even though the SEM is supposed to have resolution down to 3 nm, the pictures became more and more grainy with higher resolution, so it is hard to analyze the surface and cross-section of the selective layers; only its thickness could roughly be measured.

4.4 Gas Permeation Tests

The gas permeation tests was performed in a high pressure rig, and the optimized operating conditions from the specialization project was used, see section 3.6. The feed gas flow rate was kept constant at 2000 ml/min and the sweep gas flow rate at 50 ml/min at 1.2 bar. The retentate gas flow was also kept at pressure of 1.2 bar. Throughout the experiments the temperature was about 30°C and the feed and sweep gas humidity 100% to maintain a water saturated membrane.

4.4.1 High Pressure Rig

All the permeation tests were conducted in a High Pressure Pilot Scale Membrane Permeation Rig, which has the purpose of examine the recovery of CO_2 from high pressure gas with FSC membranes. The operation procedure is described in a manual developed by Memfo, NTNU, based on the guidelines for HSE (Health, Safety and the Environment). The experimental set-up of the high pressure rig can be seen in Figure 42.

The feed and sweep gas were supplied from gas cylinders controlled by respectively mass flow controller (MFC) A and D. The pressure of the gases was controlled by regulators connected directly to the gas cylinder and by the back pressure controllers (BPC) 1 and 3. The valves allowing the feed and sweep gas to pass through the humidifiers 2, 3 and 6, namely valves v5, v6, v15, v16, were kept fully open at all times to maximize the humidity of the gases, and the relative humidity at varying pressures were measured by the humidifier indicator (HI) 1 and 3. Data from the pressure transmitters (PT) and mass flow controllers (MFC) were connected with Labview for automatic

Figure 42: Flowsheet of the High Pressure Pilot Scale Membrane Permeation Rig [116]
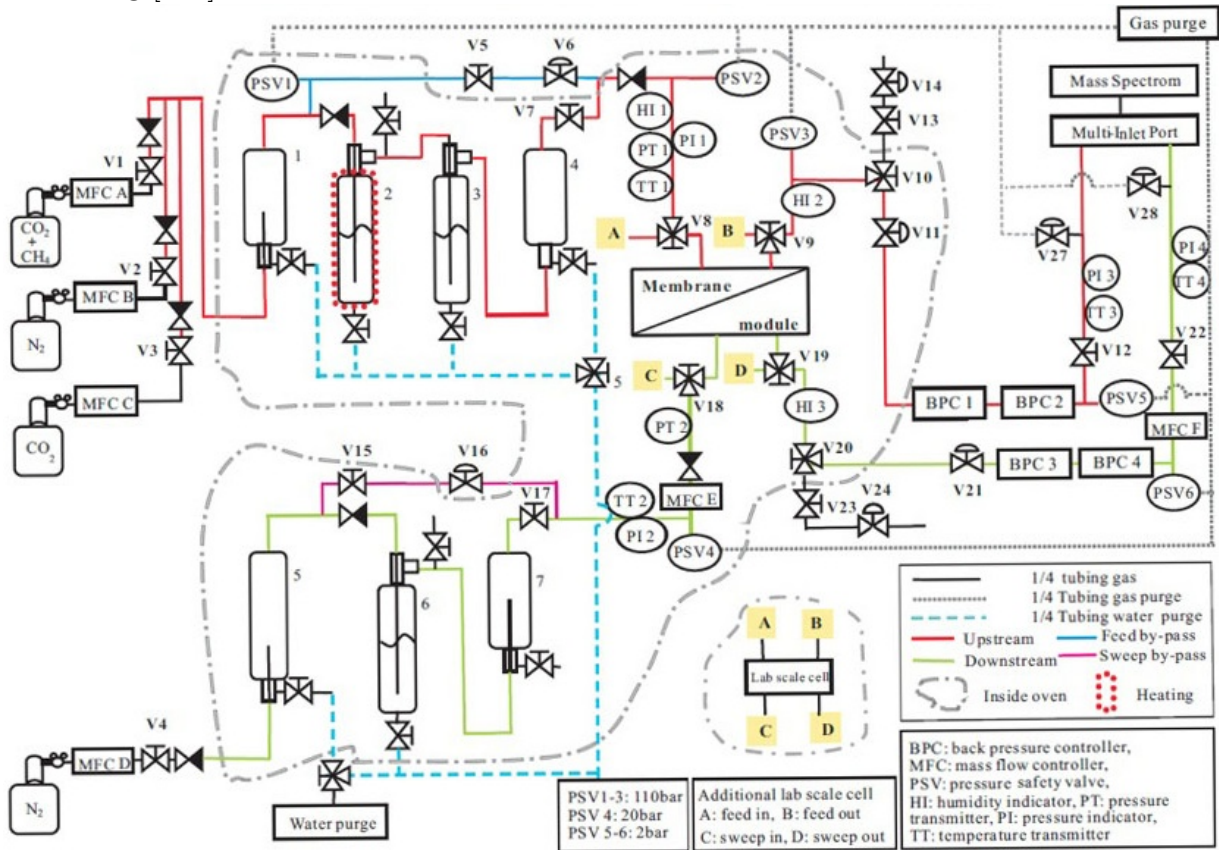
operation monitoring and controlling system [116].

The composition of the permeate gas was analyzed by a Model 8610C Gas Chromatograph from SRI Instruments. A typical run would show results in a graph similar to the one in Figure 43, with each gas component having one peak at different x-values. N_2 at around 2.190, CH_4 around 3.396 and CO_2 around 9.280. The area under the graph represents the fractional content of that component in the gas mixture. In the figure there are 5 peaks, but only three components registered. This is because one carrier registers N_2 and CH_4 whereas the other carriers registeres CO_2 in addition. A picture of the gas cromatograph used in this thesis can be seen in Figure 44.

Figure 43: Graph from analysis of permeate gas composition from GC SRI 8610C
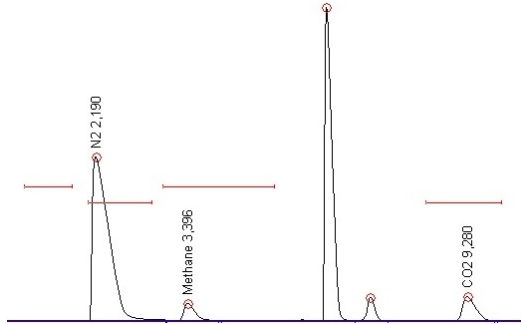
Figure 44: Picture of the GC SRI 8610C

4.4.2 Membrane Cell

For the membrane cell used for permeation tests in the high pressure rig, a circular stainless steel cell as given in Figure 45 was used. The feed is introduced at the top along with the retentate outlet, and the sweep gas inlet is at the bottom with the permeate gas outlet, as seen in Figure 46. Both the feed and sweep gas inlets are designed with a spiral current to induce a turbulent flow, which reduces potential concentration polarization problems [34].

The membrane was cut out in a circular shape with a diameter of 68 mm and placed between the top feed gas chamber and the bottom permeate gas chamber. A porous metal disk with diameter of 2 mm was positioned underneath to support the polymer membrane, and on the top of the membrane a rubber O-ring was placed, as well as in the outer O-ring track to help seal the parts. This assembly is illustrated in Figure 46. The two halves were screwed tightly together with six hexagonal head cap screws.

Figure 45: The structure of membrane cell, with the top half shown on the left and the bottom half on the right [34]
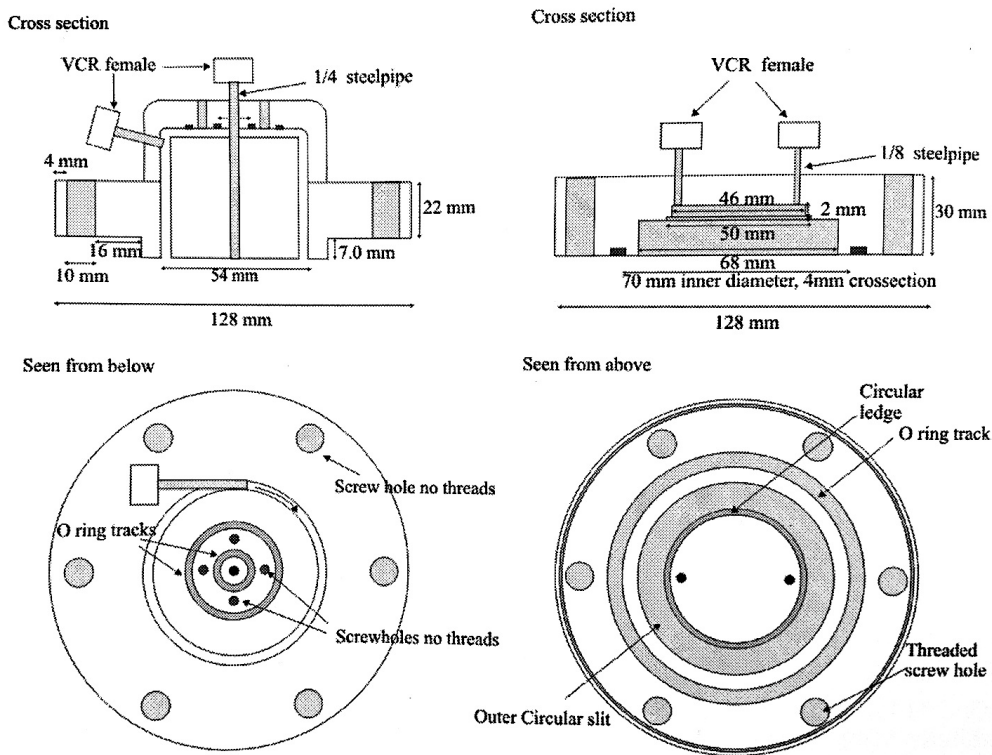
Figure 46: Picture and assembly of the membrane cell [34]
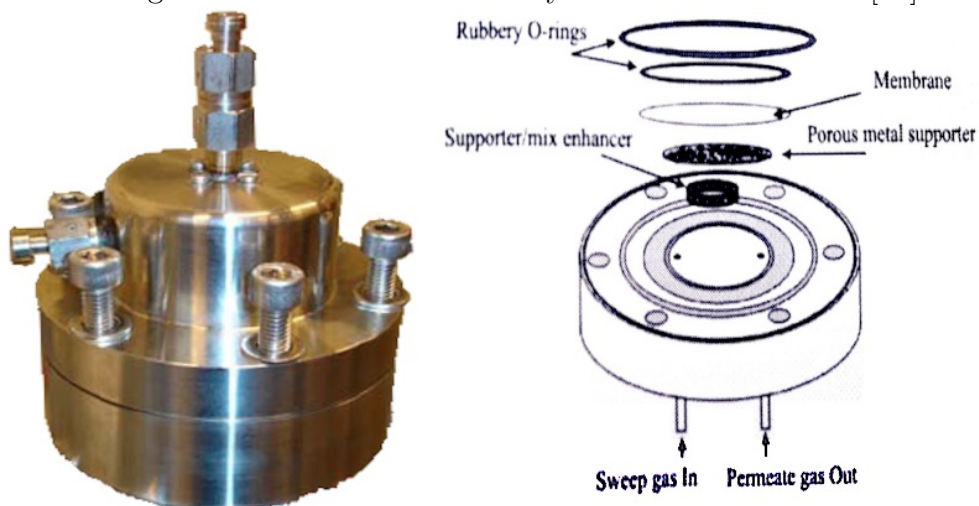
4.5   Calculation of Gas Separation Performance

CO_2 Permeance

Because of swelling, the membrane thickness is hard to measure, and therefore permeance is calculated instead of permeability, as permeance is independent of membrane thickness. The equation for calculating the CO_2 permeance is given in Equation 4.1, where P_{CO_2} is the permeance of CO_2, q_{p,CO_2} is the permeation flow rate, A is the membrane area and $\Delta p_{,CO_2}$ is the partial pressure difference between the feed side and the permeate side. The membrane radius was measured to be 2.3 cm, and thus the area is calculated to be 0.001662 m^2.

The denomination of the CO_2 permeance is $[m^3(STP)/(m^2 hbar)]$.

$$Pe_{CO_2} = \frac{q_{p,CO_2}}{A \times \Delta p_{,CO_2}} \tag{4.1}$$

CO_2/CH_4 Selectivity

The CO_2/CH_4 selectivity can be calculated both as the ratio of the CO_2 concentration in the permeate over the CH_4 concentration in the permeate or as the ratio between the CO_2 permeance over the CH_4 permeance. The latter was chosen in this project to present the permeance selectivity α_{CO_2/CH_4} as given in Equation 4.2.

$$\alpha_{CO_2/CH_4} = \frac{Pe_{CO_2}}{Pe_{CH_2}} \tag{4.2}$$

5 Results & Discussion

5.1 Characterization with SEM

5.1.1 Membrane Structure

All the pictures from the SEM characterization are appended in Appendix C, with an enumeration of membrane from Table 14. Figure 47 through Figure 50 show a cross-section of four of the membranes in different resolutions. In Figure 47 the physical structure is clear, with a woven polypropylene fiber on the bottom and a porous PSf support on top. The selective layer is not visible, as the resolution is only at 500 μm. In Figure 48 the selective layer is barely visible on the top, and the porous structure of the PSf support layer is evident. In the top section the pores are rather slim and numerous, while in the lower section the big pores open up in a from resembling a volumetric laboratory flask and the denser matter is perforated with many small pores. Figure 49 shows a clear surface with the selective layer smoothly on top and the microporous structure of the PSf underneath, and for the 5 μm resolution in Figure 50 the thickness of the selective layer is measurable, and stands in great contrast to the grainy, rough support structure with its dense and smooth composition. There seems to be an interface with very fine pores just below the selective layer, which might be a mixture of the two layers where the selective layer solution have seeped into the surface pores of the support, also known as the "pore-filling" phenomenon.

5.1.2 Support Layer

SEM-pictures of the support structure for PVDF and CA is shown in Figure 51 and Figure 52, respectively. There are obvious differences between the two. PVDF has more of an open cavern-like pore structure quite similar to that of PSf depicted in the previous section, whilst CA has a much denser and packed structure. In addition, the CA layer of the CA support membrane is only about 22 μm thick, whereas the PVDF layer is more than three times this with 77 μm.

5.1.3 Thickness of Selective Layer

The thickness of selective layer for all the membranes was measured roughly from the SEM-pictures, and is presented in Figure 53. Based on the fact that the selective layer thickness varies depending on where on the membrane the

Figure 47: Macroscale SEM-picture: Membrane #11, 500 μm
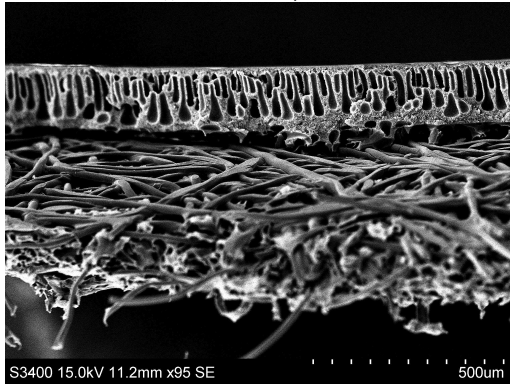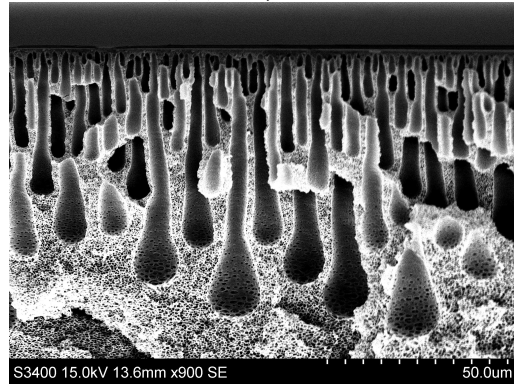

Figure 48: Microscale SEM-picture: Membrane #6, 50 μm
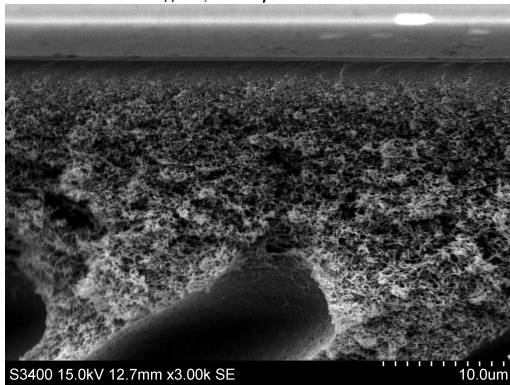

Figure 49: Microscale SEM-picture: Membrane #9, 10 μm
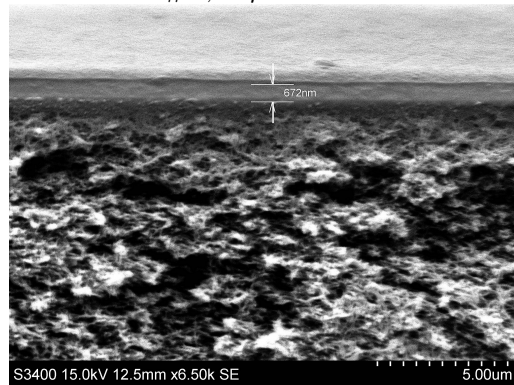

Figure 50: Nanoscale SEM-picture: Membrane #8, 5 μm

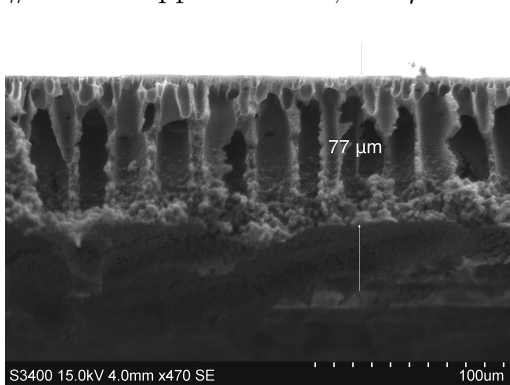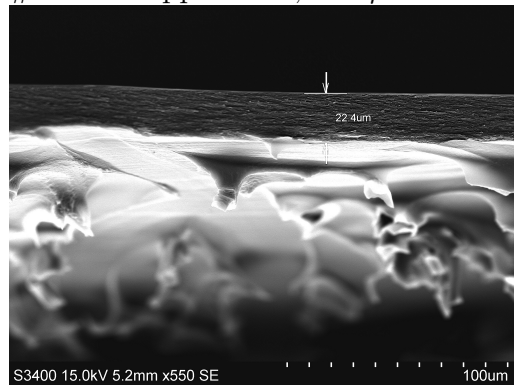Figure 51: SEM-picture of membrane #4 with support PVDF, 100 μm

Figure 52: SEM-picture of membrane #5 with support CA, 100 μm

sample is taken from, and that the blurred pictures give inaccurate measurements, an estimated margin of error lies around ± 200 nm. Still, the attained average measured thickness was 629 nm.

Figure 53: Thickness of the membranes as seen from SEM-pictures
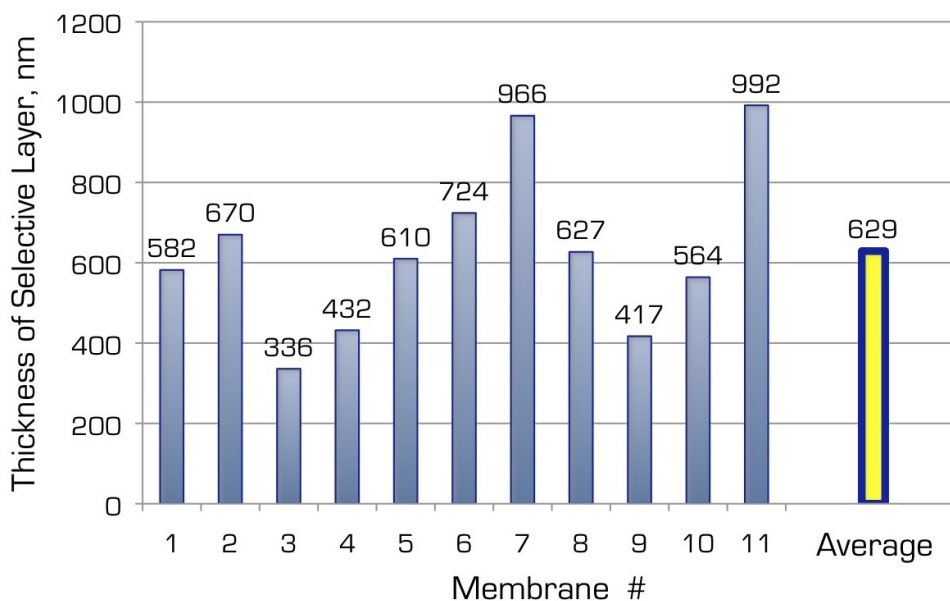
5.2 Effect of Operating Conditions

5.2.1 Effect of pressure

The effect of pressure on CO_2 permeance and CO_2/CH_4 selectivity were studied under the conditions of approximately 30°C and 100% humidity. The feed gas mass flow was kept constant at 2000 ml/min and the sweep gas flow at 50 ml/min. The feed gas pressure was varied between 10 and up to 80 bar for some membranes, and both the permeate gas pressure and the sweep gas pressure was kept constant at 1.2 bar. The reasons for not testing all 11 membranes up to 80 bar was manifold. Some membranes experienced a sudden decrease in permeation properties, probably caused by membrane rupture, whilst in some cases there were technical problems with the high pressure pilot rig leading to shutdown. Other reasons were that the pressure in the feed gas mixture bottle was decreasing beyond 80 and in some cases 60 bar, and some membrane permeation tests were terminated due to impermissible poor permeation properties.

Figure 54: Effect of pressure on CO_2 permeance
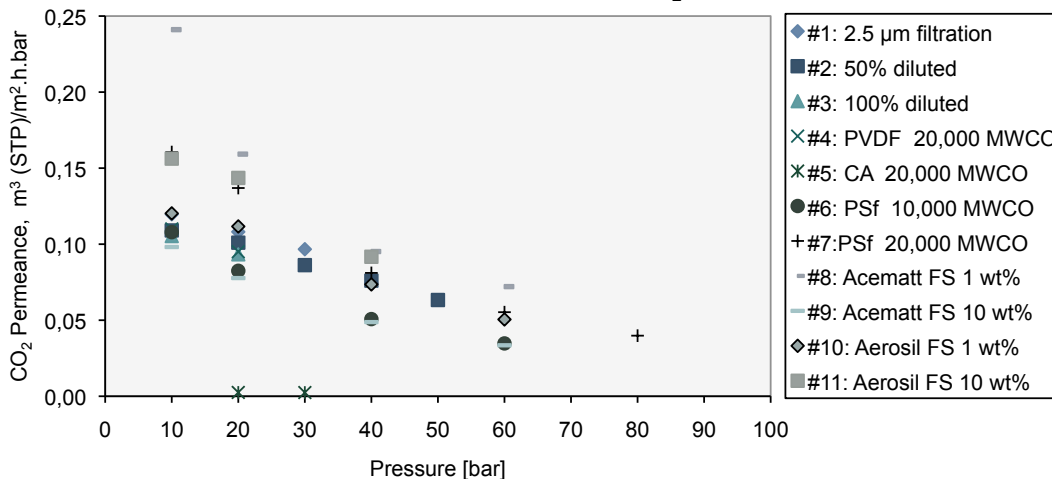
Figure 54 shows the CO_2 permeance results from the 11 different membranes tested in this thesis, and they all show a clear decrease with increasing feed gas pressure. The overall best CO_2 permeance is achieved by the membrane with the nanofiller fumed silica from Acematt at a 1wt% concentration with a CO_2 permeance of 0.159 and 0.095 $m^3(STP)/m^2.h.bar$ at feed gas pressures of 20 and 40 bar, respectively. Other good CO_2 permeances was found for the membrane with the nanofiller fumed silica from Aerosil at 10wt% concentration and the CNTs at 1% concentration. Interestingly, the membrane with the nanofiller fumed silica from Acematt at a 10wt% concentration showed the poorest permeance.

Figure 55 shows the CO_2/CH_4 selectivity results from the 11 different membranes. The general trend seems to be an increase of selectivity from 10 to 40 bar, and then a decrease from 40 bar to 80 bar. The two membranes that were tested at 80 bar show a steep decrease in selectivity from 60 bar, which gives reason to speculate that this trend would be similar for the other membranes as well. The best results varies with pressure, but the membrane with a PSf support with a MWCO of 10,000 seems to exhibit the best selectivities overall, with selectivities of 26.7 at 20 bar, 29.4 at 40 bar and 27.3 at 60 bar. Both the membranes with the nanofiller fumed silica from Acematt with a concentration at 1wt% and 10wt% also showed good selectivities, especially at 60 bar, with a selectivity of 26.9 and 27.7, respectively. The membranes with fumed silica from Aerosil as nanofiller showed the lowest selectivities at lower pressures, while the membrane with PSf MWCO 20,000 as support gave the lowest selectivity of the membranes tested at 60 bar.

Figure 55: Effect of pressure on CO_2/CH_4 selectivity
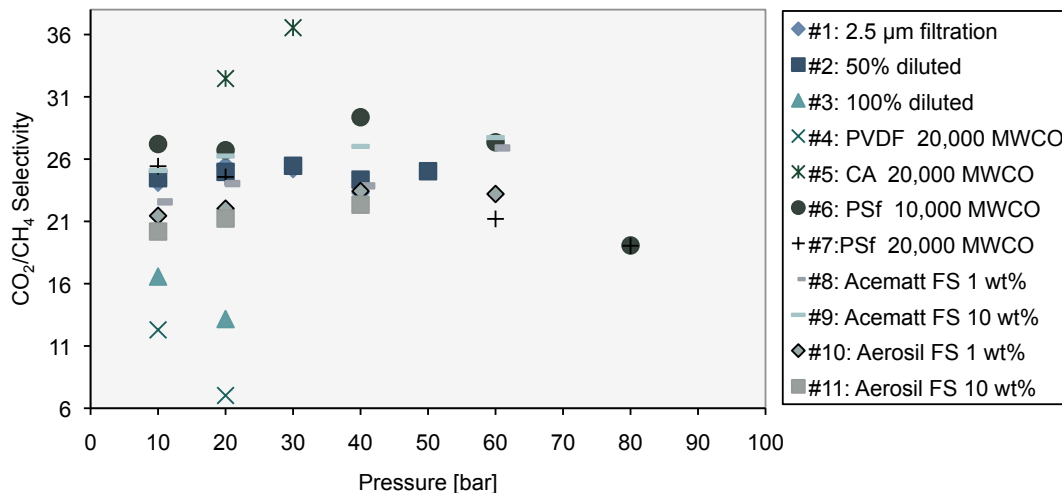
This decrease of both CO_2/CH_4 selectivity and CO_2 permeance as the feed gas pressure increases is one of the characteristics of facilitated transport membranes [117]. As the pressure increases, the limited number of available carrier sites approaches saturation, and the contribution of the facilitated transport mechanism to the permeation of CO_2 stops, and only the solution-diffusion mechanism contributes to the gas transport properties of the membrane at high pressures. This was explained by Ho and Dalrymple [118] in that a saturation of carrier occurs when the partial pressure of CO_2 is higher than a criticalCO_2 partial pressure, and a maximum concentration of the reaction product between the carrier and CO_2 is reached. This maximum will stay constant with increasing CO_2 partial pressure, and thus a higher CO_2 permeance will not be obtained from the facilitated transport mechanism. From the results of CO_2/CH_4 selectivity, this point of maximum carrier-CO_2 concentration might correspond to the observed maximum at 40 bar.

The decrease of permeance for both CO_2 and CH_4 with increasing pressure may also be attributed to the compaction of membrane at high pressures, where the physical force will pack the polymer chains closer together and reduce the free volume of the polymer inwhich the diffusion of gas molecules occur. The permeance from the solution-diffusion mechanism will then decrease. Another factor that might contribute to lower permeance at higher pressure is that the selective layer will be forced into the pores of the support layer, and thereby lose some of its excellent transport properties. This may lead to a denser membrane surface as the selective layer and support layer

are intertwined, and hinder the diffusion of gas. This may also deprive the selective layer of its CO_2/CH_4 selectivity, and be a possible influence on lower selectivity at higher pressures.

The overall decrease in selectivity over 40 bar may also be a sign of plasticization of the membrane. The higher the pressure, the higher CO_2 content in the membrane, and because of the chemical similarity of CO_2 and especially the sulfone group in the PSf support, the CO_2 will sorb into the polymer and increase the chain spacing and the mobility of the polymer chains, and thus increase the free volume of the membrane. This swelling will enhance the diffusion transport of CH_4 through the membrane, and as a consequence, the selectivity decreases. As the pressure increases, the gas molecule density increases as well, and at some point the CO_2 will have to compete not only on the sorption sites, but on the diffusion pathways in the polymer matrix as well, and this coupling effect may further decrease selectivity.

5.3 Effect of Membrane Preparation Conditions

5.3.1 Effect of Nanofillers

The four membranes with fumed silica as nanofiller is compared with the CNT-incorporated membrane in Figure 56. They all seem to exhibit the same trend of decreasing CO_2 permeance with increasing pressure, with the membrane with 1wt% FS from ACEMATT®having the highest permeance at all tested pressures. Also the membrane with 10wt% FS from AEROSIL®shows good permeance performance just over the membrane with 1wt% CNTs as nanofiller.

The general trend for the FS membranes is an increasing CO_2/CH_4 selectivity with increasing pressure, which is quite the opposite trend of the membrane with CNTs. This indicates that the role of the nanofiller is very different for FS and CNT in a membrane. The membrane with 10wt% ACEMATT®holds the best selectivity, and has a selectivity of almost 28 at 60 bar, with the 1wt% ACEMATT®at next best with a selectivity of about 27. This extraordinary behavior is hard to understand, as these fumed silica particles in theory are 9.5 μm in diameter, which is more than ten times the thickness of the selective layer. However, the solution was both sonicated and filtrated before application on the support membrane, which may have resulted in smaller FS particles in the selective layer. They are still significantly larger than the FS particles provided by AEROSIL®and the CNTs, which makes this a very interesting discovery. What advantages could drawn from having

91

microparticles in the selective layer? One speculation is that they spread evenly out in the selective layer without agglomerating, and provide a mechanical strength which prevents the membrane from compaction at higher pressures. That in turn keeps the facilitated transport mechanism from failing at higher pressures. It could also be that the microparticles block the larger pores in the surface of the porous ultrafiltration support membrane, inwhich the larger CH_4 molecules would have an easier access. In both cases a higher selectivity would result.
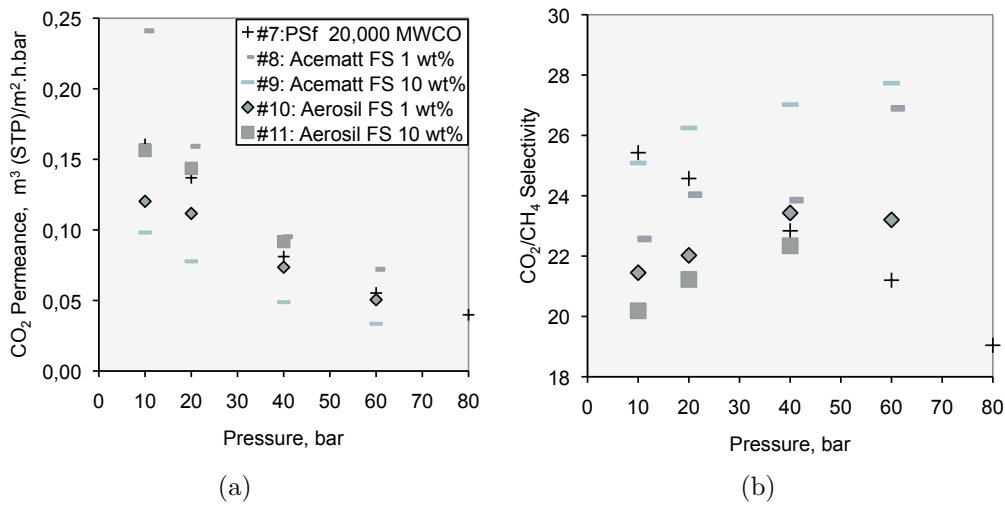
Figure 56: Effect of pressure on PVAm/PVA blend membranes with fumed silica compared to membrane #7 with 1 wt% CNTs (a): CO_2 permeance (b): CO_2/CH_4 selectivity

5.3.2 Effect of Solution Filtration

Due to the tendency for carbon nanotubes to agglomerate, the CNT-containing PVAm/PVA solution was filtrated through a filter syringe. Two different filtration methods were used in this thesis to investigate the influence of filtration on the membrane permeation properties. Both solutions were filtered through a 5 μm filter, but only one was further filtered through a 2.5 μm filter. At 10 bar, the 5 μm showed both better CO_2 permeance and better CO_2CH_4 selectivity, whereas the 2.5 μm had a slightly higher selectivity at 40 bar with 28.3 over 27.8, and an almost identical permeance around $0.08\ m^3(STP)/m^2.h.bar$. This may indicate that agglomeration size of CNT nanofillers in the selective layer has an influence on permeation properties at lower pressures, but that this difference is insignificant for pressures at

40 bar and higher. The reason for a 5 μm filtration being better than a 2.5 μm filtration is unclear, but one possible reason could be that more CNT is held back when the filtration size decreases, and as a result the product membrane contains less CNT in the selective layer. This leads to less nanofillers to strengthen the membrane and counteract the forces of high pressures leading to compaction, and thus diffusion through the compacted membrane decreases.
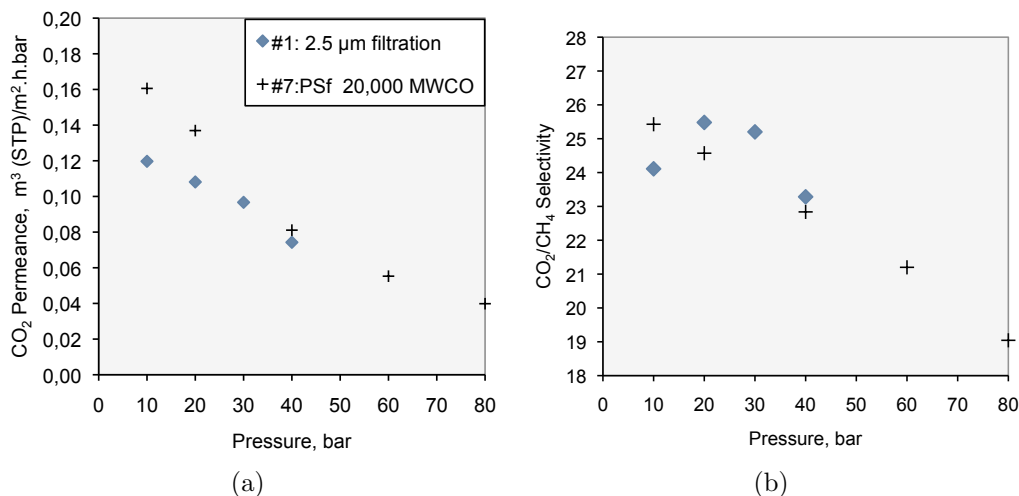

Figure 57: Effect of pressure on PVAm/PVA blend membrane filtrated with 2.5μm filter compared to membrane #7 with 5μm filter (a): CO_2 permeance (b): CO_2/CH_4 selectivity

5.3.3 Effect of Solution Dilution

As the thickness of the dense selective layers plays an important role in permeation of gas through the membrane, an idea was to try to reduce this thickness to increase the CO_2 permeance while maintaining the CO_2/CH_4 selectivity. The current application method of dripping the solution on the support membrane and spreading it out evenly by rolling a glass syringe carefully over the surface seemed unimprovable, and another approach was attempted where the solution was diluted with water by adding 50% and 100% of the weight of the solution. The same amount of diluted solution was applied on the support membrane as for the undiluted solution, and as a result the selective layer should become thinner through drying and evaporation of water. The results were, however, quite disappointing, and especially for the 100% diluted membrane, the selectivity plummeted to 16.5 and 13.2 for 10 and 20 bar as seen from Figure 58, with only mediocre CO_2 permeances of

0.105 and 0.093 $m^3(STP)/m^2.h.bar$, so further examinations at higher pressures were discontinued. The membrane with a 50% diluted selective layer actually showed higher selectivites than the undiluted one between 20 and 50 bar, with a maximum at 30 bar of 25.5, but had considerably lower CO_2 permeance at lower pressures. With increasing pressures, the permeance difference for these two membranes diminished, and at 40 bar they both had a permeance of about 0.08 $m^3(STP)/m^2.h.bar$. One reason why the selectivity results for the 100% diluted membrane were so low could be that the selective layer simply had a too low concentration of amine carriers, leading to a gas transport mainly supported by the solution-diffusion mechanism. This would also explain why the selectivity dropped with higher pressure, as there would be competitive sorption between CO_2 and CH_4. With 9 times more methane in the gas mixture, the CO_2 could easily be outstripped of sorption sites, and more methane would flow through with increasing gas molecule density due to higher pressure. This does not explain why the permeation results for the 50% diluted membrane is higher at 40 bar though. One possible thought could be that the amount of carriers in the selective layer is still high enough to keep the facilitated transport mechanism working, but that a thinner selective layer will increase the solution-diffusion permeance of CO_2 as well.

(a)   (b)
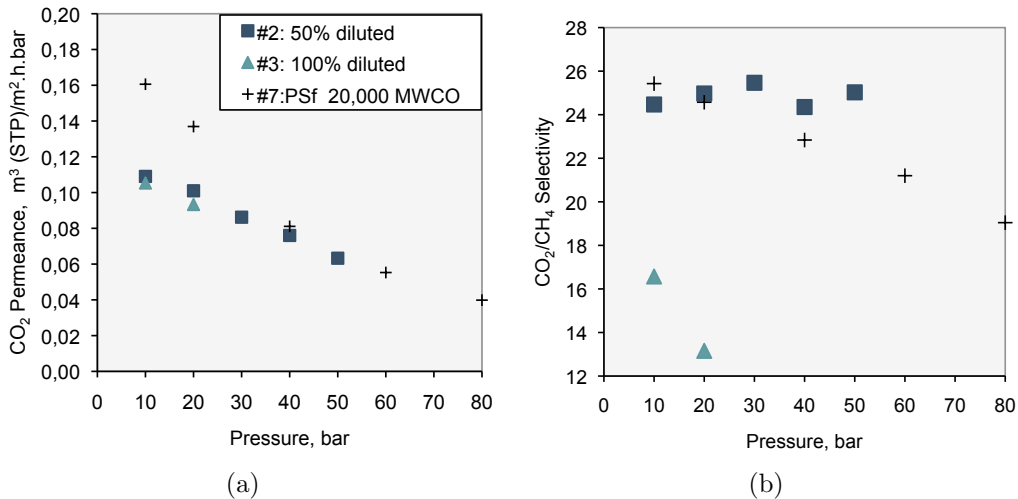
Figure 58: Effect of pressure on PVAm/PVA blend membrane diluted with 50% and 100% water compared to the undiluted membrane #7 (a): CO_2 permeance (b): CO_2/CH_4 selectivity

5.3.4 Effect of Support Membrane

The results from the permeation tests of the three different support membranes PVDF, CA and PSf, all with 20,000 MWCO, are rather surprising and confusing. The CA membrane shows a very high CO_2/CH_4 selectivity, but has an extremely low CO_2 permeance, as seen from Figure 59. This may be attributed to the dense-looking layer as seen from the SEM-picture in Figure 52. As with all polymer membranes there exists a trade-off between selectivity and permeance, and this would be an extreme example of that. Another theory could be that the selective layer and the porous CA support have mixed together in an interfacial layer, creating a dense barrier for the gas molecules to cross. The PVDF support membrane on the other hand, shows an opposite tendency, namely a moderately high permeance, but an intolerable low selectivity. As seen from the aforementioned SEM-picture, the pores of the PVDF were quite open and large, and could theoretically transport large volumes of gas, but with a lower selectivity for increasing pressures. However, these results are not quite convincing, and any conclusions would have to require several parallel tests to find accordance with the very low selectivity of PVDF and the very low permeance of CA.
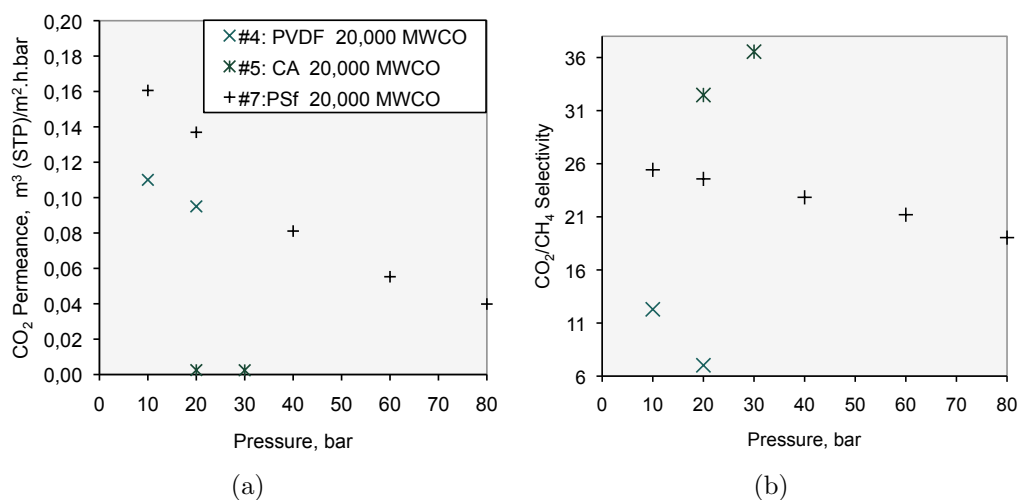
Figure 59: Effect of pressure on PVAm/PVA blend membrane with PVDF and CA support compared to membrane #7 with a PSf support (a): CO_2 permeance (b): CO_2/CH_4 selectivity

95

5.3.5 Effect of MWCO in Support Membrane

The CO_2 permeance and CO_2/CH_4 selectivity for two membranes with identical preparation procedures, except that one membrane was cast on a 10,000 MWCO PSf support and the other on 20,000 MWCO PSf support. Figure 60 shows a similar decreasing permeance trend with increasing pressure, with a higher permeance for the higher MWCO membrane. This may be explained by the fact that the pores are in average twice as big, and thereby permit more gas to flow through the membrane. As expected, the selectivity for the higher MWCO membrane is therefore lower than for the 10,000 MWCO membrane. However, the 10,000 MWCO membrane undergoes an increase in selectivity between 20 and 40 bar, despite the decreasing trend with increasing pressure. There are several explanations for why these two membranes behave differently. Primarily, the smaller pore size of the lower MWCO membrane could prevent the selective layer from being pressed down into the pores (pore-filling phenomenon) so that the facilitated transport mechanism is less affected. Secondarily, the lower MWCO membrane has a denser pore structure, and may not be as susceptible to compaction at higher pressures. Nonetheless, this advantage over the 20,000 MWCO membrane seems to disappear when the pressure approaches 80 bar, at which the MWCO difference in selectivity has vanished.

(a)   (b)
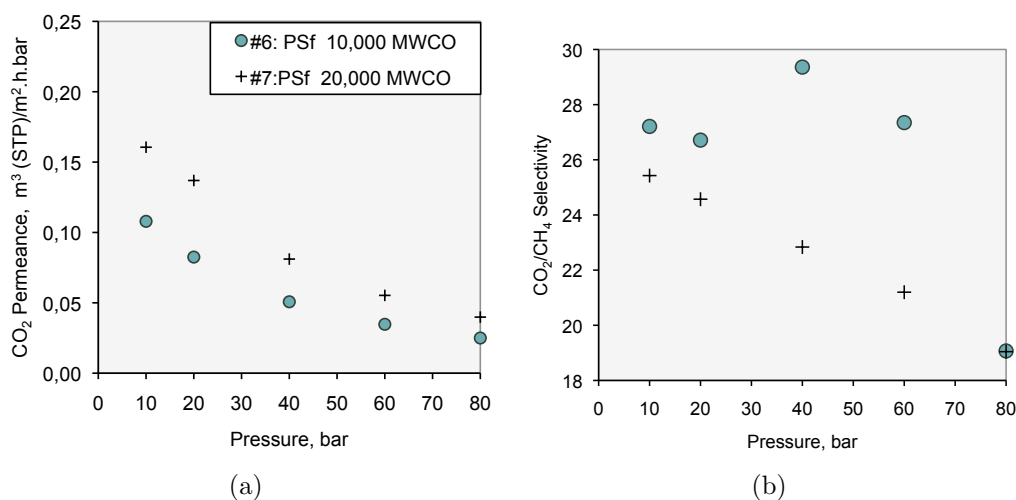
Figure 60: Effect of pressure on PVAm/PVA blend PSf MWCO 10,000 support membrane compared to membrane #7 with a PSf MWCO 20,000 support (a): CO_2 permeance (b): CO_2/CH_4 selectivity

5.4 Uncertainty

One large source of uncertainty was the fact that both permeance and selectivity of the membrane changes over time, and even though results were usually noted and conditions changed every 1-2 hours, experiments over longer time showed that the values of permeance and selectivity continue to decrease even after 4 hours, and indicates that the membrane needs quite a long time to stabilize.

The potential for human errors when preparing the membranes is quite large, especially for the method of selective layer solution casting on the support membrane. In theory, this should give an even top layer with equal thickness everywhere, but since the layer is so thin, there is no doubt that lab scale casting produces an unevenly distributed selective layer, which in turn gives varying results in the peremation tests. Another factor is that the membrane must be treat with utter care when prepared, since even a fingerprint may destroy the selective layer before dried and cross-linked.

Other significant sources of uncertainty are the conditions inside the membrane cell in the pilot rig. Changing of gas bottles, changing of permeation gas analysis method and drying of pipelines to remove harmful condensation due to sudden or even short term pressure drops may cause irreparable damage to the membrane, thereby inhibiting the separation performance of the membrane.

6 Conclusion

Eleven different polyvinyl amine/polyvinyl alcohol blend fixed-site carrier membranes were prepared with different nanofillers, supports and techniques, and good results were achieved for many of them. The best overall performance was by a PVAm/PVA blend FSC membrane with 1wt% fumed silica from ACEMATT®cast on a 20,000 MWCO polysulfone membrane, with a CO_2/CH_4 selectivity of 26.9 and a CO_2 permeance of 0.072 $m^3(STP)/m^2.h.bar$ at a pressure of 60 bar. The general trend was a decreasing permeance with increasing pressure until the carriers in the selective layer were saturated. The decrease in permeance at high pressure was much more insignificant than at lower pressures, which is a typical trait for facilitated transport membranes. The selectivity trend seemed to reach a maximum at 40 bar, before decreasing with further increasing pressure.

The 10,000 MWCO PSf membrane seemed to be advantageous at pressures of 40 and 60 bar, with CO_2/CH_4 selectivities close to 30 with only slightly lower CO_2 permeance compared to the 20,000 MWCO PSf membrane. There were indications that a thinner selective layer may lead to higher selectivities, but a good way of further reducing the thickness of the selective layer is needed. From the results it appears that both CA and PVDF are unfit to act as support for the PVAm/PVA blend FSC membrane for natural gas sweetening at high pressures, but further investigation would be needed before excluding these polymers. Good results in both selectivity and permeance was found for the membranes with fumed silica, and this should be investigated more in detail in order to improve the existing FSC membrane.

The nanoparticle reinforced PVAm/PVA blend FSC membrane combines the advantages of both the polymers PVAm and PVA in addition to the dispersed nanofillers to achieve higher and better CO_2/CH_4 selectivity and CO_2 permeance, as well as high stability to high pressures up to 80 bar. Characteristics of the membrane makes it simple and practical to be reproduced or up-scaled, and the materials are commercially available and inexpensive. The use of membranes in natural gas sweetening has a promising future, and may already replace conventional sweetening methods both offshore and in smaller natural gas processing plants. The greatest challenges are the need for costly pretreatment of the natural gas before entering the membrane system, and developing cheap membranes with sufficient permeability and selectivity to surmount the Robeson's upper bound. This would to reduce the required membrane area and the energy needed for permeate gas recompression.

References

[1] J. Conti and P. Holtberg, "International energy outlook 2011," tech. rep., U.S. Energy Information Administration, 2011.

[2] S. Sridhar, B. Smitha, and T. M. Aminabhavi, "Separation of carbon dioxide from natural gas mixtures through polymeric membranes—a review," *Separation and Purification Reviews*, vol. 36, no. 2, pp. 113–174, 2007.

[3] "U.s. environmental protection agency." http://www.epa.gov/ climatechange/.

[4] "Intergovernmental panel on climate change." http://www.ipcc.ch/publications_and_data/ar4/syr/en/spms3.html.

[5] "Natural gas supply association." http://www.naturalgas.org/ environment/naturalgas.asp.

[6] A. J. Kidnay and W. R. Parrish, *Natural Gas Processing*. CRC Press, Taylor and Francis Group, 2006.

[7] "Ssb: Naturgass." http://www.ssb.no/naturgass/.

[8] Statoil, "Statoilhydro's annual and sustainability report," tech. rep., Statoil, 2008.

[9] M. Ree and O. K. Helgesen, "Snøhvit-co2 sprenger reservoaret," *Teknisk Ukeblad*, 2011.

[10] S. Sridhar, R. Veerapur, M. Patil, K. Gudasi, and T. Aminabhavi, "Matrimid polyimide membranes for the separation of carbon dioxide from methane," *Journal of Applied Polymer Science*, vol. 106, pp. J. Appl. Polym. Sci. 106 1585–1594, 2007.

[11] J. S. Gudmundsson, "Produsert og prosessert naturgass." Teaching slide in TPG4140 Natural Gas, November 2006.

[12] R. W. Baker, *Membrane Technology and Applications*. John Wiley and Sons, Ltd, 2nd ed., 2004.

[13] L. Deng, T.-J. Kim, M. Sandru, and M.-B. Hägg, *PVA/PVAm Blend FSC Membrane for Natural Gas Sweetening*. PhD thesis, NTNU, 2009.

[14] T. D. C. Company, "Gas sweetening," tech. rep., The Dow Chemical Company, 1998.

[15] P. Bernardo, E. Drioli, and G. Golemme, "Membrane gas separation: A review/state of the art," *Industrial and Engineering Chemistry Research (ACS Publication)*, vol. 48, pp. 4638–4661, 2009.

[16] H. Lin, E. V. Wagner, R. Raharjo, B. D. Freeman, and I. Roman, "High-performance polymer membranes for natural-gas sweetening," *Advanced Materials*, vol. 18, pp. 39–44, 2006.

[17] R. W. Baker, "Future directions of membrane gas separation technology," *Industrial and Engineering Chemistry Research*, vol. 41, pp. 1393–1411, 2002.

[18] M. Mulder, *Basic Principles of Membrane Technology*. Kluwer Academic Publishers, second edition ed., 1996.

[19] M. Kraume, *Membranverfahren in der kommunalen und industriellen Abwasserbehnadlung*. Fachgebiet Verfahrenstechnik, TU Berlin, 2010.

[20] Y. Zhang, Z. Wang, and S. Wang, "Selective permeation of co2 through new facilitated transport membranes," *Desalination*, vol. 145, pp. 385–388, 2002.

[21] M.-B. Hägg, "Nanostructured membranes for gas separation," FUNMAT, 2006.

[22] H. Yang, Z. Xu, M. Fan, R. Gupta, R. B. Slimane, A. E. Bland, and I. Wright, "Progress in carbon dioxide separation and capture: A review," *Journal of Environmental Sciences*, vol. 20, pp. 14–27, 2008.

[23] C. A. Scholes, S. E. Kentish, and G. W. Stevens, "Carbon dioxide separation through polymeric membrane systems for flue gas applications," *Recent Patents on Chemical Engineering*, vol. 1, pp. 52–66, 2008.

[24] D. Shekhawat, D. R. Luebke, and H. W. Pennline, "A review of carbon dioxide selective membranes - a topical report," tech. rep., National Energy Technology Laboratory, United States Department of Energy, 2003.

[25] M.-B. Hägg, *Handbook of Membrane Separations*. Taylor and Francis Group, 2009.

[26] H. Yang, Z. Xu, M. Fan, R. Gupta, R. B. Slimane, A. E. .Bland, and I. Wright, "Progress in carbon dioxide separation and capture: A review," *Journal of Environmental Sciences*, vol. 20, pp. 14–27, 2008.

[27] Y. Yampolskii and B. Freeman, *Membrane Gas Separation*. Wiley, 2010.

[28] P. Scholander, "Oxygen transport through hemoglobin solution," *Science*, vol. 131, p. 585, 1960.

[29] W. J. W. III and W. L. Robb, "Carbon dioxide-oxygen separation: Facilitated transport of carbon dioxide across a liquid film," *Science*, vol. 156, no. 3781, pp. 1481–1484, 1967.

[30] H. C. Ferraz, L. T. Duarte, M. D. Luccio, T. L. M. Alves, A. C. Habert, and C. P. Borges, "Recent achievements in facilitated transport membranes for separation processes," *Brazilian Journal of Chemical Engineering*, vol. 24, pp. 101–118, 2007.

[31] Y. Jiang, Z. Zhou, Z. Jiao, L. Li, Y. Wu, and Z. Zhang, "So2 gas separation using supported ionic liquid membranes," *Journal of Physical Chemistry*, vol. 111, pp. 5058–5061, 2007.

[32] P. Scovazzo, J. Kieft, D. Finan, C. Koval, D. DuBois, and R. Noble, "Gas separations using non-hexafluorophosphate [pf6]- anion supported ionic liquid membranes," *Journal of Membrane Science*, vol. 238, pp. 57–63, 2004.

[33] Y. Yampolskii, I. Pinnau, and B. D. Freeman, *Materials Science of Membranes for Gas and Vapor Separation*. John Wiley and Sons Ltd,, 2006.

[34] L. Deng, *Development of Novel PVAm/PVA Blend FSC Membrane for CO2 Capture*. PhD thesis, NTNU, 2009.

[35] K. Ebert, D. Fritsch, J. Koll, and C. Tjahjawiguna, "Influence of inorganic fillers on the compaction behaviour of porous polymer based membranes," *Journal of Membrane Science*, vol. 233, pp. 71–78, 2004.

[36] J. D. Wind, C. Staudt-Bickel, D. R. Paul, and W. J. Koros, "The effects of crosslinking chemistry on co2 plasticization of polyimide gas separation membrane," *Industrial and Engineering Chemistry Research*, vol. 41, pp. 6139–6148, October 2002.

[37] D. D. Iarikov and S. T. Oyama, *Membrane Science and Technology, Chapter 5 - Review of CO2/CH4 Separation Membranes*, vol. 14. Elsevier B.V., 2011.

[38] L. M. Robeson, "Correlation of separation factor versus permeability for polymeric membranes," *Journal of Membrane Science*, vol. 62, pp. 165–185, February 1991.

101

[39] L. M. Robeson, "The upper bound revisited," *Journal of Membrane Science*, vol. 320, pp. 390–400, April 2008.

[40] K. Ghosal and B. Freeman, "Gas separation using polymer membranes; an overview," *Polymers for Advanced technology*, vol. 5, pp. 673–697, 1994.

[41] A. F. Ismail, T. D. Kusworo, A. Mustafa, and H. Hasbullah, *Understanding the solution-diffusion mechanism in gas separation membrane for engineering students.* PhD thesis, Universiti Teknologi Malaysia, 2005.

[42] Y. Zhang, Z. Wang, and S. Wang, "A study on facilitated transport membranes for removal of co2 from ch4," *Fuel Chemistry Division Preprints*, vol. 47, no. 1, pp. 73–74, 2002.

[43] T.-J. Kim, B. Li, and M.-B. Hägg, "Novel fixed-site–carrier polyvinylamine membrane for carbon dioxide capture," *Wiley InterScience*, 2004.

[44] C. Dong, Z. Wang, C. Yi, and S. Wang, "Preparation of polyvinylamine/polysulfone composite hollow-fiber membranes and their co2/ch4 separation performance," *Journal of Applied Polymer Science*, vol. 101, pp. 1885–1891, 2006.

[45] M. P. Chenar, M. Soltanieh, T. Matsuura, A. Tabe-Mohammadi, and K. Khulbe, "The effect of water vapor on the performance of commercial polyphenylene oxide and cardo-type polyimide hollow fiber membranes in co2/ch4 separation applications," *Journal of Membrane Science*, vol. 285, pp. 265–271, 2006.

[46] S. Li, Z. Wang, X. Yu, J. Wang, and S. Wang, "High-performance membranes with multi-permselectivity for co2 separation," *Advanced Materials*, pp. 1–5, 2012.

[47] C. A. Scholes, G. W. Stevens, and S. E. Kentish, "Membrane gas separation applications in natural gas processing," *Fuel*, 2012.

[48] V. E. Reinsch, A. R. Greenberg, S. S. Kelley, R. Peterson, and L. J. Bond, "A new technique for the simultaneous, real - time measurement of membrane compaction and performance during exposure to high - pressure gas," *Journal of Membrane Science*, vol. 171, pp. 217–228, 2000.

[49] R. W. Baker and K. Lokhandwala, "Natural gas processing with membranes: An overview," *Industrial and Engineering Chemistry Research*, vol. 47, pp. 2109–2121, 2008.

[50] T.-J. Kim, M. W. Uddin, M. Sandru, and M.-B. Hägg, "The effect of contaminants on the composite membranes for co2 separation and challenges in up-scaling of the membranes," *Energy Procedia*, vol. 4, pp. 737–744, 2011.

[51] G. C. Institute and P. Brinckerhoff, *Accelerating the Uptake of CCS: Industrial Use of Captured Carbon Dioxide*. Global CCS Institute, 2011.

[52] D. Yang, Z. Wang, J. Wang, and S. Wang, "Parametric study of the membrane process for carbon dioxide removal from natural gas," *Industrial and Engineering Chemistry Research*, vol. 48, pp. 9013–9022, 2009.

[53] B. Bhide and S. Stern, "Membrane processes for the removal of acid gases from natural gas. i. process configurations and optimization of operating conditions," *Journal of Membrane Science*, vol. 81, pp. 209–237, 1993.

[54] M. Chen, G. Goff, and J. Vanommeren, "Process for separating co2 and h2s from hydrocarbons." United States Patent No. US 4589896, 1986.

[55] P. Cook and M. Losin, "Membranes provide cost effective natural gas processing," *Hydrocarbon Processing*, vol. 74, pp. 79–84, 1995.

[56] L. Peters, A. Hussain, M. Follmann, T. Melin, and M.-B. Hägg, "Co2 removal from natural gas by employing amine absorption and membrane technology—a technical and economical analysis," *Chemical Engineering Journal*, vol. 172, pp. 952–960, 2011.

[57] E. F. et al., "Membrane processes for pre-combustion carbon dioxide capture: a parametric study," *Energy*, vol. 31, pp. 2556–2570, 2006.

[58] T. C. Merkel, M. Zhou, and R. W. Baker, "Carbon dioxide capture with membranes at an igcc power plant," *Journal of Membrane Science*, vol. 289, pp. 441– 450, 2012.

[59] K. Guthrie, "Capital cost estimating," *Chemical Engineering*, March 1969.

[60] L. B. et al., *Systematic Methods of Chemical Process Design,*. Prentice Hall International Series, 1999.

[61] B. D. B. et al., "Hybrid process for the removal of acid gases from natural gas," *Journal of Membrane Science*, vol. 140, pp. 27–49, 1998.

[62] "U.s. energy information administration." http://www.eia.doe.gov/.

[63] C. Richardson's, ed., *Chemical Engineering - Chemical Engineering Design*, vol. 6. Elsevier Butterworth-Heinemann,, 4th ed., 2005.

[64] e. a. J. Hao, "Upgrading low-quality natural gas with h2s- and co2-selective polymer membranes. part i. process design and economics of membrane stages without recycle streams," *Journal of Membrane Science*, vol. 209, pp. 177–206, 2002.

[65] A. Brunetti, F. Scura, G. Barbieri, and E. Drioli, "Membrane technologies for co2 separation," *Journal of Membrane Science*, vol. 359, pp. 115–125, 2009.

[66] M. B. Hägg, L. Deng, and A. Hussain, "Natural gas sweetening by the use of a selective membrane process," *Journal of Membrane Science*, vol. 24, pp. 426–436, 2004.

[67] C. Chi and H. Lee, "Natural gas purification by 5a molecular sieves and its design method," *AIChE Symposium Series*, vol. 69, 1973.

[68] R. W. Baker, "Future directions of membrane gas separation technology," *Industrial and Engineering Chemistry Research*, vol. 41, pp. 1393–1411, 2002.

[69] K. Kamide and M. S. M., "Cellulose and cellulose derivatives: recent advances in physical chemistry.," in *Advances in Polymer Science*, Springer, 1987.

[70] S. Stern, P. Rice, and J. Hao, "Upgrading natural gas via membrane separation processes," tech. rep., Federal Energy Technology Center U.S.Department of Energy Morgantown,WV, 2000.

[71] Y. Yampolskii, "Polymeric gas separation membranes," *Macromolecules*, vol. 45, pp. 3298–3311, 2012.

[72] C. A. Scholes, S. E. Kentish, and G. W. Stevens, "Effects of minor components in carbon dioxide capture using polymeric gas separation membranes," *Separation and Purification Reviews*, vol. 38, pp. 1–44, 2009.

[73] Cameron, "Cynara®co2 membrane separation solutions." Product Information, 2010.

[74] Honeywell, "Uop separex ™membrane technology." Product Information, 2009.

[75] J. LePree, "Membranes for gas separation," *Chemical Engineering*, 2012.

[76] I. Pinnau and L. Toy, "Gas and vapor transport properties of amorphous perfluorinated copolymer membranes based on 2,2-bistrifluoromethyl-4,5- difluoro-1,3-dioxole/tetrafluoroethylene," *Journal of Membrane Science*, vol. 109, pp. 125–133, 1996.

[77] P. Hale and K. Lokhandwala, "Advances in membrane materials provide new solutions in the gas business," tech. rep., Randall Gas Technologies-ABB Lummus Global Inc. and Membrane Technology and Research, Inc., 2004.

[78] M. Sandru, T.-J. Kim, and M.-B. H€agg, "High molecular fixed-site-carrier pvam membrane for co2 capture," *Desalination*, vol. 240, pp. 298–300, 2009.

[79] L. Deng, T.-J. Kim, and M.-B. Hägg, "Facilitated transport of co2 in novel pvam/pva blend membrane," *Journal of Membrane Science*, vol. 340, pp. 154–163, 2009.

[80] L. Deng and M.-B. Hägg, "Swelling behavior and gas permeation performance of pvam/pva blend fsc membrane," *Journal of Membrane Science*, vol. 363, pp. 295–301, 2010.

[81] H. Matsuyama, M. Teramoto, and H. Sakakura, "Selective permeation of co 2 through poly(2-(n,n-dimethyl) aminoethyl methacrylate) membrane prepared by plasma-graft polymerization technique," *Journal of Membrane Science*, vol. 114, pp. 193–200, 1996.

[82] J. Shen, L. Wu, L. Zhang, Y. Dong, H. Chen, and C. Gao, "Selective permeation of co2 through a composite membrane with a separation layer of 2-n,n-dimethyl aminoethyl methacrylate and acrylic acid copolymer," *Desalination*, vol. 193, pp. 327–334, 2006.

[83] J. Shen, J. Qiu, L. Wu, and C. Gao, "Facilitated transport of carbon dioxide through poly(2-n,n-dimethyl aminoethyl methacrylate-co-acryclic acid soidum) membrane," *Separation and Purification Technology*, 2006.

[84] Z. Wang, C. Yi, Y. Zhang, J. Wang, and S. Wang, "Co2-facilitated transport through poly(n-vinyl-γ-sodium aminobutyrate-co-sodium acrylate)/polysulfone composite membranes," *Journal of Applied Polymer Science*, vol. 100, pp. 275–282, 2006.

[85] J. Zou and W. W. Ho, "Co2-selective polymeric membranes containing amines in crosslinked poly(vinyl alcohol)," *Journal of Membrane Science*, vol. 286, pp. 310–321, 2006.

[86] "Gas transport property of polyallylamine–poly(vinyl alcohol)/ polysulfone composite membranes,"

[87] E. of pressure and temperature on fixed-site carrier membrane for CO2 separation from natural gas *Frontiers in Chemical Engineering China*, vol. 4, pp. 127–132, 2010.

[88] X. Yu, Z. Wang, Z. Wei, S. Yuan, J. Zhao, J. Wang, and S. Wang, "Novel tertiary amino containing thin film composite membranes prepared by interfacial polymerization for co2 capture," *Journal of Membrane Science*, vol. 362, pp. 265–278, 2010.

[89] Y. Zhang, Z. Wang, and S. Wang, "Novel fixed-carrier membranes for co2 separation," *Journal of Applied Polymer Science*, vol. 86, pp. 2222–2226, 2002.

[90] L. Deng and M.-B. Hägg, *Carbon Nanotube Reinforced PVAm/PVA Blend FSC Nanocomposite Membrane for CO2 separation*. PhD thesis, NTNU, 2009.

[91] W. Chen, X. Tao, P. Xue, and X. Cheng, "Enhancedmechanicalproperties and morphological characterizations of poly(vinyl alcohol)–carbon nanotube composite films," *Applied Surface Science*, vol. 252, pp. 1404–1409, 2005.

[92] F. Peng, C. Hu, and Z. Jiang, "Novel ploy(vinyl alcohol)/carbon nanotube hybrid membranes for pervaporation separation of benzene/cyclohexane mixtures," *Journal of Membrane Science*, vol. 297, pp. 236–242, 2007.

[93] Z. Wang, *Reinforcing Efficiency of Carbon Nanotubes in Poly (vinyl alcohol) Composites*. PhD thesis, university of London, 2007.

[94] T. C. Merkel, B. D. Freeman, R. J. Spontak, Z. He, I. Pinnau, P. Meakin, and A. J. Hill, "Ultrapermeable, reverse-selective nanocomposite membranes," *Science Magazine*, vol. 296, pp. 519–522, 2002.

[95] Z. He, I. Pinnau, and A. Morisato, "Nanostructured poly(4-methyl-2-pentyne)/silica hybrid membranes for gas separation," *Desalination*, vol. 146, pp. 11–15, 2002.

[96] M. Wahab, A. Ismail, and S. Shilton, "Studies on gas permeation performance of asymmetric polysulfone hollow fiber mixed matrix membranes using nanosized fumed silica as fillers," *Separation and Purification Technology*, vol. 86, pp. 41–48, 2011.

[97] L. Shao, J. Samseth, and M.-B. Hägg, "Crosslinking and stabilization of nanoparticle filled pmp nanocomposite membranes for gas separations," *Journal of Membrane Science*, vol. 326, pp. 285–292, 2008.

[98] Y. Kong, H. Du, J. Yang, D. Shi, Y. Wang, Y. Zhang, and W. Xin, "Study on polyimide/tio, nanocomposite membranes for gas separation," *Desalination*, vol. 146, pp. 49–55, 2002.

[99] S. Kim, L. Chen, J. K. Johnson, and E. Marand, "Polysulfone and functionalized carbon nanotube mixed matrix membranes for gas separation: Theory and experiment," *Journal of Membrane Science*, vol. 294, pp. 147–158, 2007.

[100] J. Ahn, W.-J. Chung, I. Pinnau, and M. D. Guiver, "Polysulfone/silica nanoparticle mixed-matrix membranes for gas separation," *Journal of Membrane Science*, vol. 314, pp. 123–133, 2008.

[101] M. W. Uddin, *Durability of PVAm/PVA Blend Membrane in Natural Gas Sweetening*. PhD thesis, NTNU, 2012.

[102] "Polymers netbase." Polymers Netbase, http://www.polymersnetbase.com/.

[103] "Polymer processing." Polymer Processing, http://www.polymerprocessing.com/.

[104] D. M. Marquis, É. Guillaume, and C. Chivas-Joly, *Nanocomposites and Polymers with Analytical Methods: Properties of Nanofillers in Polymer*. InTech, 2011.

[105] E. T. Thostenson, Z. Ren, and T.-W. Chou, "Advances in the science and technology of carbon nanotubes and their composites: a review," *Composites Science and Technology*, vol. 61, pp. 1899–1912, October 2001.

[106] E. T. Thostenson, Z. Ren, and T.-W. Chou, "Advances in the science and technology of carbon nanotubes and their composites: a review," *Composites Science and Technology*, vol. 61, pp. 1899–1912, 2001.

[107] "Azom." http://www.azom.com/article.aspx?ArticleID=1386.

[108] "Aerosil." http://www.aerosil.com/product/aerosil/.

[109] T. C. M. et al., "Ultrapermeable, reverse-selective nanocomposite membranes," *Science magazine*, vol. 296, April 2002.

[110] "Aerosil." http://www.specialchem4adhesives.com/tds/aerosil-150/evonik/1586/index.aspx.

[111] E. Industries, "Product information acematt®3300." http://www.acematt.com/.

[112] L. K. Wang, J. P. Chen, Y.-T. Hung, and N. K. Shammas, eds., *Membrane and Desalination Technologies*, vol. 13. Humana Press, 2011.

[113] N. N. Li, A. G. Fane, W. S. W. Ho, , and T. Matsuura, eds., *Advanced Membrane Technology and Applications*. John Wiley and Sons, Inc., 2008.

[114] M. J. El-Hibri and D. R. Paul, "Gas transport in poly(viny1idene fluoride): Effects of uniaxial drawing and processing temperature," *Journal of Applied Polymer Science*, vol. 31, pp. 2533–2560, 1986.

[115] S. Sridhar, R. Suryamurali, B. Smitha, and T. Aminabhavi, "Development of crosslinked poly(ether-block-amide) membrane for co2/ch4 separation," *Colloids and surfaces*, vol. 297, no. 1-3, pp. 267–274, 2007.

[116] M.-B. Hägg, L. Deng, M. W. Uddin, and T.-J. Kim, *Operation Manual for High Pressure Pilot Scale Membrane Permeation Rig (Level 1)*. Memfo, NTNU, December 2010.

[117] R. Quinn, J. Appleby, and G. Pez, "New facilitated transport membranes for the separation of carbon dioxide from hydrogen and methane," *Journal of Membrane Science*, vol. 104, pp. 139–146, 1996.

[118] W. Ho and D. Dalrymple, "Facilitated transport of olefins in ag+- containing polymer membranes," *Journal of Membrane Science*, vol. 91, pp. 13–25, 1994.

Appendices

A   Risk Assessment

	Utarbeidet av	Nummer	Dato
	HMS-avd.	HMSRV2603	04.02.11
	Godkjent av	Side	Erstatter
	HMS-avd.	Side	

Unit: Memfo Group, Dep. Chemical Engineering

Line manager: May-Britt Hägg

Participants in the identification process (including their function): May-Britt Hägg (Group leader), Liyuan Deng (post doc), Anders Sørheim (student)

Date: 14.09.2011

Signatures:

ID no.	Activity from the Identification process form	Potential undesirable incident/strain	Likelihood (1-5)	Consequence: Human (A-E)	Environment (A-E)	Economy/ material (A-E)	Reputation (A-E)	Risk value Human	Comments/status Suggested measures
1	High Pressure	Leakage	4	A	B	A	A		
2	Methane	Explotion	1	E	B	D	E		
3	CO_2	Leakage	4	A	A	A	A		
4	Carbon nano tube	Inhale powder	1	B	C	A	A		
5	Condensation	Formation of hydrates will affect MFC Malfunction of valves	3	A	A	A	A		
6	Membrane rapture	and pressure build up	3	A	A	A	A		
7	Power failure	No ventilation, no control	3	A	A	A	A		

B   Original Master's Thesis Proposal

Proposal for master thesis for Anders Sørheim

Testing and Optimization of Nanoparticles Reinforced PVAm/PVA Blend

FSC Membranes for High Pressure Natural Gas Sweetening

This project will focus on the testing and optimizing of the nano particles reinforced polyvinylamine/polyvinylalcohol (PVAm/PVA) blend membrane for natural gas sweetening at high pressures. The objective of this project is to improve the target membrane to be more resistant at high pressures (up to 80bar) without the loss of the CO_2 separation efficiency. Carbon nanotubes (CNTs) and fumed silica nano particles (SiO_2) have been considered as the nano-fillers in making the PVAm/PVA blend nanocomposite membranes. The functions of the CNTs and SiO_2 in this membrane include the reinforcement of the membrane mechanical properties and the improvement of the membrane swelling capacity (and hence CO_2 separation efficiency) at high pressures due to the nano spacer effect of the nanofillers.

The scope of this work can be specified as follows:

(1) Optimization of the membrane preparation conditions based on the membrane separation performance at high pressures. The effects of support membrane and membrane thickness will be investigated and the optimized membrane preparation condition determined.

(2) Permeation tests of the membranes at high pressures (10bar, 20bar, 40bar, 60bar, 80bar) at constant flow rate. The membranes will be prepared with various thicknesses, compositions and support membranes. The tests will be performed in an advanced high-pressure pilot scale rig with an automatic operation monitoring and controlling system and a mass spectrometer for determining permeate gas composition.

(3) Characterizations of the membranes using SEM.

The master thesis will be delivered by the end of July 2012.

Supervisor: Prof. May-Britt Hägg

Co-supervisor: Xuezhong He

28th of February 2012

C   Tabulated Results

Membrane	Selectivity							
	10	**20**	**30**	**40**	**50**	**60**	**70**	**80**
#1: 2.5 µm filtration	24,111	25,481	25,202	23,283				
#2: 50% diluted	24,469	24,973	25,465	24,353	25,027			
#3: 100% diluted	16,572	13,159						
#4: PVDF 20,000 MWCO	12,293	7,023						
#5: CA 20,000 MWCO		32,470	36,550					
#6: PSf 10,000 MWCO	27,210	26,713		29,361		27,349		19,069
#7:PSf 20,000 MWCO	25,427	24,572		22,837		21,200		19,044
#8: Acematt FS 1 wt%	22,568	24,035		23,854		26,897		
#9: Acematt FS 10 wt%	25,085	26,247		27,021		27,731		
#10: Aerosil FS 1 wt%	21,449	22,024		23,430		23,202		
#11: Aerosil FS 10 wt%	20,186	21,226		22,341				

Membrane	Permeance							
	10	**20**	**30**	**40**	**50**	**60**	**70**	**80**
#1: 2.5 µm filtration	0,120	0,108	0,097	0,074				
#2: 50% diluted	0,109	0,101	0,086	0,076	0,063			
#3: 100% diluted	0,105	0,093						
#4: PVDF 20,000 MWCO	0,110	0,095						
#5: CA 20,000 MWCO		0,003	0,002					
#6: PSf 10,000 MWCO	0,108	0,083		0,051		0,035		0,025
#7:PSf 20,000 MWCO	0,161	0,137		0,081		0,055		0,040
#8: Acematt FS 1 wt%	0,241	0,159		0,095		0,072		
#9: Acematt FS 10 wt%	0,098	0,078		0,049		0,034		
#10: Aerosil FS 1 wt%	0,120	0,112		0,074		0,051		
#11: Aerosil FS 10 wt%	0,156	0,144		0,092				

D SEM-pictures
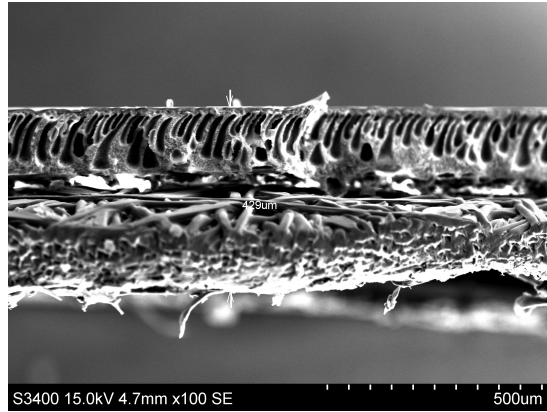
(a) Membrane #1, 500 μm
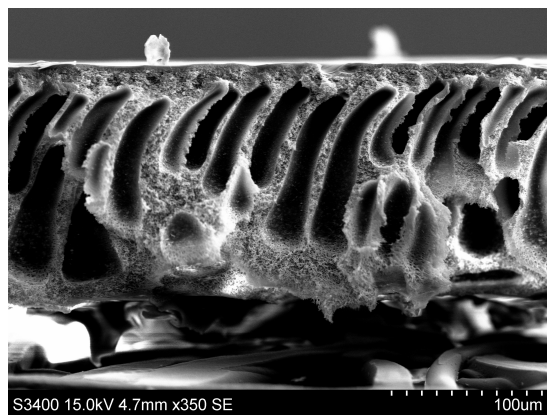
(b) Membrane # 1, 100 μm
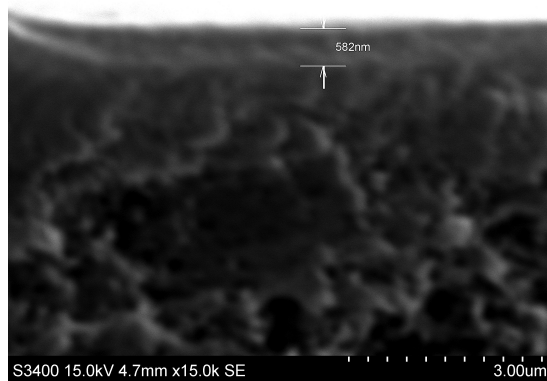
(c) Membrane #1, 3 μm

Figure 61: SEM-pictures of membrane #1
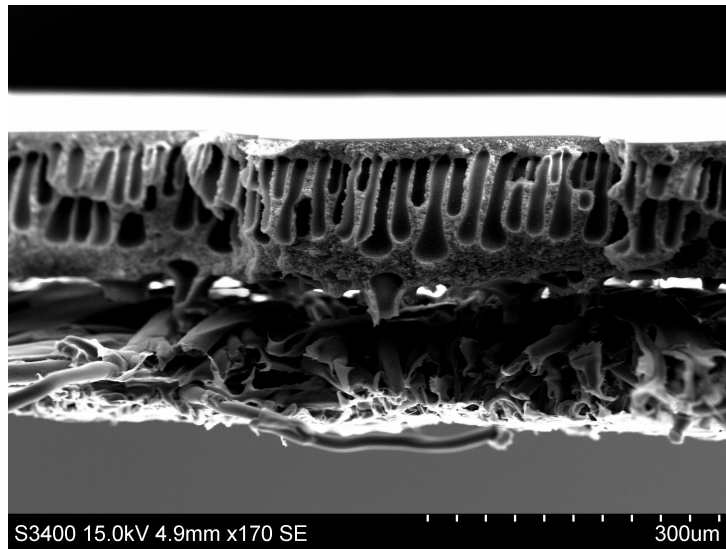
(a) Membrane #2, 300 μm
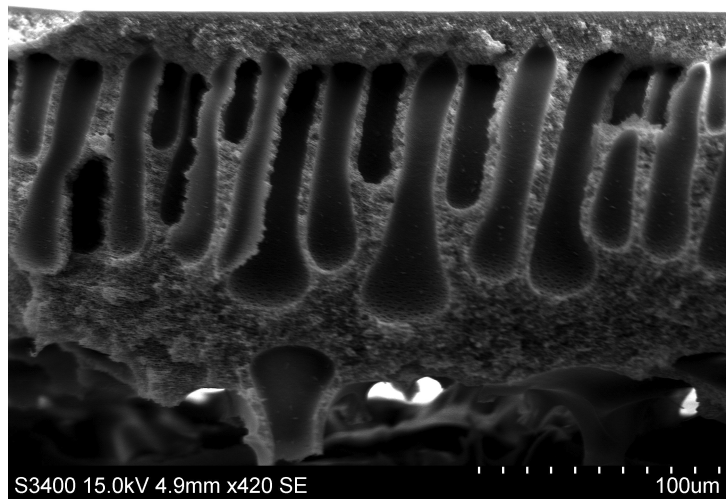
(b) Membrane #2, 100 μm
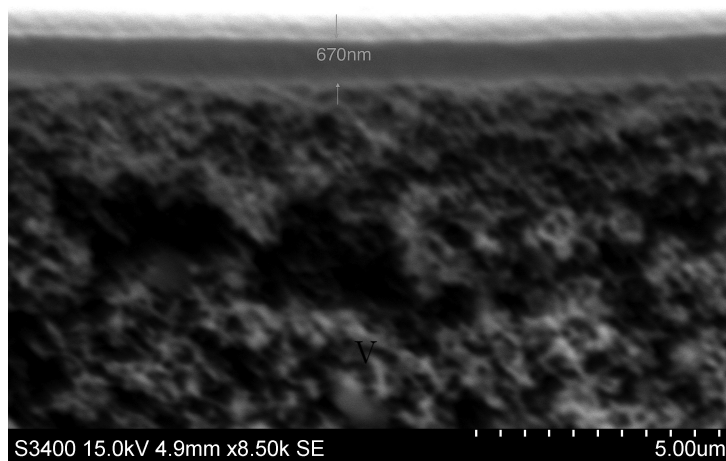
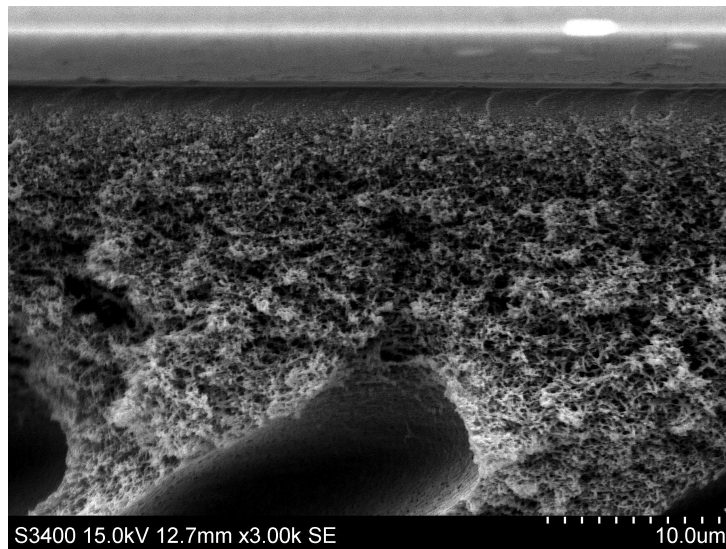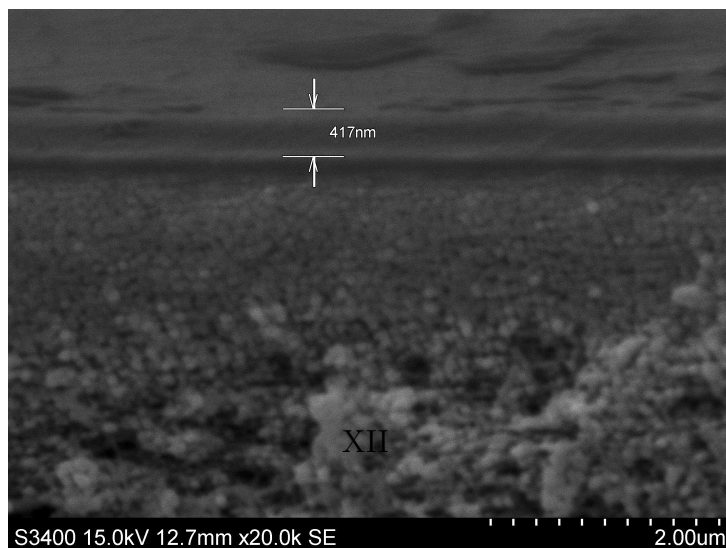(c) Membrane #2, 5 μm

Figure 62: SEM-pictures of membrane #2
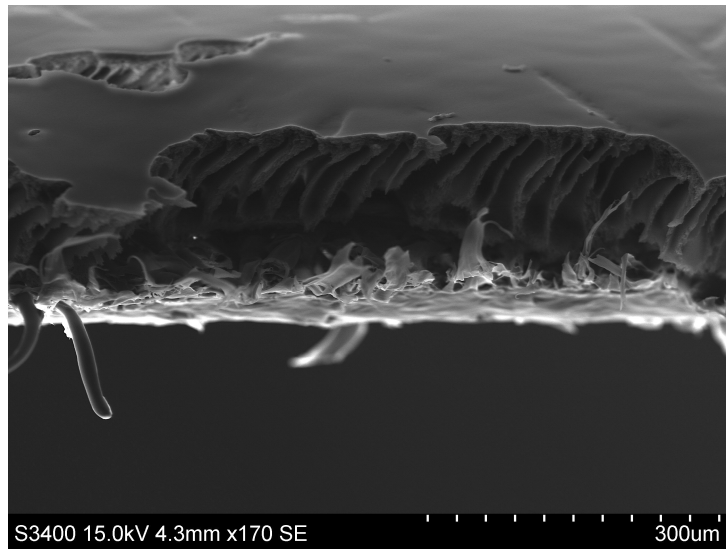
(a) Membrane #3, 300 μm
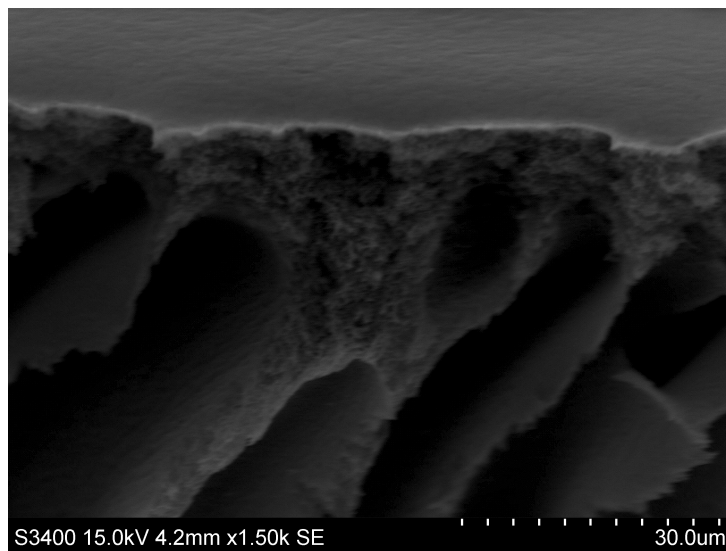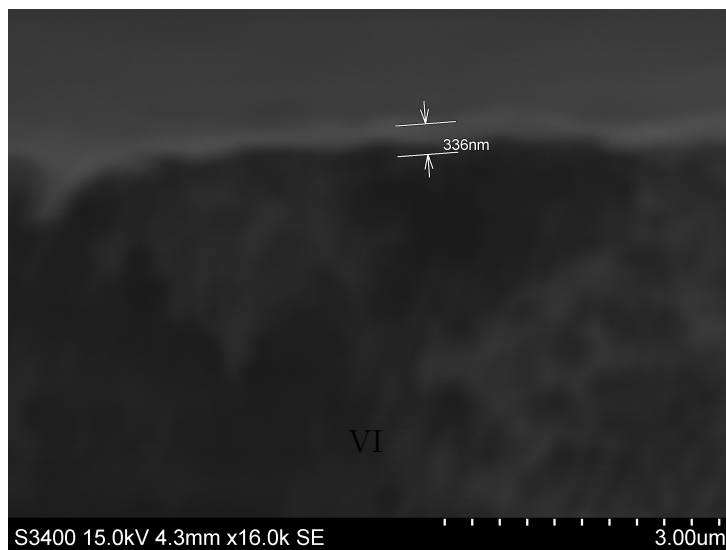
(b) Membrane #3, 30 μm

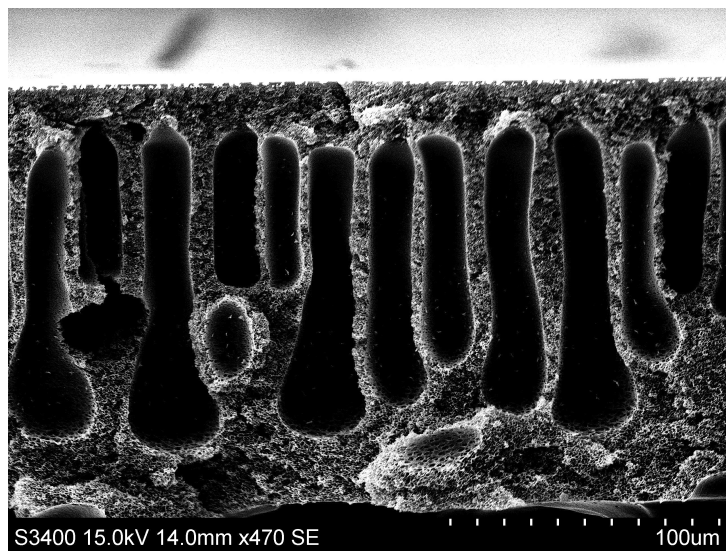

(c) Membrane #3, 3 μm

Figure 63: SEM-pictures of membrane #3
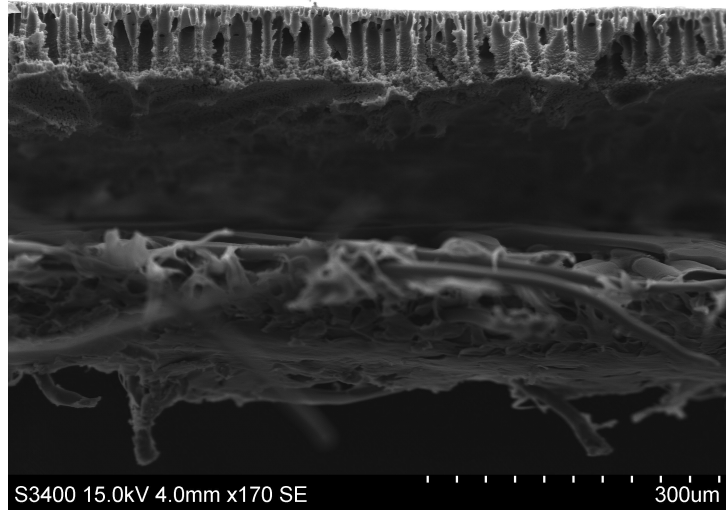
(a) Membrane #4, 300 μm
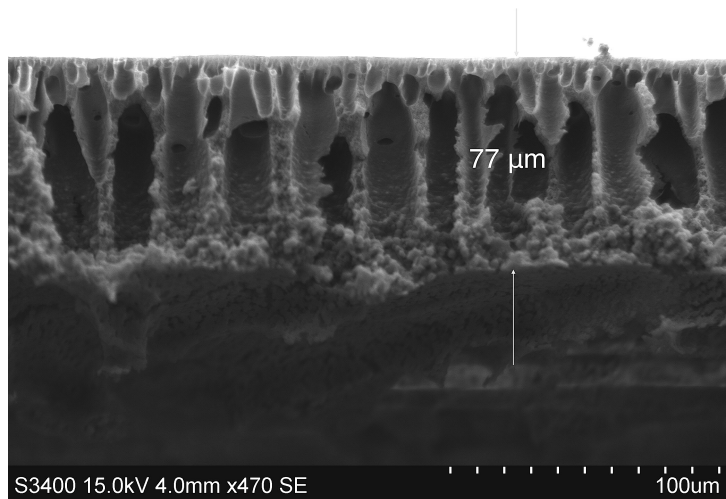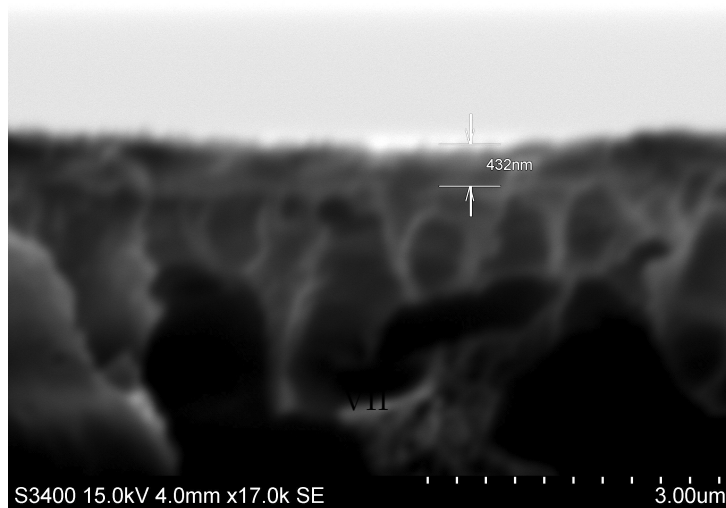
(b) Membrane #4, 100 μm

(c) Membrane #4, 3 μm

Figure 64: SEM-pictures of membrane #4
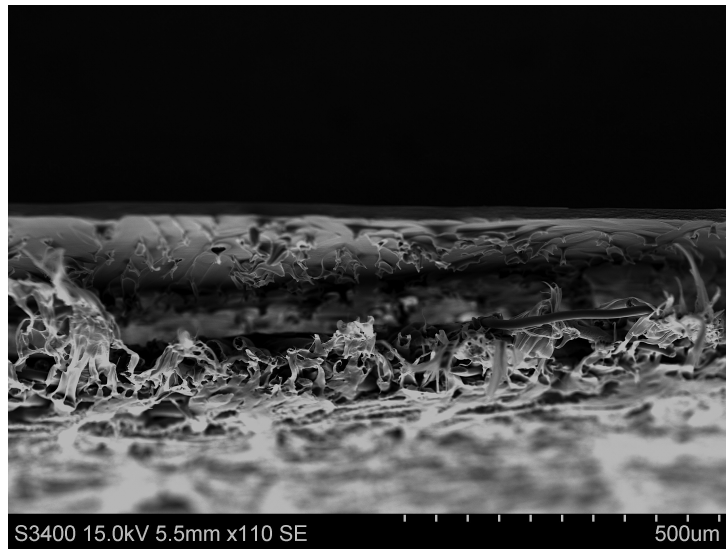
(a) Membrane #5, 500 μm
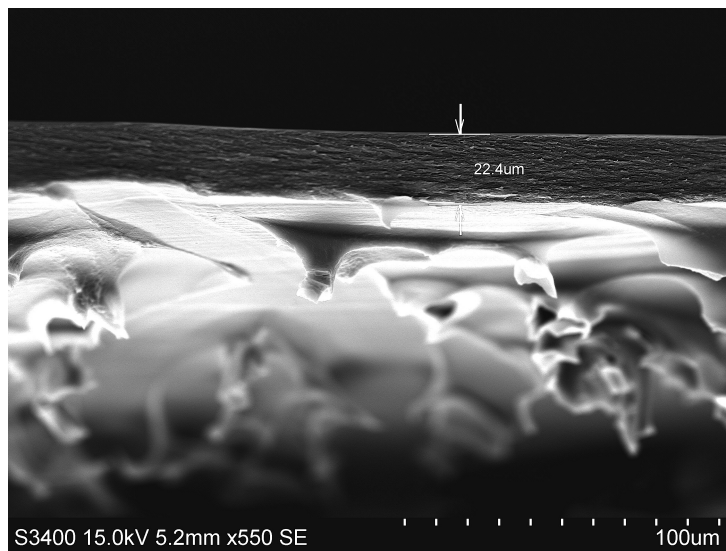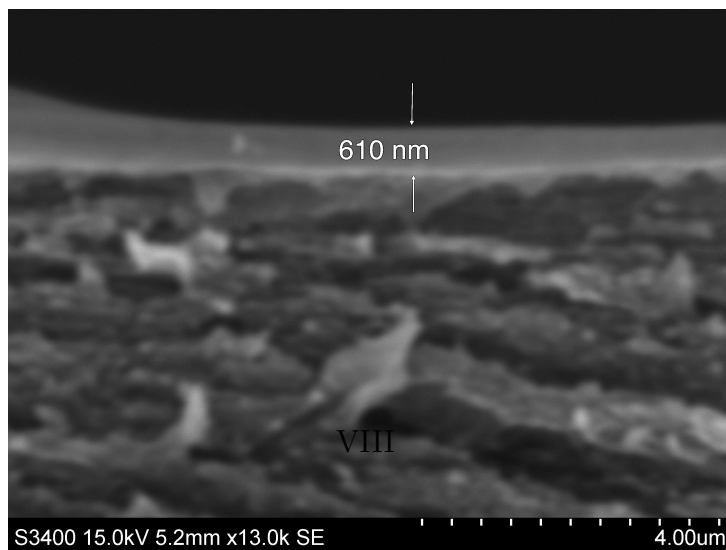
(b) Membrane #5, 100 μm

(c) Membrane #5, 4 μm

Figure 65: SEM-pictures of membrane #5
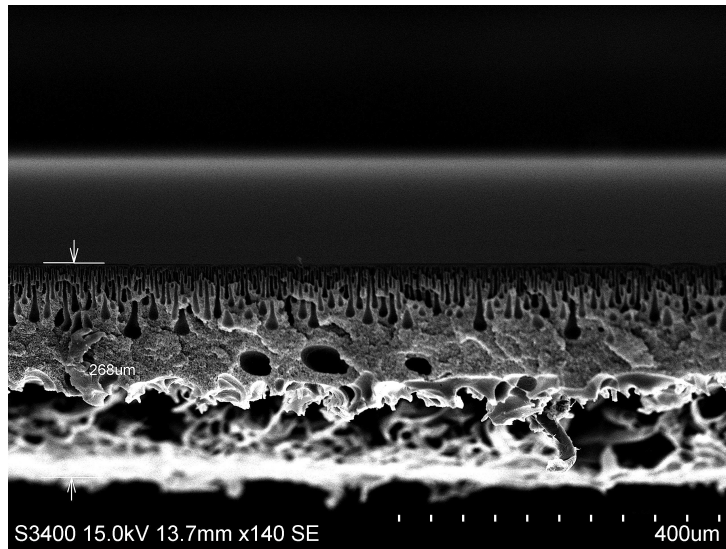
(a) Membrane #6, 400 μm
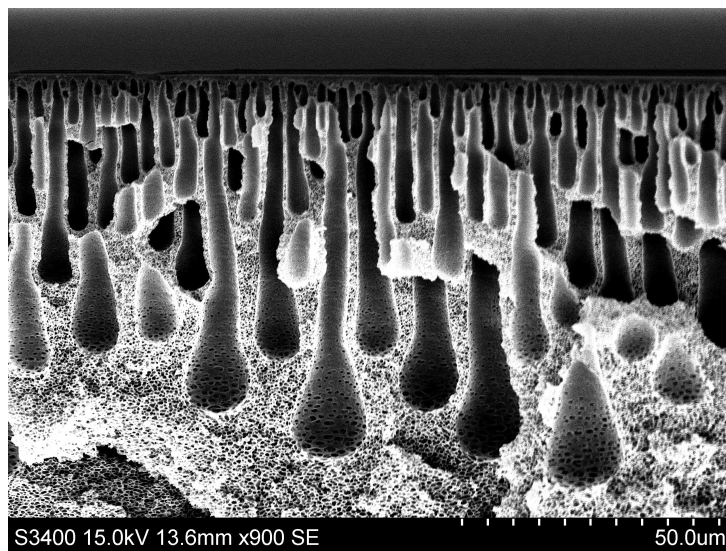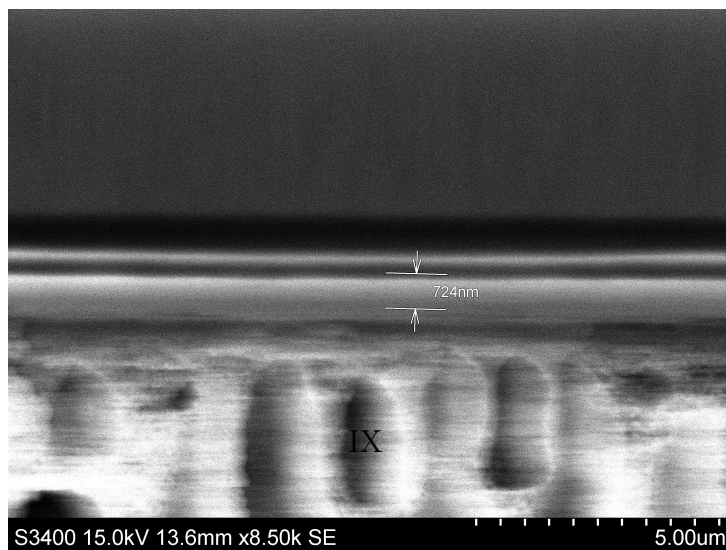
(b) Membrane #6, 50 μm

(c) Membrane #6, 5 μm

Figure 66: SEM-pictures of membrane #6
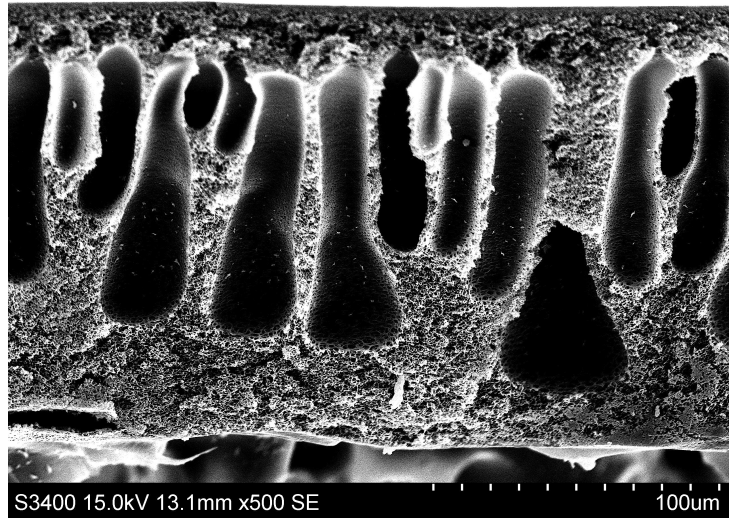
(a) Membrane #7, 100 μm
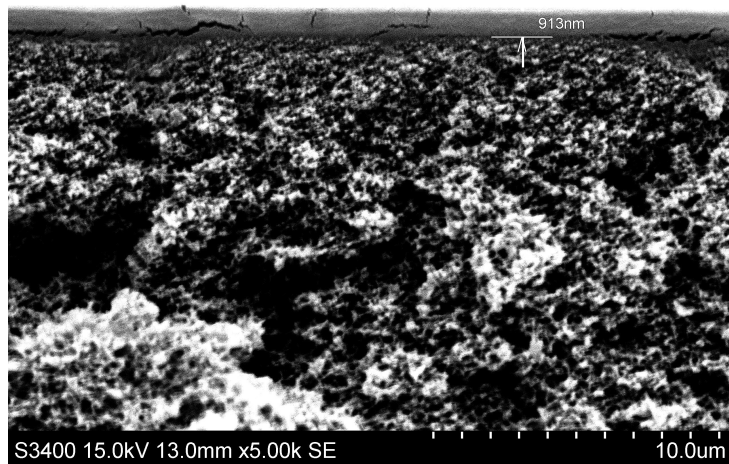
(b) Membrane #7, 10 μm
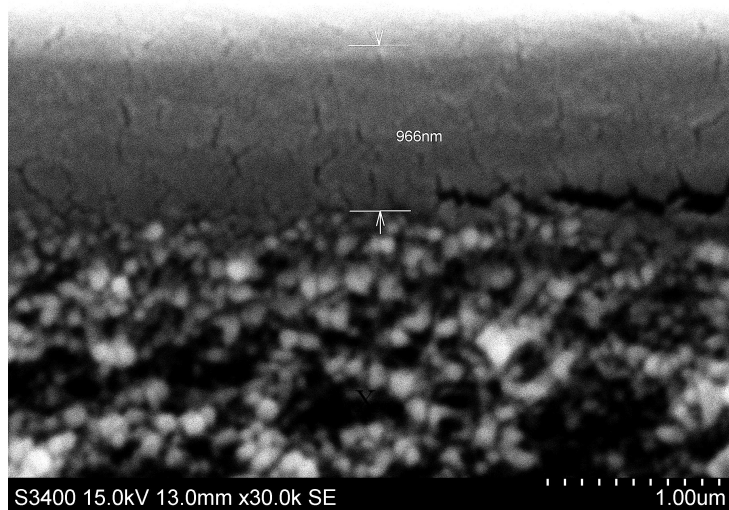
(c) Membrane #7, 1 μm

Figure 67: SEM-pictures of membrane #7
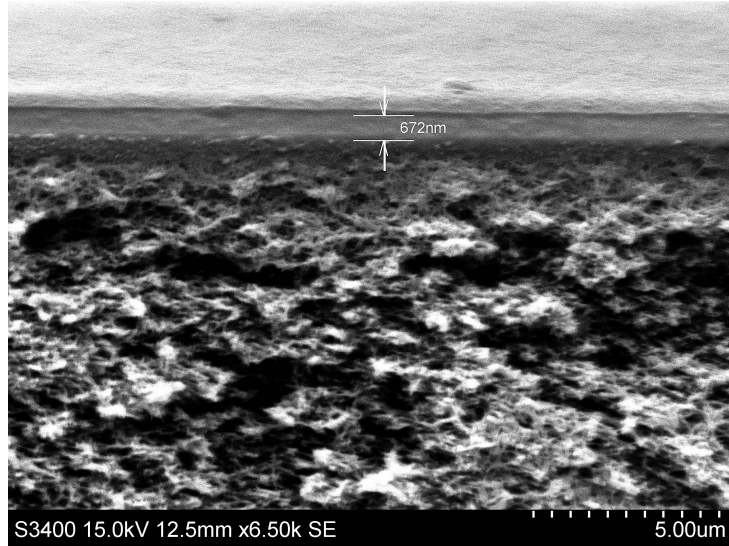
(a) Membrane #8, 5 μm
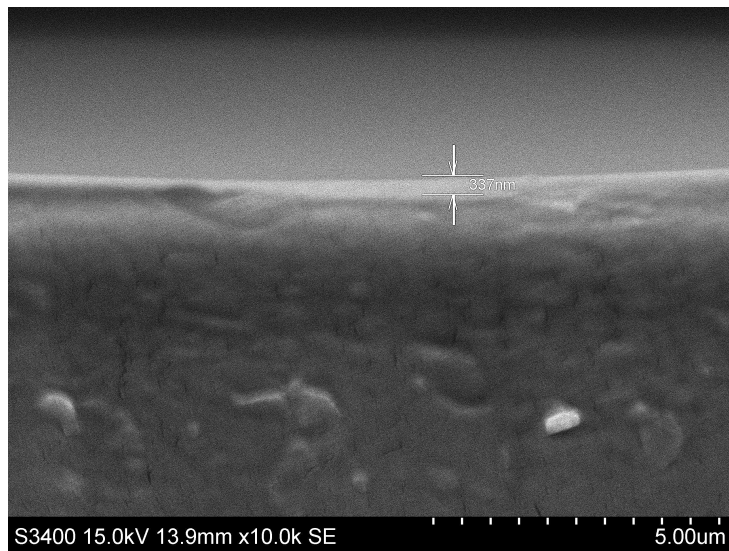
(b) Membrane #8, 5 μm

Figure 68: SEM-pictures of membrane #8
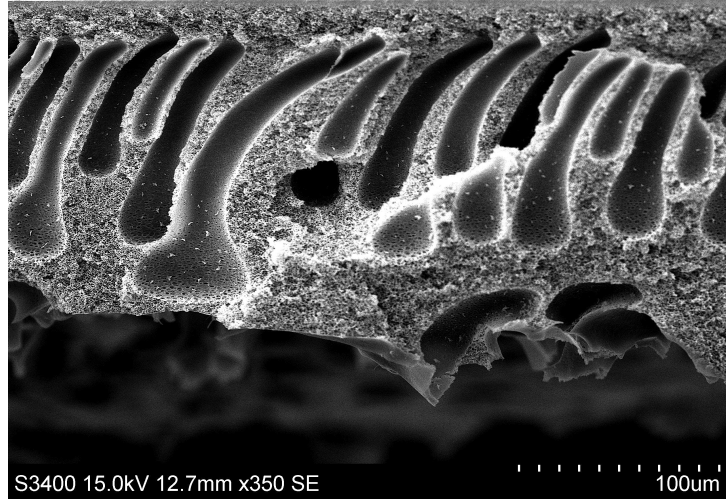
(a) Membrane #9, 100 μm

(b) Membrane #9, 10 μm

(c) Membrane #9, 2 μm
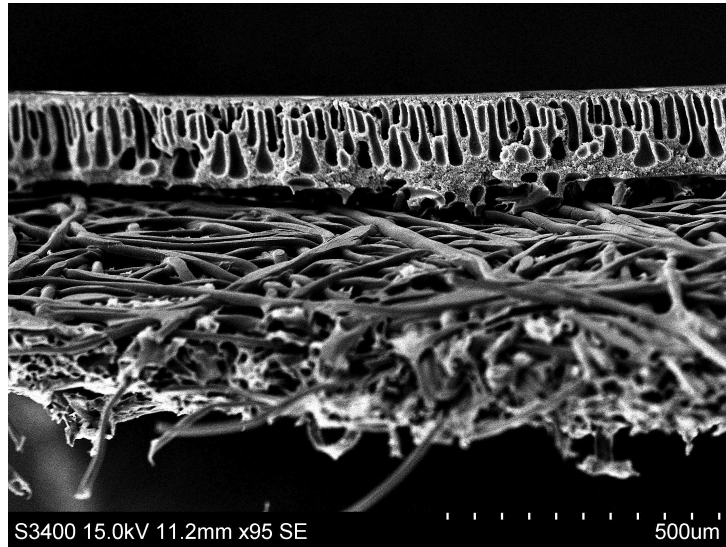
Figure 69: SEM-pictures of membrane #9
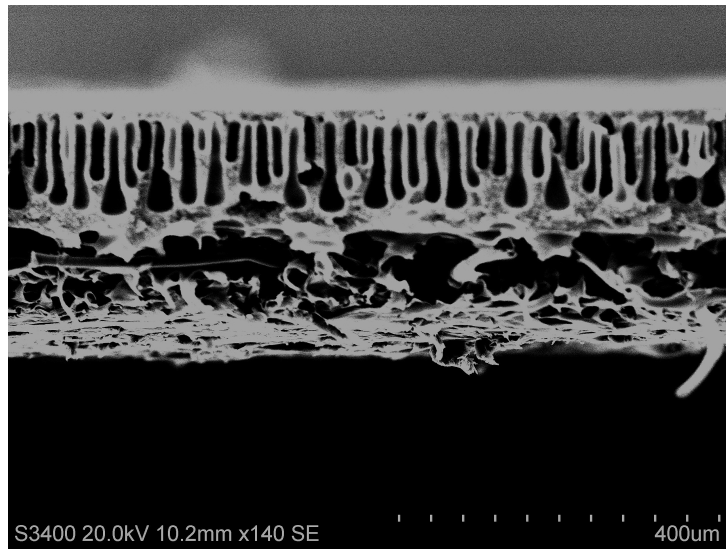
(a) Membrane #10, 400 μm
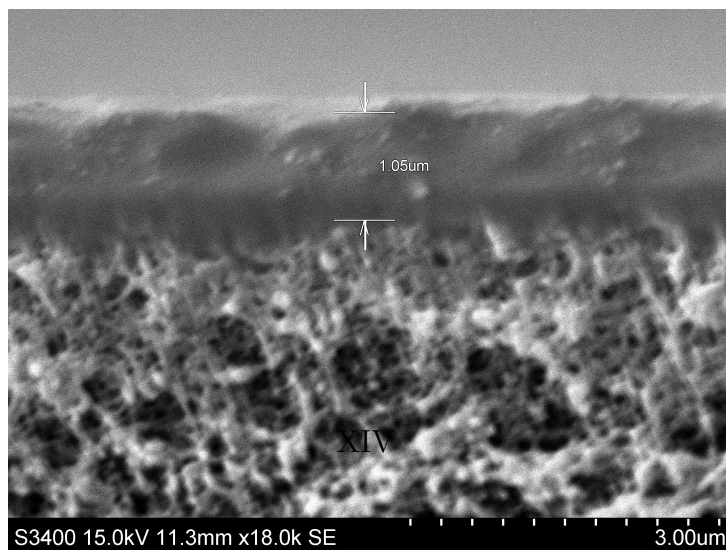

(b) Membrane #10, 100 μm
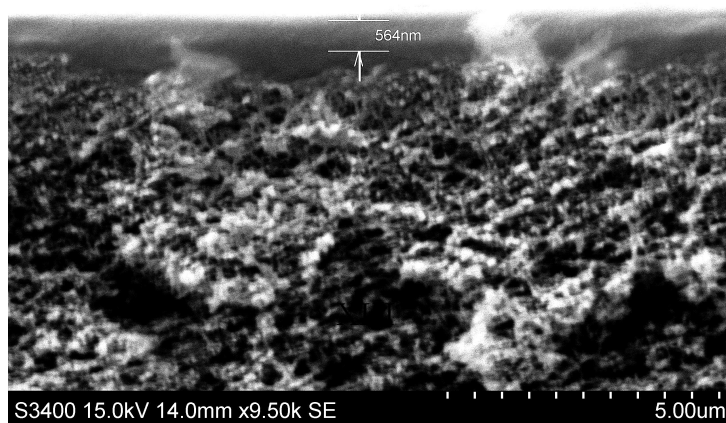
(c) Membrane #10, 5 μm

Figure 70: SEM-pictures of membrane #10

(a) Membrane #11, 500 μm

(b) Membrane #11, 5 μm

(c) Membrane #11, 3 μm

Figure 71: SEM-pictures of membrane #11

E   CD-ROM with Data from Experiments